

INFORMATION TO USERS

This reproduction was made from a copy of a document sent to us for microfilming. While the most advanced technology has been used to photograph and reproduce this document, the quality of the reproduction is heavily dependent upon the quality of the material submitted.

The following explanation of techniques is provided to help clarify markings or notations which may appear on this reproduction.

1. The sign or "target" for pages apparently lacking from the document photographed is "Missing Page(s)". If it was possible to obtain the missing page(s) or section, they are spliced into the film along with adjacent pages. This may have necessitated cutting through an image and duplicating adjacent pages to assure complete continuity.
2. When an image on the film is obliterated with a round black mark, it is an indication of either blurred copy because of movement during exposure, duplicate copy, or copyrighted materials that should not have been filmed. For blurred pages, a good image of the page can be found in the adjacent frame. If copyrighted materials were deleted, a target note will appear listing the pages in the adjacent frame.
3. When a map, drawing or chart, etc., is part of the material being photographed, a definite method of "sectioning" the material has been followed. It is customary to begin filming at the upper left hand corner of a large sheet and to continue from left to right in equal sections with small overlaps. If necessary, sectioning is continued again—beginning below the first row and continuing on until complete.
4. For illustrations that cannot be satisfactorily reproduced by xerographic means, photographic prints can be purchased at additional cost and inserted into your xerographic copy. These prints are available upon request from the Dissertations Customer Services Department.
5. Some pages in any document may have indistinct print. In all cases the best available copy has been filmed.

**University
Microfilms
International**
300 N. Zeeb Road
Ann Arbor, MI 48106

1327838

Karimnassae, Ali

FLEXURAL BEHAVIOR OF LIGHTLY REINFORCED UNBONDED POST-TENSIONED CONCRETE BEAMS

The University of Arizona

M.S.

1986

**University
Microfilms
International** 300 N. Zeeb Road, Ann Arbor, MI 48106

PLEASE NOTE:

In all cases this material has been filmed in the best possible way from the available copy. Problems encountered with this document have been identified here with a check mark .

1. Glossy photographs or pages
2. Colored illustrations, paper or print _____
3. Photographs with dark background
4. Illustrations are poor copy _____
5. Pages with black marks, not original copy _____
6. Print shows through as there is text on both sides of page _____
7. Indistinct, broken or small print on several pages
8. Print exceeds margin requirements _____
9. Tightly bound copy with print lost in spine _____
10. Computer printout pages with indistinct print _____
11. Page(s) _____ lacking when material received, and not available from school or author.
12. Page(s) _____ seem to be missing in numbering only as text follows.
13. Two pages numbered _____. Text follows.
14. Curling and wrinkled pages _____
15. Dissertation contains pages with print at a slant, filmed as received _____
16. Other _____

University
Microfilms
International

FLEXURAL BEHAVIOR OF LIGHTLY REINFORCED
UNBONDED POST-TENSIONED CONCRETE BEAMS

by

Ali Karimnassaei

A Thesis Submitted to the Faculty of the
DEPARTMENT OF CIVIL ENGINEERING AND
ENGINEERING MECHANICS
In Partial Fulfillment of the Requirements
For the Degree of
MASTER OF SCIENCE
WITH A MAJOR IN CIVIL ENGINEERING
In the Graduate College
THE UNIVERSITY OF ARIZONA

1 9 8 6

STATEMENT BY AUTHOR

This thesis has been submitted in partial fulfillment of requirements for an advanced degree at The University of Arizona and is deposited in the University Library to be made available to borrowers under rules of the Library.

Brief quotations from this thesis are allowable without special permission, provided that accurate acknowledgment of source is made. Requests for permission for extended quotation from or reproduction of this manuscript in whole or in part may be granted by the head of the major department or the Dean of the Graduate College when in his or her judgment the proposed use of the material is in the interests of scholarship. In all other instances, however, permission must be obtained from the author.

SIGNED: Ali Korumassae

APPROVAL BY THESIS DIRECTOR

This thesis has been approved on the date shown below:

M. R. Ehsani 5/5/86
Mohammed R. Ehsani Date
Assistant Professor of Civil Engineering
and Engineering Mechanics

DEDICATION

to my parents

ACKNOWLEDGMENT

It is a pleasure to acknowledge some of the people who helped and encouraged me in the preparation of this thesis. I would like to begin by expressing my sincere gratitude to my major advisor, Dr. Mohammad R. Ehsani, for his invaluable assistance and advice in the planning, organization, and completion of this thesis.

Special thanks are extended to the members of my committee, Doctors Reidar Bjorhovde and Edward A. Nowatzki, for reviewing this manuscript.

Thanks are also extended to Mr. Tariq Al-Faris for his assistance throughout the entire project.

Appreciation is extended to the Department of Civil Engineering for providing the equipment, as well as funds for this study.

Finally, my deepest appreciation goes to those whose love, support, and encouragement made this achievement possible: my parents, my family who all deserve to be recognized here, my wife, and all of my friends.

TABLE OF CONTENTS

	page
LIST OF ILLUSTRATIONS	v
LIST OF TABLES	xi
ABSTRACT	xii
1. INTRODUCTION	1
1.1. General	1
1.2. Flexural Behavior of Unbonded Post-tensioned Members	3
1.3. Effect of Reinforcement Ratio on Mode of Failure	9
1.4. Objective and Scope	12
2. DESIGN AND CONSTRUCTION OF SPECIMENS	14
2.1. General	14
2.2. Design for Flexural	14
2.3. Design for Shear	17
2.4. Construction of Specimens	17
2.5. Material Properties	27
3. INSTRUMENTATION AND TEST SET-UP	37
3.1. Instrumentation	37
3.2. Test Set-Up	46
3.3. Test Procedures	46
4. BEHAVIOR OF SPECIMENS UNDER THE TEST	54
5. DISCUSSION OF RESULTS	87
5.1. Effects of Primary Variables	87
5.2. Comparison of Test Results With Existing Theories	92
5.3. Reinforcing Index, ω	107

TABLE OF CONTENTS--Continued

	page
6. SUMMARY AND CONCLUSIONS	114
6.1. Summary	114
6.2. Conclusions	115
6.3. Recommendations for Further Research	117
APPENDIX A: DERIVATION OF $\bar{\omega}$	1118
APPENDIX B: LIST OF NOTATION	121
REFERENCES	124

LIST OF ILLUSTRATIONS

Figure		page
1.1	Distribution of Additional Strain in the Strand due to the Externally Applied Load, $\Delta\epsilon_s$, for Bonded and Unbonded Tendons	4
2.1	Flow Chart of Experimental Program	15
2.2	Details of Specimens 1 and 4	18
2.3	Details of Specimens 2 and 3	19
2.4	Details of Specimens 5 and 8	20
2.5	Details of Specimens 6 and 7	21
2.6a	Construction of Forms	23
2.6b	Interior Dividers used in the Forms	23
2.7	Location of Strain Gages	25
2.8	Constructed Form Prior to Concrete Pouring	26
2.9	Typical Plot of Stress vs. Strain for Concrete	30
2.10	Typical Plot of Stress vs. Strain for Prestressing Tendon	32
2.11	Typical Plot of Load vs. Strain for Obtaining the Apparent E Value	34
2.12	Typical Plot of Stress vs. Strain for Nonprestressed Steel	36
3.1	MTS Control System	39
3.2a	Typical Strain Gages Attached to a Stirrup	41

LIST OF ILLUSTRATIONS--Continued

Figure		page
3.2b	Typical Strain Gages Attached to a Strand	41
3.3	The Load Cell Constructed for the Study	42
3.4	Connections of Strain Gages for Building the Load Cells	44
3.5	Load Cell Calibration Curve	45
3.6	Test Set-Up Inside the Frame	47
3.7	A Typical Support for the Specimens	48
3.8	Locations of LPSRSM's	50
3.9	Typical Chuck Anchor for a Single Tendon (Courtesy Supreme Products Corporation)	51
3.10a	Assemblage of Dead End of the Specimens	52
3.10b	Assemblage of Live End of the Specimen	52
4.1	Location of Strain Gages and LPSRSM's for Specimens 1, 2, 3, and 5	56
4.2	Applied Load vs. Strain in the Longitudinal Reinforcement in the Bottom of Specimen 1	57
4.3	Applied Load vs. Strain in the Compression Reinforcement for Specimen 1	59
4.4	Applied Load vs. Deflection for Specimen 1	60
4.5	Specimen 1 During the Test	61
4.6	Applied Load vs. Deflection for Specimen 2	63
4.7	Specimen 2 at the Conclusion of the Test	64
4.8	Applied Load vs. Strain in the Compression Reinforcement for Specimen 3	66

LIST OF ILLUSTRATIONS--Continued

Figure		page
4.9	Applied Load vs. Deflection for Specimen 3	67
4.10	Specimen 3 Near the Failure	68
4.11	Location of Strain Gages and LPSRSM's for Specimens 4, 6, 7, and 8	69
4.12	Specimen 4 During the Test	71
4.13	Applied Load vs. Deflection for Specimen 4	72
4.14	Applied Load vs. Deflection for Specimen 5	73
4.15	Specimen 5 at the Conclusion of the Test	74
4.16	Applied Load vs. Deflection for Specimen 6	76
4.17	Specimen 6 at the Conclusion of the Test	77
4.18	Applied Load vs. Strain in the Longitudinal Reinforcement in the Bottom of Specimen 7	79
4.19	Applied Load vs. Deflection for Specimen 7	80
4.20	Specimen 7 Near the Failure	81
4.21	Specimen 7 at the Conclusion of the Test	82
4.22	Applied Load vs. Strain in the Longitudinal Reinforcement in the Bottom of Specimen 8	83
4.23	Applied Load vs. Deflection for Specimen 8	85
4.24	Specimen 8 at the Conclusion of the Test	86

LIST OF ILLUSTRATIONS--Continued

Figure		page
5.1	Effect of Shear Span on Δf_s	89
5.2	Distribution of $\Delta \epsilon_s$ in Unbonded Tendons for Different Loading Conditions	91
5.3	Comparison of Eq. 18-4 of ACI-318-83 Code to the Test Results	94
5.4	Comparison of Modified Eq. 18-4 of ACI-381-83 Code to the Test Results	97
5.5	Comparison of Pannell-Tam Equation to the Test Results	99
5.6	Effect of Shear Span on the Coefficient ν	101
5.7	Comparison of Modified Pannell-Tam Equation to the Test Results	103
5.8	Comparison of the British Code Values to the Test Results	105
5.9	Comparison of the British Code Values to the Test Results	106
5.10	Ratio of Actual $\bar{\omega}$ to the $\bar{\omega}$ Obtained from Eq. 5.8 vs. Specimens	111
5.11	Ratio $M_U/b_w d$ vs. Reinforcing Index $\bar{\omega}$	113

LIST OF TABLES

Table	page
2.1 Capacity of the Designed Specimens	22
2.2 Concrete Mix Proportions	27
2.3 Results of Concrete Cylinder Tests	29
2.4 Properties of Strands	31
4.1 Details of Specimens	55
5.1 Primary Variables and Some of the Test Results	88
5.2 Values of Δf_s (ksi)	93
5.3 British Code Values for Ultimate Stress in Unbonded Tendons	104
5.4 Reinforcing Index, $\bar{\omega}$	110

ABSTRACT

Effect of shear span on the magnitude of additional strain due to externally applied loads ($\Delta\epsilon_s$) in unbonded post-tensioned concrete beams is investigated in this study.

Full-scale test results are reported for specimens with eight different shear spans. It is concluded that length of the shear span does influence the magnitude of $\Delta\epsilon_s$.

The values of $\Delta\epsilon_s$ obtained from this experiment are compared with those obtained from the most widely used expressions. Some modification factors which include the effect of shear span on magnitude of $\Delta\epsilon_s$ are proposed.

CHAPTER 1

INTRODUCTION

1.1. General

Tensile strength of concrete is much lower than its compressive strength. This results in preventing its usage in those structural members which require high tensile strength. During the second half of the nineteenth century, this problem was overcome by using steel bars in those places which would be subjected to tensile stress during their lifetime⁽¹⁾. Such a combination of steel and concrete is known as reinforced concrete.

In most reinforced concrete members subjected to flexure, tension cracks are formed at loads significantly smaller than the ultimate capacity of the section. This cracking of the member reduces the stiffness of the section considerably and may result in early deterioration and rusting of the reinforcing steel due to the penetration of water through these cracks. In order to delay the cracking of concrete, compressive stresses can be introduced initially to the parts of the cross section which would experience tensile stresses under service loads. This compressive stress will counteract some or all of the tensile stresses that will be introduced to the member during its

lifetime. This imposition of stress to the member is called a prestressing and the specimen which is subjected to the prestressing is called prestressed concrete member.

Prestressing of concrete members is usually done by means of high-strength steel tendons which were first used for prestressing by the Spaniard Eduard Torroja, in the members of the Tempul Aqueduct in 1925⁽²⁾. These high-strength steel tendons are stressed and then anchored. The prestressing process can be carried out in two ways: pre-tensioning and post-tensioning. The primary difference between the two methods is the condition of the concrete at the time of application of the prestressing force. In the pre-tensioned members, the tendons are stressed before the casting of concrete, but in the post-tensioned members the tendons are stressed after the concrete has hardened and has obtained enough strength to support the stress.

Prestressing tendons can be either "bonded" or "unbonded." Bonded tendons are tendons which are bonded to the concrete throughout their entire length. Almost all of the pre-tensioned tendons and some of the post-tensioned tendons which are placed in ducts and grouted are considered "bonded." Unbonded tendons are those whose bond to the concrete throughout the entire length is prevented by wrapping the tendon in waterproof paper and greasing it or placing the tendon inside a flexible duct. All of the

specimens which were tested for the purpose of this investigation were unbonded post-tensioned beams.

1.2. Flexural Behavior of Unbonded Post-tensioned Members

If the prestressing steel is bonded to the concrete, then the change in strain in the tendon at any point along the length of the span is equal to the change in the strain of concrete at that particular point. This means that the strain compatibility equations can be used for analysis of the section subjected to flexure as given by Libby⁽³⁾ or Nilson⁽⁴⁾. However, if the prestressing tendon is unbonded, the change in strain in the tendon is distributed over the entire length of the tendon rather than being "more concentrated" at the section of maximum moment. Distributions of the additional strain due to the externally applied loads, $\Delta\epsilon_s$, for a bonded and an unbonded tendon are shown in Fig. 1.1. As can be seen in this figure, the magnitude of $\Delta\epsilon_s$ in the unbonded tendon is smaller than that of the bonded one. Since stress is directly proportional to strain, the reduction in strain because of the lack of bond between the steel and concrete results in a reduction in the additional stress due to the externally applied loads, Δf_s .

The stress in steel at ultimate load (f_{ps}) in a prestressed concrete beam can be expressed as:

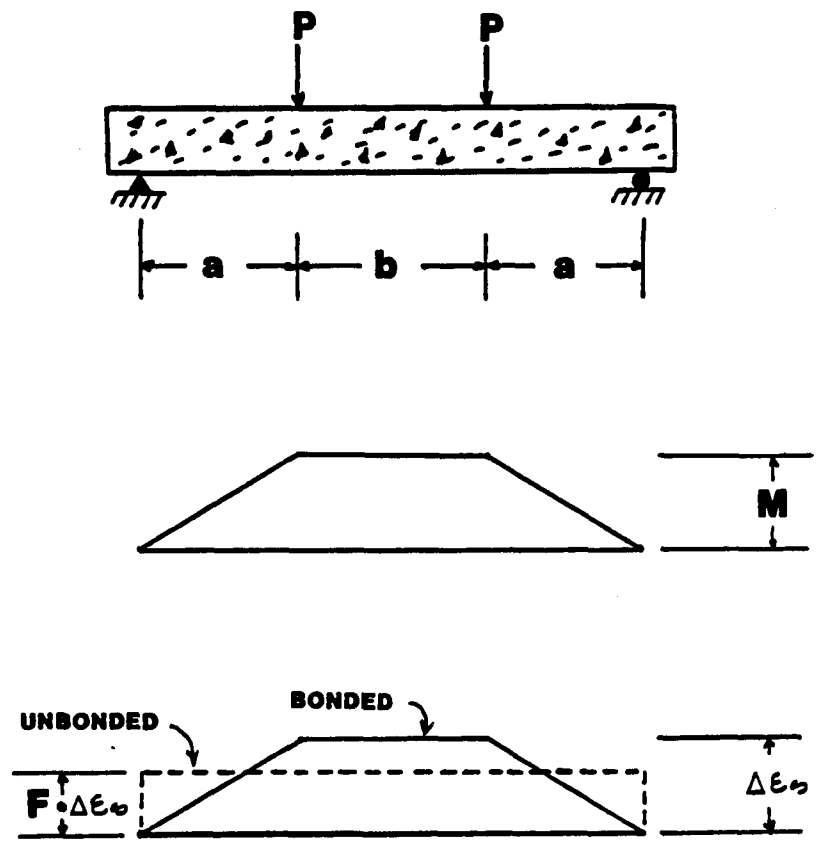


Fig. 1.1. Distribution of Additional Strain in the Strand due to the Externally Applied Load, $\Delta\epsilon_s$, for Bonded and Unbonded Tendons

$$f_{ps} = f_{se} + \Delta f_s \quad (1.1)$$

where f_{se} is the effective prestress in the steel tendon after all the prestress losses have taken place, and Δf_s is the additional stress due to the externally applied loads. From the above equation it can be concluded that a reduction in the value of Δf_s due to the lack of bond results in a lower value of f_{ps} and ultimate moment capacity of unbonded post-tensioned members.

Baker⁽⁵⁾ was the first one who recognized that loss of bond between the prestressing steel and concrete lowers the ultimate moment capacity of the prestressed concrete beams. He introduced a bond factor F to account for these losses. The factor F is the ratio of change in the strain in the tendon to the change in the strain in the concrete adjacent to the tendon at failure. The value of F is a function of several variables including the value of strain in the tendon at ultimate load. For this reason, Baker suggested that the bond factor should be obtained experimentally. However, for the purpose of design and simplified analysis, he suggested the use of a safe value of 0.1. The bond factor, F , can be multiplied by Δf_s obtained from strain compatibility equations to calculate $\Delta \epsilon_s$ in unbonded post-tensioned beams.

Tests performed by Janny et al.⁽⁶⁾ at the Research and Development Laboratories of the Portland Cement

Association showed that the strength of pre-tensioned and the corresponding post-tensioned bonded beams was nearly equal, but that the strength of post-tensioned unbonded beams was between 20 to 40 percent lower than that of the corresponding bonded beams. Values of Δf_s in unbonded tendons were found to vary from 40,000 to 60,000 psi. However, Eq. 26-7 of ACI 318-63⁽⁷⁾ code gave a constant value of 15,000 psi for Δf_s in post-tensioned unbonded tendons. The reason for limiting Δf_s to such a low and conservative value was the lack of detailed information and test results on the behavior of post-tensioned specimens with unbonded tendons. This resulted in more experiments and investigations.

Twenty-six unbonded post-tensioned beams were tested at the University of Illinois.⁽⁸⁾ The results showed that Δf_s was a function of the reinforcement ratio, ρ_p , as well as the compressive strength of concrete f'_c . The values of Δf_s were found to vary from about 10,000 to 80,000 psi. Warwaruk⁽⁸⁾ plotted Δf_s against ρ_p/f'_c and obtained the following equation for Δf_s ;

$$\Delta f_s = 30,000 - 10^{10} \frac{\rho_p}{f'_c} \quad (1.2)$$

where $\rho_p = \frac{A_{ps}}{b_w d}$

A_{ps} = area of prestressed reinforcement in tension zone

b_w = width of compression face of member

d = distance from extreme compression fiber to centroid of prestressing steel.

Based on the results of tests by Mattock, Yamazaki and Kattula⁽⁹⁾ on seven simply supported and three continuous beams performed at the University of Washington, the following equation was obtained for Δf_s .

$$\Delta f_s = 1.4 \frac{f'_c}{100 \rho_p} + 10,000 \quad (1.3)$$

Mattock⁽⁹⁾ plotted the values obtained from Eq. 1.3 against ρ_p/f'_c and compared them to the test results of Warwaruk⁽⁸⁾, Mattock⁽¹⁰⁾, Janney et al.⁽⁶⁾, Imperial College S.D.I.R. Group⁽¹¹⁾ and Gifford⁽¹²⁾ and found that Eq. 1.3 gave a lower bound to all of those test results.

ACI-ASCE Committee 423 replaced the factor 1.4 in Eq. 1.3 by 1.0 to make it slightly more conservative. It is this form for Δf_s that is used in the ACI-318-71⁽¹³⁾ code for Δf_s , i.e.,

$$f_{ps} = f_{pe} + \Delta f_s \quad (1.4)$$

where

$$\Delta f_s = \frac{f'_c}{100 \rho_p} + 10,000$$

The value of Δf_s in this equation is limited to a maximum value of 60,000 psi and f_{ps} is limited to the yield stress of prestressing steel f_{py} .

Several investigators⁽¹⁴⁻¹⁷⁾ have shown that the span/depth ratio, l/d , also influences the magnitude of Δf_s in addition to ρ_p and f'_c included in Eq. 1.4. Mojtahedi and Gamble⁽¹⁶⁾ found that the value of Δf_s given by Eq. 1.4 was over-estimated for the beams with l/d greater than 40. This means that Eq. 1.4 cannot be applied to those structural members with $l/d \geq 40$, including typical slabs which have an l/d ratio of about 45. For this reason Park and Gamble⁽¹⁸⁾ suggested that until further tests have been conducted and Eq. 1.4 is modified, the conservative equation given by ACI 318-63⁽⁷⁾ should be used for the determination of Δf_s in post-tensioned unbonded members with $l/d > 40$.

Equation 18.4 of ACI-318-83⁽¹⁹⁾ limited the use of Eq. 1.4 to those specimens with l/d less than or equal to 35 and introduced the following equation for specimens with l/d greater than 35:

$$f_{ps} = f_{se} + \Delta f_s \leq f_{py} \quad (1.5)$$

where

$$\Delta f_s = \frac{f'_c}{300 \rho_p} + 10,000$$

This value of Δf_s is limited to a maximum value of 30,000 psi and f_{ps} is limited to the value of f_{py} .

In post-tensioned members in which the unbonded tendons are the only flexural reinforcement of the member, after the first flexural crack appears it increases rapidly in depth and width and the member behaves as a shallow tied arch, rather than as a flexural member. For this reason, ACI-ASCE Committee 423⁽²⁰⁾ required a minimum amount of bonded reinforcement. This amount was given as 0.2 percent of the gross area of concrete. From the results of the experiment conducted by Mattock⁽⁹⁾, he concluded that the above requirement would ensure a satisfactory serviceability characteristic in beams with unbonded tendons. However, Mattock suggested that the amount of this minimum reinforcement should be 0.4 percent of the area of that part of the beam section between the flexural tension face and the neutral axis of the cross section. This is the same amount of reinforcement that is required by Section 18.9 of the ACI-318-83 Code.⁽¹⁹⁾

1.3. Effect of Reinforcement on Mode of Failure

There are three terms which are used for defining the amount of reinforcement in reinforced as well as

prestressed concrete members. These are: balanced, underreinforced and overreinforced conditions.

A beam in which the reinforcing steel starts to yield at exactly the same load as the concrete reaches its ultimate strain is said to be in its balanced condition. If a beam has less reinforcement than that required for a balanced condition, it is said to be underreinforced. If it has more, it is said to be overreinforced.

In an underreinforced beam the prestressing steel yields before the compression concrete reaches its ultimate stress. As a result, large deflection and cracks will be observed before the failure occurs. This is the most desirable mode of failure, because it warns the user of the structure before failure occurs. If the amount of steel reinforcement is much too small, the ultimate resisting moment of the section will be less than the cracking moment. As a result, a brittle failure by fracture of steel occurs. Such beams are often referred to as too lightly reinforced. If a beam is overreinforced, the compression concrete reaches its ultimate stress before the steel yields. The failure of such a beam would be sudden and unexpected to the users of structures.

The most desirable mode of failure for a concrete beam is that of underreinforced beams which give a noticeable amount of deflection and large enough cracks

prior to the failure. In order to prevent the sudden and brittle failure associated with overreinforced or too lightly reinforced beams, a lower and an upper limit for the amount of reinforcement should be set. For reinforced concrete beams, the ACI Code⁽¹⁹⁾ provides a minimum amount of steel ratio ρ_{\min} which is equal to $200/f_y$, where f_y is the specified yield strength of tension reinforcement in psi. This value of ρ_{\min} was obtained by calculating the cracking moment of a plain concrete section and equating it to the strength of a reinforced concrete section of the same size multiplied by a safety factor of 2 and solving for the steel ratio, ρ . The maximum amount of reinforcement in reinforced concrete beams is given as 75 percent of the steel required for the balanced condition. This guarantees that the beam will never reach its balanced condition and will always behave as an underreinforced beam.

For prestressed concrete beams the minimum amount of reinforcement is not given in terms of reinforcement ratios. It is rather given indirectly in terms of ultimate resisting moment (M_u) and cracking moment (M_{cr}). According to Section 18.8.3 of the ACI Code⁽¹⁹⁾, the design nominal moment capacity of the section must be at least 20 percent higher than that of cracking moment. An expression for minimum amount of reinforcement can be obtained in terms of reinforcement index, $\bar{\omega}$, where

$$\bar{\omega} = \omega_p + \omega - \omega'$$

$$\omega_p = \rho_p \frac{f_{ps}}{f'_c}$$

$$\omega = \rho \frac{f_y}{f'_c} ; \quad \rho = \frac{A_s}{b_w d}$$

$$\omega' = \rho' \frac{F'_s}{F'_c} ; \quad \rho' = \frac{A'_s}{b_w d}$$

A_s = area of nonprestressed tension reinforcement

A'_s = area of compression reinforcement

f_y = specified yield strength of nonprestressed reinforcement

f'_s = stress in compression reinforcement at nominal strength.

This expression can be obtained by writing the design nominal moment capacity of a section as a function of $\bar{\omega}$ and setting it equal to a factor multiplied by the cracking moment of the cross section. This procedure was done by Naaman^(21,22) for a typical prestressed concrete beam. The derivation of such an equation for partially reinforced beams with unbonded tendon is given in Appendix A of this report.

1.4. Objective and Scope

This experiment was undertaken to study the flexural behavior of unbonded post-tensioned members with

the minimum amount of reinforcement and the effect of shear span, a , on additional stress due to externally applied loads, Δf_s . Eight full-size unbonded post-tensioned concrete beams were constructed and tested for the purpose of this investigation. The primary variables of the experiment consisted of dimensions of the cross section, the amount of prestressing force, p_e , and the a/l ratio where a is the shear span and l is the clear length of the span. In the experimental portion of this investigation effects of such parameters on Δf_s are investigated. In the analytical portion of this study the results of the experiments are compared to the values obtained from some of the existing equations and some modification factors are recommended.

CHAPTER 2

DESIGN AND CONSTRUCTION OF SPECIMENS

2.1. General

Eight unbonded post-tensioned beams were tested during this experiment. The primary purpose of this experiment was to study the flexural behavior of lightly reinforced post-tensioned beams with varying shear span. The major variables of the experiment consisted of dimensions of the cross section, the amount of prestressing force, P_e , and the a/l ratio, where a is the shear span and l is the clear length of the span. Four of the specimens were "large size" which were 14 x 20 in. and the other four were "small size" which were 12 x 18 in. A flow chart of the experimental program is shown in Fig. 2.1.

2.2. Design for Flexural

The size and amount of prestressing steel for each specimen was chosen so that a section with a design nominal moment of 20 percent higher than the cracking moment as suggested by the ACI Code was obtained. A larger section was then chosen to make the cracking moment higher. The ultimate moment capacities were calculated by using

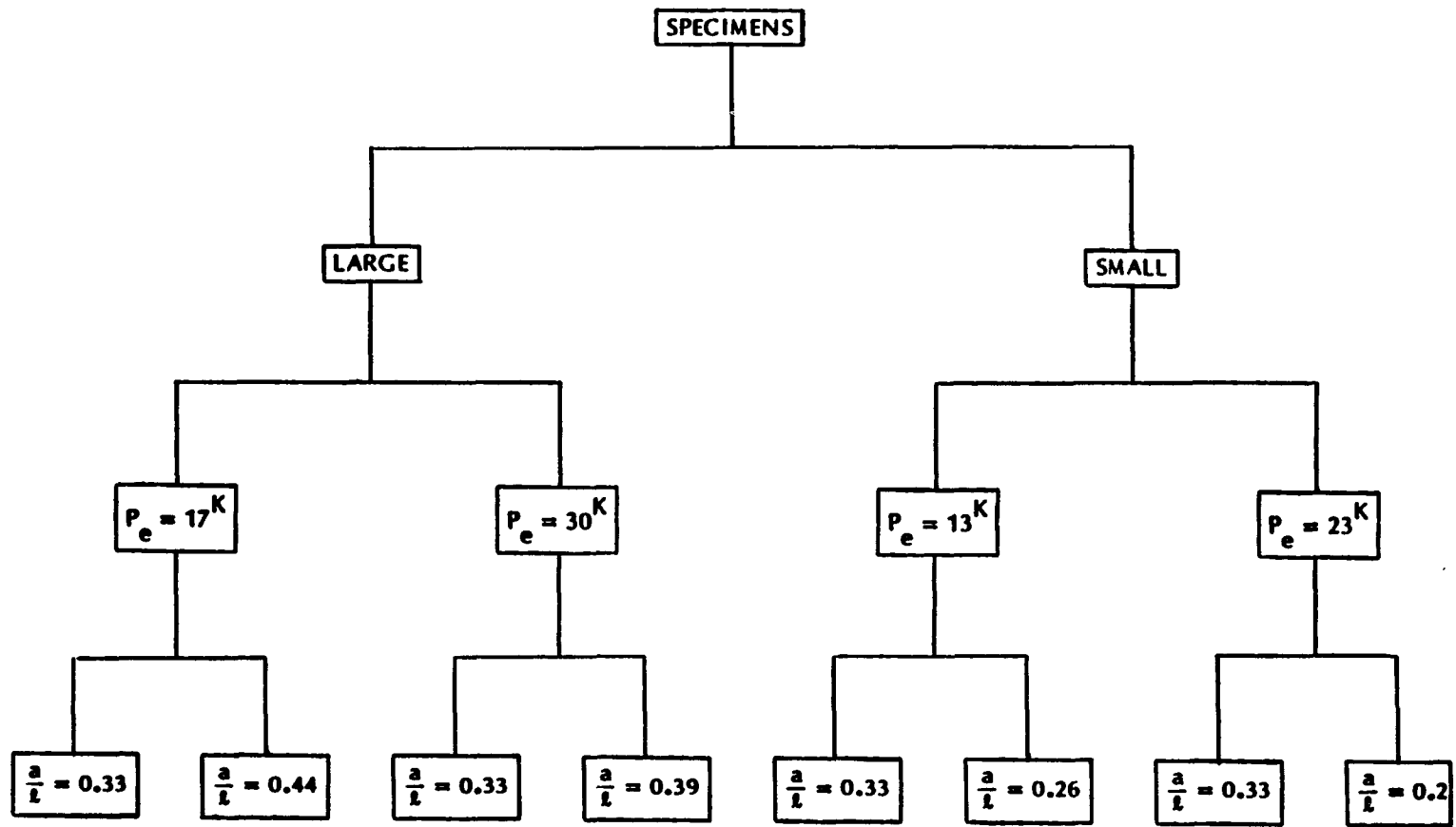


Fig. 2.1. Flow Chart of Experimental Program.

18-4 of the ACI code and cracking moments were calculated from the following equation.

$$M_{Cr} = P_e \left(\frac{r^2}{y_b} + e_o \right) + \frac{f_r I}{y_b}$$

where

r = radius of gyration of cross section

$$r = \left(\frac{I}{A_c} \right)$$

I = moment of inertia of gross concrete section about neutral axis, in⁴.

A_c = gross area of concrete, in²

y_b = distance from the tension face of the specimen to the neutral axis, in.

e_o = distance from the center of the prestressing steel to the neutral axis of cross section, in.

f_r = modulus of rupture of concrete, psi.

$$f_r = 7.5 f'_c$$

f'_c = specified compressive strength of concrete, psi.

Since all of the beams had unbonded tendons, a minimum area of bonded reinforcement was added as required by Section 18.9.2 of the ACI code which is given by the equation $A_s = 0.004 A$, where A is the area of that part of the cross section between flexural tension face and the

center of gravity of the cross section. Figures 2.2-2.5 show the dimensions and details of test specimens.

After adding this amount of steel area, the sections were analyzed again. These new values of nominal and cracking moments are shown in Table 2.1.

2.3. Design for Shear

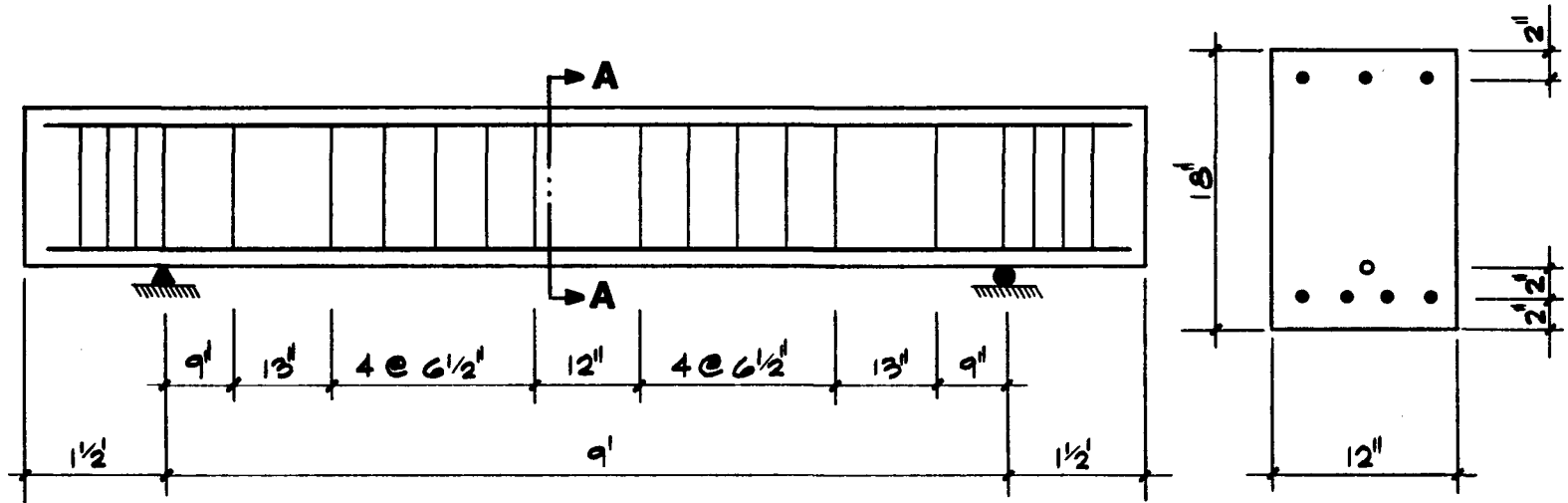
The amount of shear reinforcement and spacing of stirrups were obtained from equations given in Section 11.4 and 11.5 of the ACI code.

The values of load (V) and moment (M) that were used in these equations were obtained from the nominal capacity of the section and a shear span a of 4 feet. Figures 2.2-2.5 give the spacing of stirrups for all of the specimens.

2.4. Construction of Specimens

One large wooden form was used to cast all of the beams. The form was constructed of $3/4$ inch thick plywood and was designed to accommodate four beams side by side at one time, as shown in Fig. 2.6a. The beams were separated by means of interior dividers which were slid into the form as shown in Fig. 2.6b.

The form was then waterproofed with bulls eye shellac coating and oiled prior to casting. Electrical resistance strain gages manufactured by Micromasurements

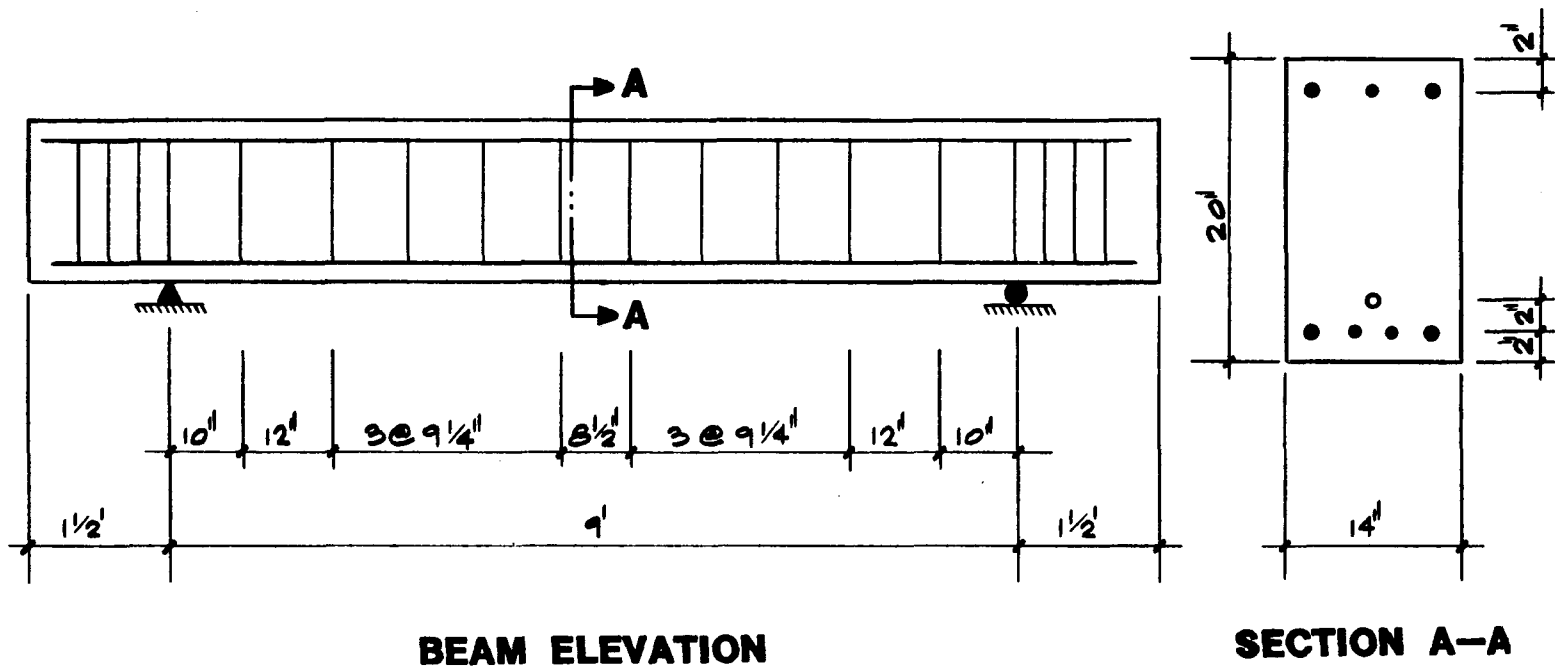


BEAM ELEVATION

SECTION A-A

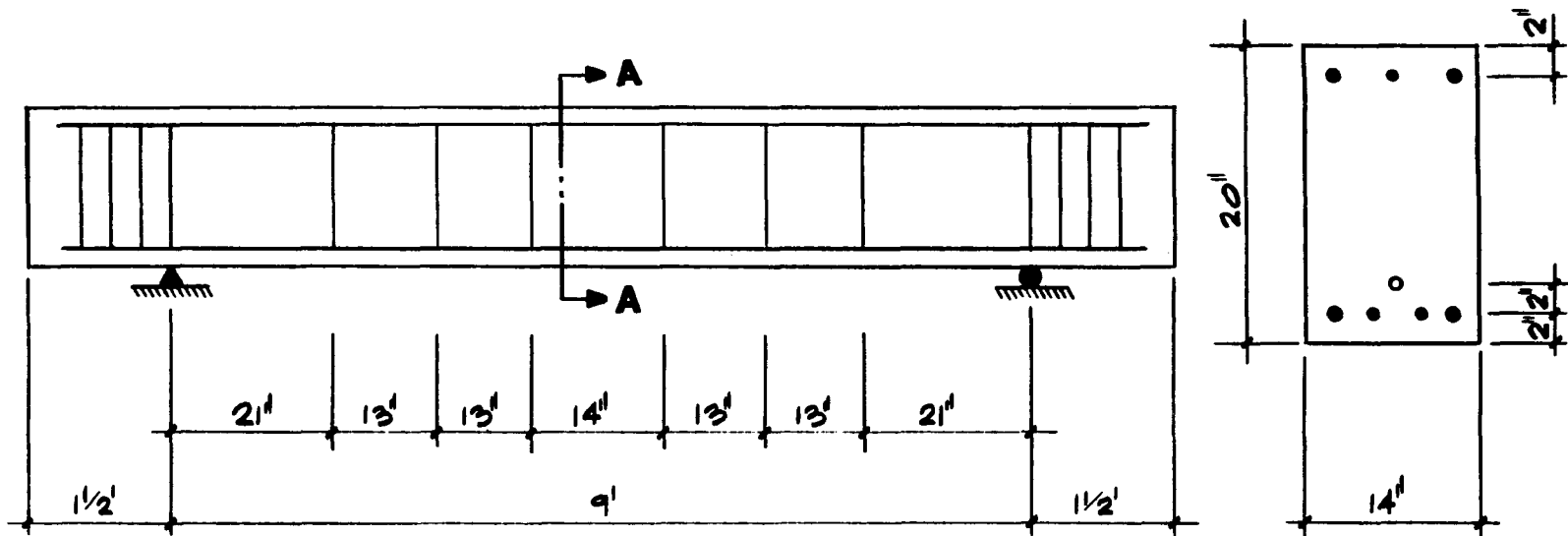
- #3 GR. 40 STEEL
- 1/2" DIAM. GR. 270 SEVEN WIRE STRAND

Fig. 2.2. Details of Specimens 1 and 4



- #3 GR. 40 STEEL
- #4 GR. 40 STEEL
- 1/2" DIAM. GR. 270 SEVEN WIRE STRAND

Fig. 2.3. Details of Specimens 2 and 3

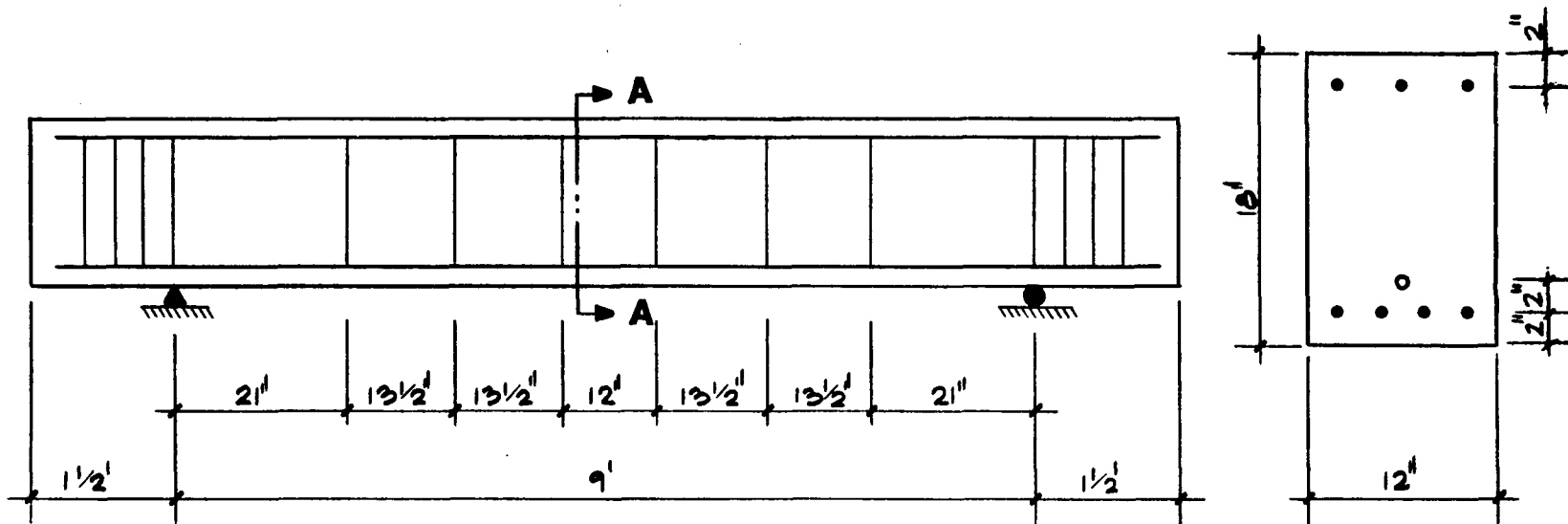


BEAM ELEVATION

SECTION A-A

- #3 GR. 40 STEEL
- #4 GR. 40 STEEL
- 1/2" DIAM. GR. 270 SEVEN WIRE STRAN

Fig. 2.4. Details of Specimens 5 and 8



BEAM ELEVATION

SECTION A-A

- #3 GR. 40 STEEL
- 1/2" DIAM. GR. 270 SEVEN WIRE STRAND

Fig. 2.5. Details of Specimens 6 and 7

Table 2.1
Capacity of the Designed Specimens

Specimen Number	Size	P_e (k)	$\bar{\nu}$	M_n k-ft	ϕM_n	M_{cr}	$1.2 M_{cr}$
1 & 4	12x18	13.1	0.0348	46.83	42.90	34.33	41.95
2 & 3	14x20	17.0	0.0321	69.83	62.85	50.10	60.11
5 & 8	14x20	30.0	0.0463	85.84	77.26	60.19	72.22
6 & 7	12x14	23.1	0.0506	57.59	51.83	41.0	49.19

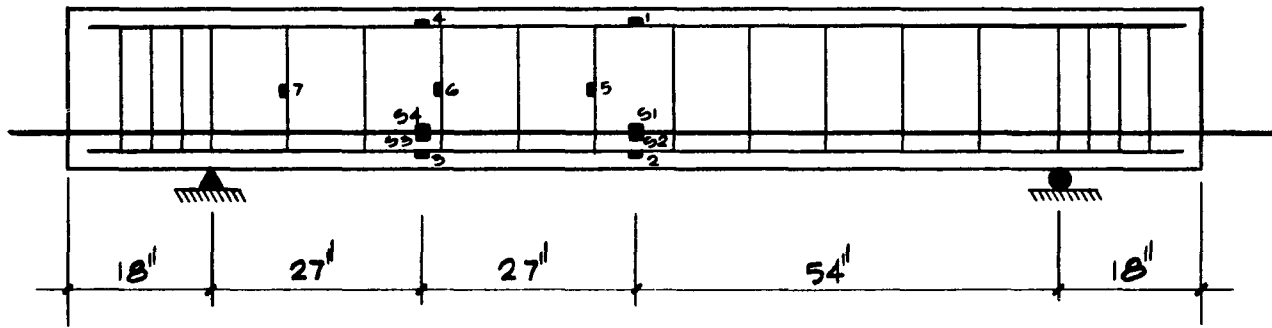


Fig. 2.6a. Construction of Forms



Fig. 2.6b. Interior Dividers used in the Forms

were attached to the longitudinal steel reinforcement, stirrups and prestressing tendons in the designated locations shown in Fig. 2.7. The longitudinal steel reinforcement and stirrups were assembled and tied together. After the assemblage was done, several 1 1/2 in. diameter by 2 in. "chairs" were placed in the oiled form, and the cages were placed on top of them. This was done for the purpose of providing the 2 in. concrete cover for the lower longitudinal bars. Since the strands were longer than the form, and some portion of the strands had to be extended outside the form on each side, a 5/8 in. diameter hole was made at the location of the strands on each side of the form and the strands were passed through these holes. It was desirable to keep the tendon on the center line of the specimen so that no lateral eccentricity of the post-tensioning force could exist. This was achieved by tying the strand on both sides of the form with end anchorages, as shown in Fig. 2.8. Before placing the concrete, the tendons were wrapped in plastic tape and were lubricated by a thin film of grease to eliminate the bonding of the tendons to the concrete. The concrete for all beams was supplied by the Tanner Companies in Tucson, Arizona, and followed the mix proportion as given in Table 2.2. At the time of casting, a hand-held electrical vibrator was used to consolidate the concrete inside the



• STRAIN GAGE

Fig. 2.7. Location of Strain Gages



Fig. 2.8. Constructed Form Prior to Concrete Pouring

form. Fourteen concrete cylinders were cast from each batch of concrete.

The beams and the concrete cylinders were moist-cured in the formwork under sheets of plastic for two weeks. The forms were then removed and the specimens were left without covering under the same condition as the concrete cylinders until the day of testing.

2.5 Material Properties

The concrete used in the beams was mixed and delivered by the Tanner Companies in Tucson, Arizona. It was of normal weight concrete with a design compressive strength of 4000 psi at 28 days and mix proportions given in Table 2.2.

Table 2.2
Concrete Mix Proportions

Material	lb/cuyd
Coarse aggregate with max. size 1/2 in.	1800
Fine aggregate (sand)	1240
Portland cement, Type I	480
Water	308

Because the forms could accommodate only four beams, two batches of concrete were used to cast all eight

specimens. At the time of casting, the concrete mix for both batches had a slump of 3 1/2" and a water cement ratio of 0.55. Fourteen standard 6 in. by 12 in. concrete cylinders were cast with each batch of concrete and then cured in the same condition as the specimens. Compressive strength of the concrete cylinders at 28 days as well as the day of testing are listed in Table 2.3. It should be mentioned here that the highest and the lowest values of concrete cylinder tests are not included in the average. A typical stress versus strain curve for the concrete is shown in Fig. 2.9.

The prestressing steel used in the beams was 1/2 in. diameter, seven wire low relaxation strand. It was supplied by Sumiden Wire Products Corporation and had the properties as shown in Table 2.4. The plot of stress vs. strain for the strand is given in Fig. 2.10.

The stresses in the strands were measured, using electrical resistance strain gages attached to two of the strands. Each strain gage was attached to one wire which was spirally oriented relative to the longitudinal axis of the strand. The effect of this spiral orientation on the measurement was taken into account through the modulus of elasticity of the strand as follows: two electrical resistance strain gages were attached to two different

Table 2.3
Results of Concrete Cylinder Tests

Description	Batch No. 1	Batch No. 2
Specimens Constructed with each Batch	1, 2, 3, 4	5, 6, 7, 8
28-Day Compressive Strength (psi)	**	3820, 4490, 3840, 3930
Average of 28-Day Comp. Strength (psi)	----	4020
Test Day Compressive Strength (psi)	4740, 4670, 4580, 3290, 4420 4830, 4670, 5110*, 2760* 4600, 5080, 3220, 5080	4600, 4780, 4400, 4810* 3820*, 3940, 4070, 4550 3960, 3890
Avg. Test Day Comp. Strength (psi)	4470	4270

**No cylinder test at 28 days.

*Not included in the average.

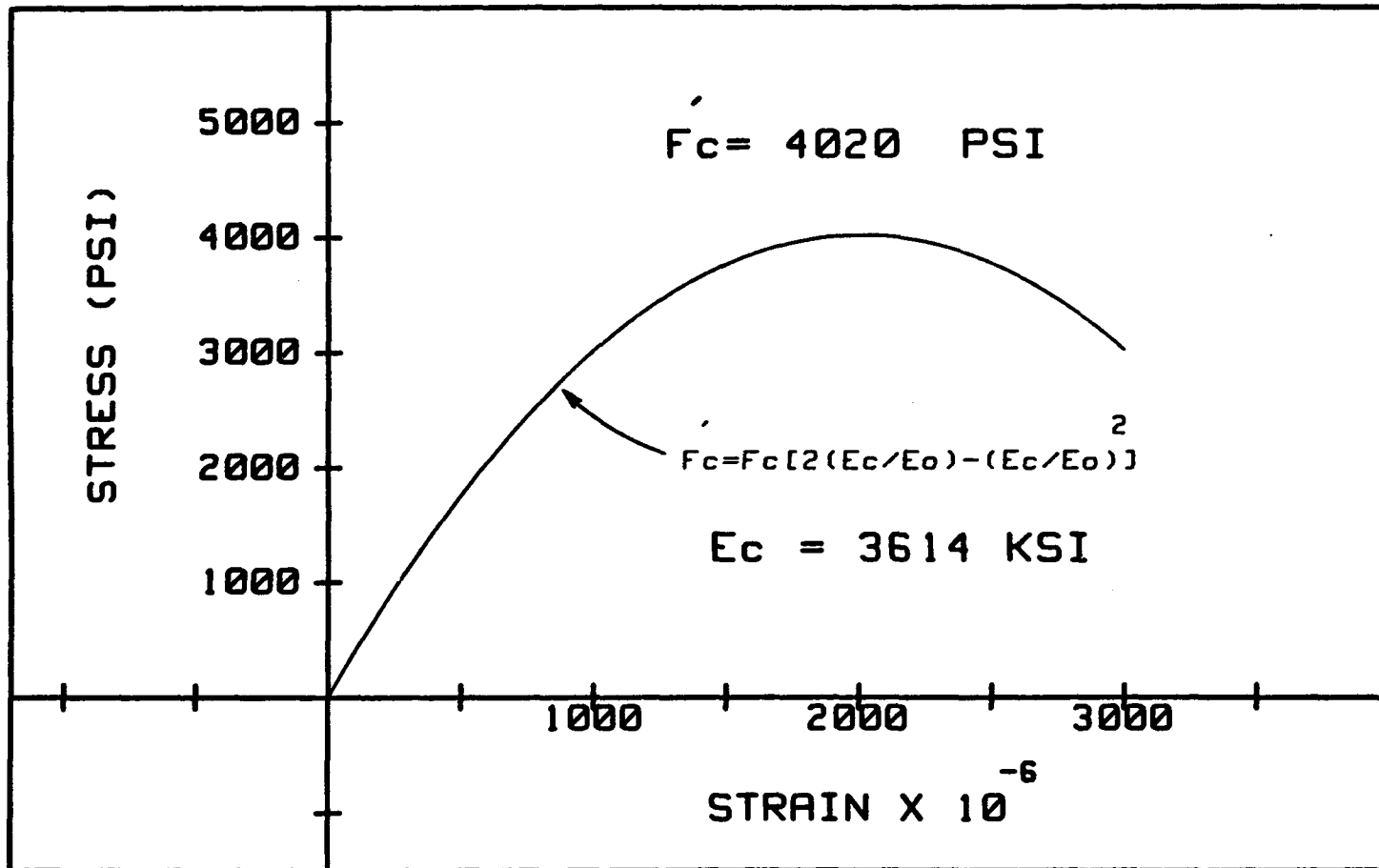


Fig. 2.9. Typical Plot of Stress vs. Strain for Concrete

Table 2.4
Properties of Strands

Ultimate stress	288	ksi
Yield stress	265.5	ksi
Cross-sectional area	0.1525	in ²
Modulus of elasticity	28800	ksi
Total strain	0.053	in/in

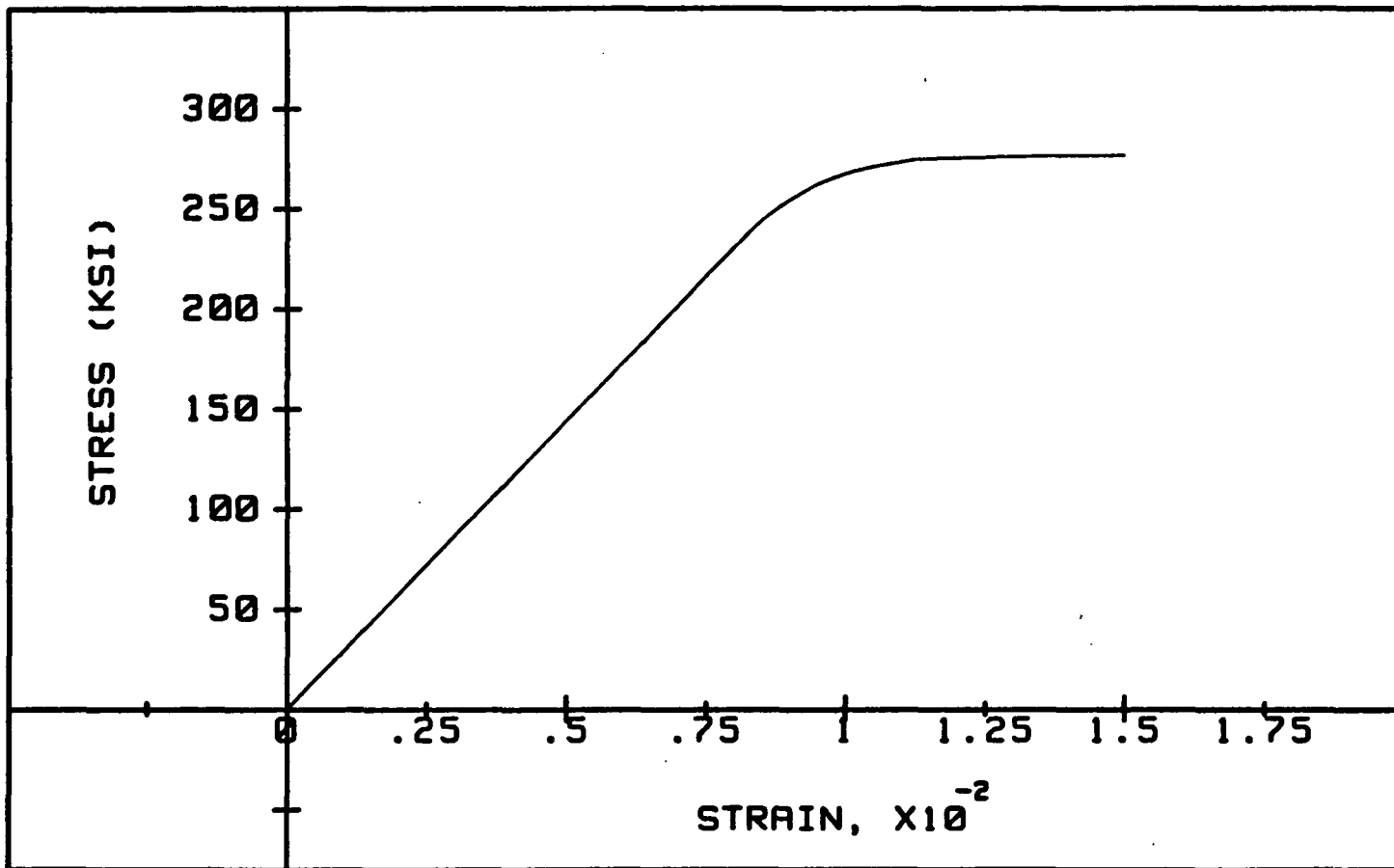


Fig. 2.10. Typical Plot of Stress vs. Strain for Prestressing Tendon

wires which were approximately on opposite faces of the strand. The strand was then subjected to tension over a length of 7 ft. The amount of load which was applied to the strand was measured by using a load cell which will be explained in detail in Chapter 3. The strain in the strand was obtained by the two electrical resistance strain gages which were explained earlier. The strand was tensioned three times up to a load of 30 kips. At 2 kips intervals both the values of load and strain were recorded by a data acquisition system. This data acquisition will also be explained in Chapter 3.

Using the above data, the load versus strain curve for each trial was obtained. The slope of each of these graphs was obtained and compared. It was found that these slopes were very close. The mean value for all of the slopes was calculated and was found to be 5150 ksi. This value was then divided by the area of the strand and the apparent E value was obtained. This apparent modulus of elasticity was used to calculate the stresses from measured strains in the strand. A typical plot of load vs. strain for obtaining the apparent E value is shown in Fig. 2.11.

The reinforcing bars used in this project consisted of No. 3 Grade 40, which were used for stirrups, longitudinal bars in the smaller cross sections and some of the longitudinal bars for the large cross sections. No. 4

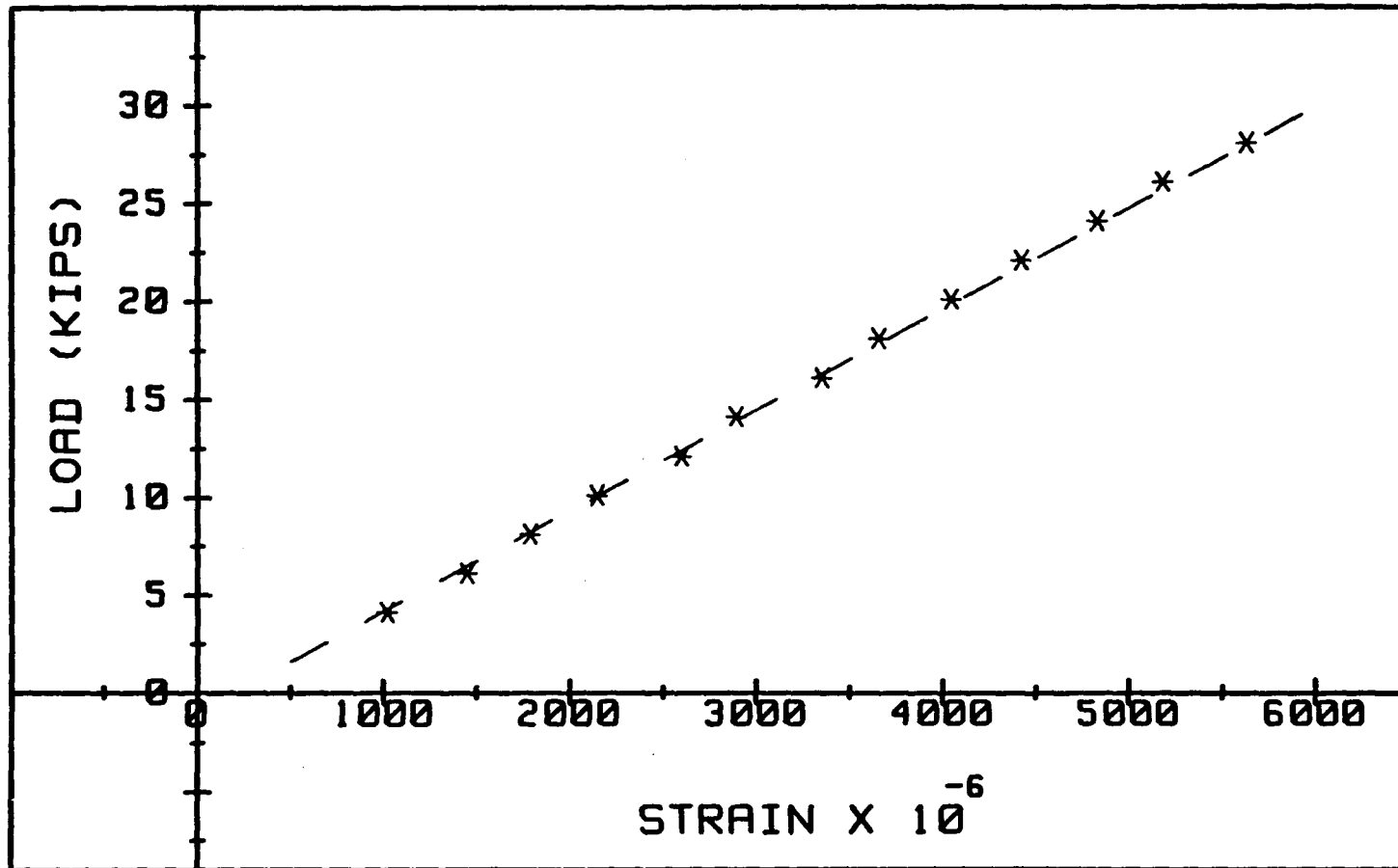


Fig. 2.11. Typical Plot of Load vs. Strain for Obtaining the Apparent E Value

Grade 40 steel was used for some of the longitudinal bars for the rest of the cross sections. Three pieces of 15-inch long samples of each size bar were randomly selected and were tested under a uniaxial tension test with an eight inch gage length. The average value of yield stress (f_y) was found to be 61.33 and 65.4 ksi for No. 3 and No. 4 bars respectively. A typical graph of stress versus strain for No. 3 bars is shown in Fig. 2.12.

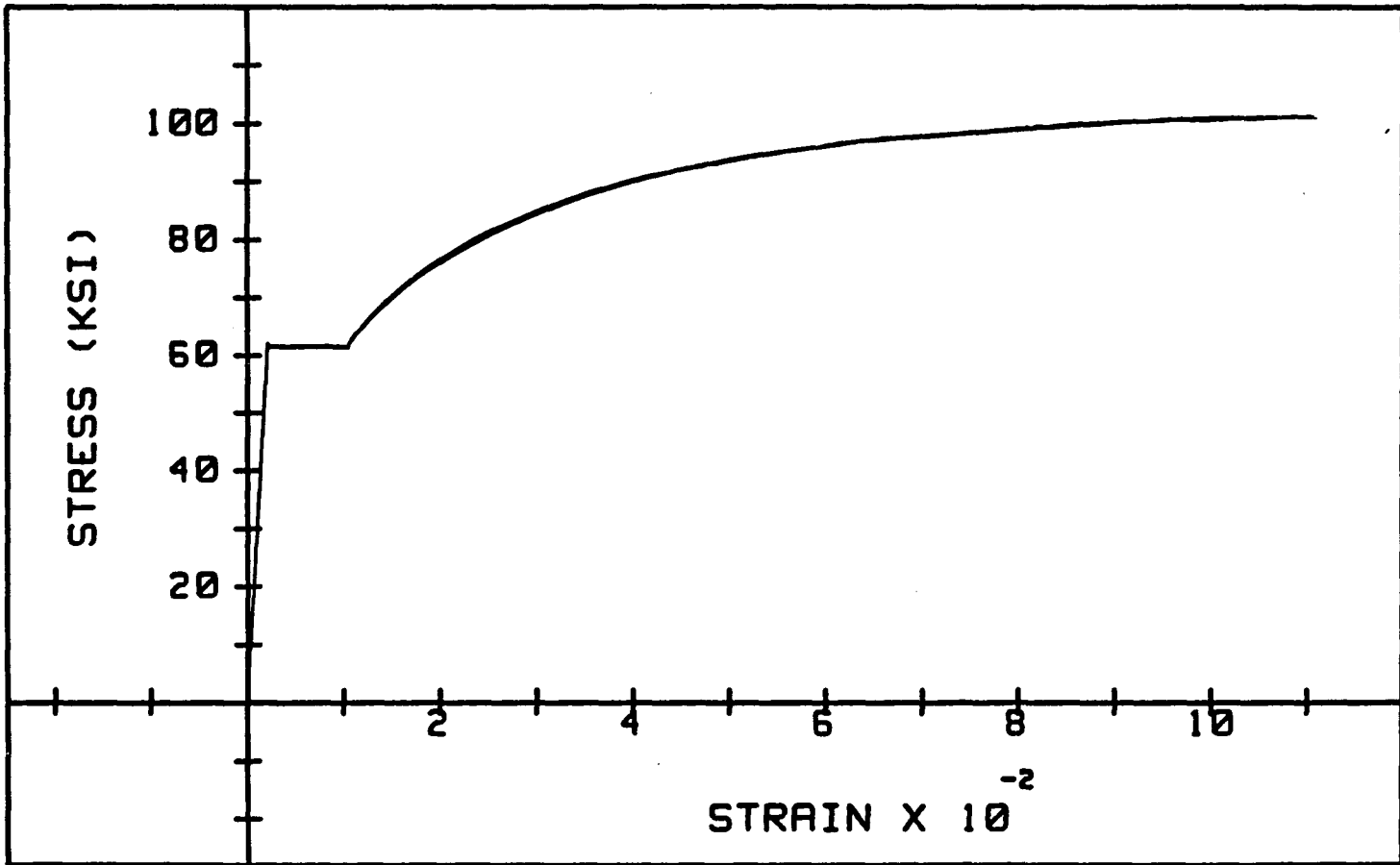


Fig. 2.12. Typical Plot of Stress vs. Strain for Nonprestressed Steel

CHAPTER 3

INSTRUMENTATION AND TEST SET-UP

3.1. Instrumentation

Four different types of measuring devices were used during the testing of specimens. These consisted of an MTS loading system which measured the amount of displacement and the load applied to the specimen, Micromasurement Inc. electrical resistance strain gages which measured the amount of strain in the strands, conventional load cells which measured the amount of load applied to the strand, and linear position spring return sensor models (LPSRSM) which measured the amount of deflection. The LPSRSMs were manufactured by Duncan Electronics, in Costa Mesa, California.

The amount of load which was applied to the specimen was controlled and measured by an MTS 436.11C control unit and an MTS 406.11 controller. The control unit was used to turn on the hydraulic power supply and select the required hydraulic pressure. The controller contained a feedback selector which enabled the user to select either the "load control" or the "displacement control" mode. It also contained a limit detector which limited the load or displacement to a certain predetermined

percentage of the full capacity. A photograph of the MTS control system is shown in Fig. 3.1.

The strain in the reinforcing steel was measured by using electrical resistance strain gages. All of the strain gages which were used throughout this experiment were type EA-06-240LZ-120 with a gage factor of 2.045 and 120 ohms electrical resistance. They were manufactured by Micromeritics Inc.

Before attaching the strain gages, the surface of the reinforcing bars and strands was smoothed by coarse and then fine sandpaper. A water-based acidic surface cleaner, "conditioner A," and a water-based alkaline surface cleaner, "neutralizer 5," were used to further prepare the surface. The strain gages and the terminals which were the type CTF-50D and manufactured by Micromeritics were placed on a cellophane tape with a clear distance of 1/8 in. between them. The tape was placed on the reinforcing steel bars and strands, making sure that the strain gages and terminals were at the prescribed locations. One end of the tape was then lifted up and Duro Contact Cement adhesive was applied to both strain gages and a conditioned surface. After ten minutes, the assemblage was placed on the surface of the bar and tightly wrapped with a rubber band for 24 hours. This was done for the purpose of maintaining the pressure required for the adhesive to cure.

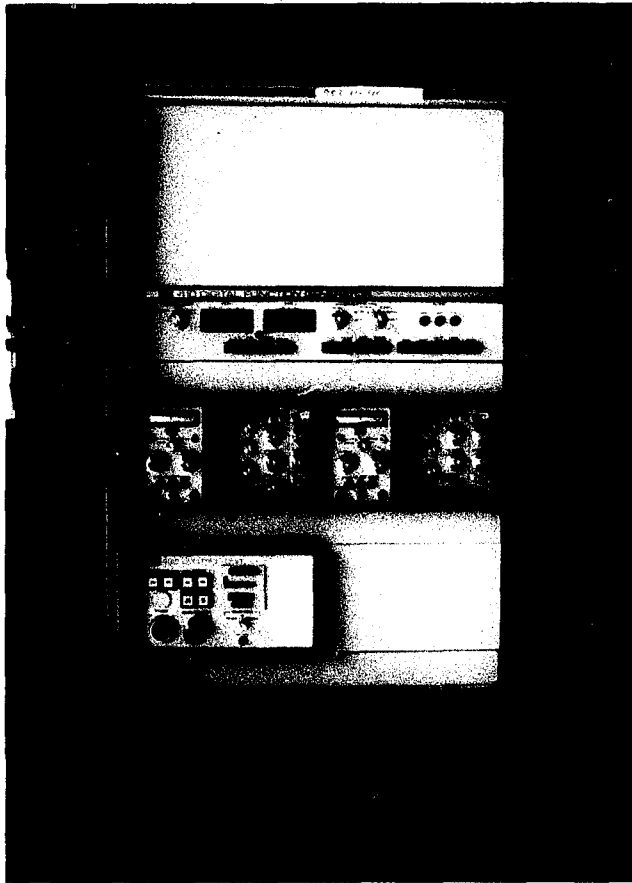


Fig. 3.1. MTS Control System

After removing the rubber band, small pieces of Teflon-coated electrical wires were used to connect the strain gages to the terminals by means of soldering. A 20 feet long three-conductor cable was then soldered to each terminal. These wires were later connected to a model 3054A data acquisition control unit system manufactured by Hewlett Packard. Photographs of strain gages attached to a stirrup and strand are shown in Figs. 3.2a and 3.2b, respectively.

In order to have a good measurement of the amount of force which was applied to the strand, a cylindrical aluminum load cell was built with a diameter of 1 1/2 inch and a height of 2 inches. The hollow core of the load cell allowed the passage of the strand through the load cell. The procedure given earlier was followed to attach four strain gages to the load cell. Two of the strain gages were attached vertically and the other two were attached horizontally. The locations of the strain gages were placed so that each strain gage was located in the mid-height of the cylinder and was 90° away from the adjacent strain gages as shown in Fig. 3.3. Since all of the strain gages which were connected to the data acquisition had 120 ohms electrical resistance, it was desirable to make the total electrical resistance of the load cell 120 ohms also. This condition was achieved by connecting two strain



Fig. 3.2a. Typical Strain Gages Attached to a Stirrup

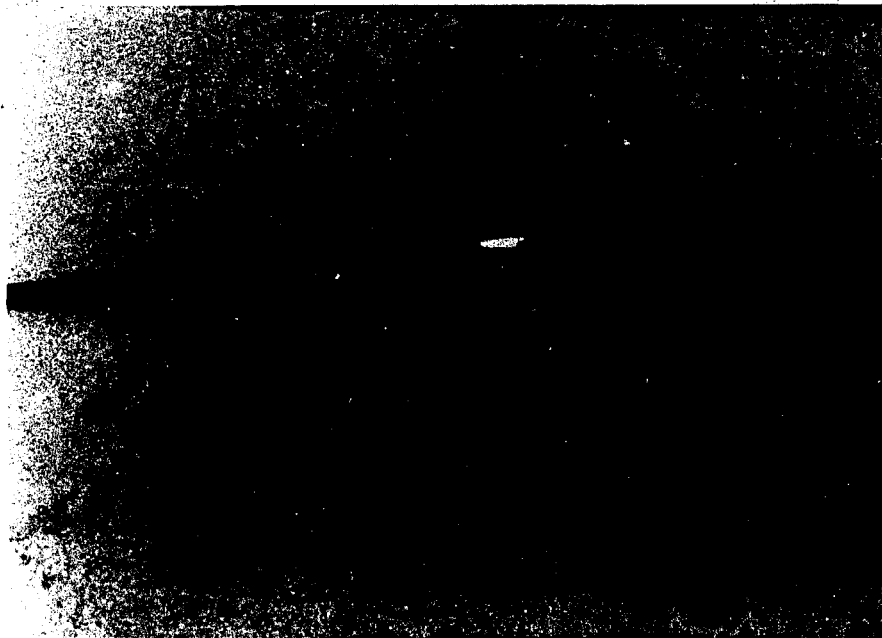


Fig. 3.2b. Typical Strain Gages Attached to a Strand

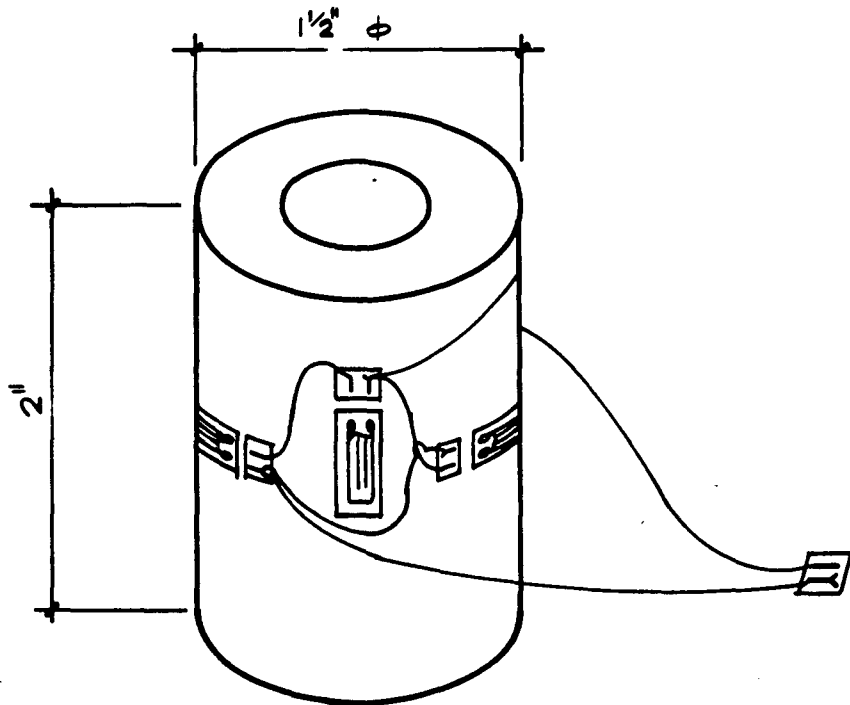


Fig. 3.3. The Load Cell Constructed for the Study

gages in parallel to each other and the other two in series, as shown in Fig. 3.4.

After the load cell was built, its calibration curve was obtained by subjecting it to compressive forces under the actuator. The amount of load applied by the actuator and the strains obtained from the strain gages were recorded at every five kips interval. This process was repeated three times for loads of up to 35 kips. The results for all of the trials were very close. At the end, the applied load was plotted versus strain and the calibration curve was obtained as shown in Fig. 3.5.

The deflections of the specimens were measured by eight linear position spring return sensor models (LPSRSM), manufactured by System Bouncan Electronic Company.

The calibration curve for each LPSRSM was obtained by displacing the spring and obtaining the change in the output of voltage for every $1/8$ of an inch increment. The change in voltage was then plotted versus the amount of displacement. This calibration curve was obtained for all of the LPSRSMs. Since all of the graphs were not identical and there were some slight differences among them, each of the LPSRSMs was numbered and its corresponding graph was identified. Deflection at each location was found by

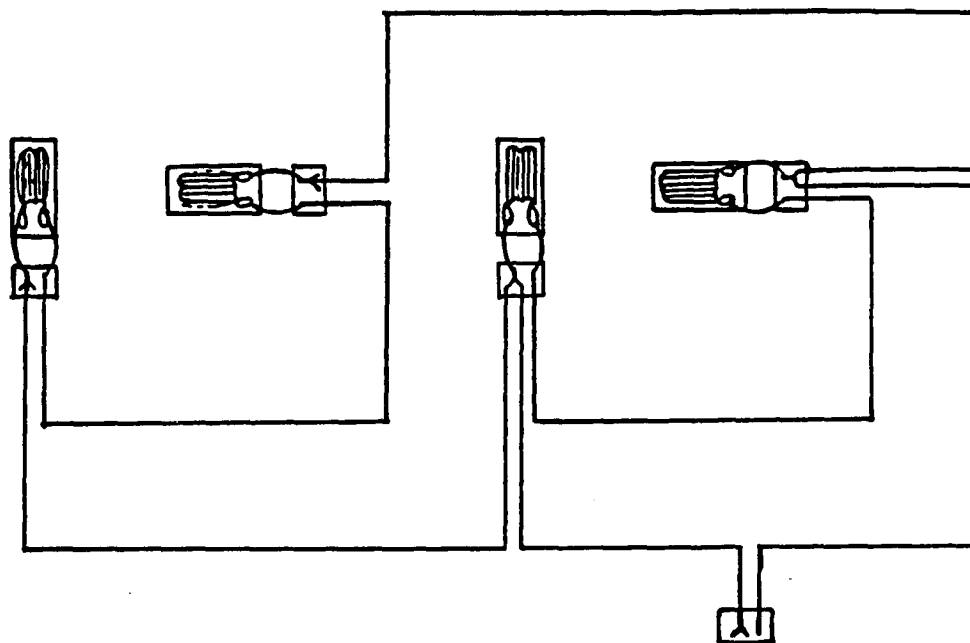


Fig. 3.4. Connections of Strain Gages for Building the Load Cells

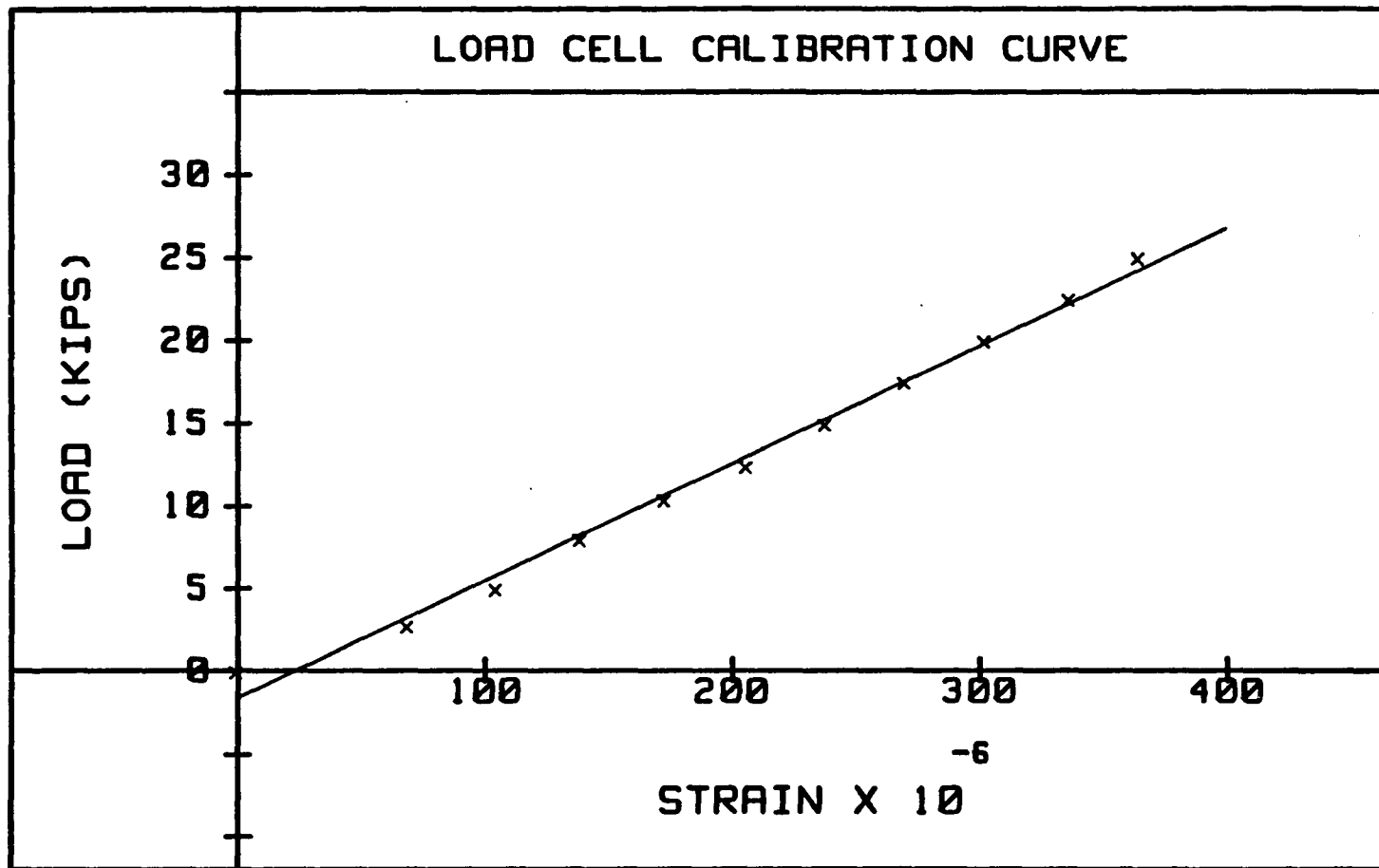


Fig. 3.5. Load Cell Calibration Curve

getting the change in voltage of that particular LPSRSM and finding the amount of deflection from the corresponding graph.

3.2. Test Set-Up

All beams were tested in a large steel frame shown in Fig. 3.6. The loads were applied through an MTS hydraulic actuator with a maximum capacity of 110 kips and a maximum stroke of 10 inches.

All specimens were 129 inches long and were supported on two 14-inch long, 1 inch diameter steel rods mounted between two grooved 1"x3"x14" steel plates as shown in Fig. 3.7. The center-to-center distance between the supports was 108 inches.

A 64-inch-long HP 10x53 steel beam stiffened with 18 1/2"x5"x10" steel plates was used as a spreader beam to transmit the load from the actuator to the specimen through two adjustable supports which were exactly the same as shown in Fig. 3.7.

3.3. Test Procedure

The specimen was placed in the frame. Linear position spring sensor models (LPSRSM) were placed at four different locations along the specimen. These locations were the centerline of the specimen, 6 inches from each side of the centerline and under one of the concentrated

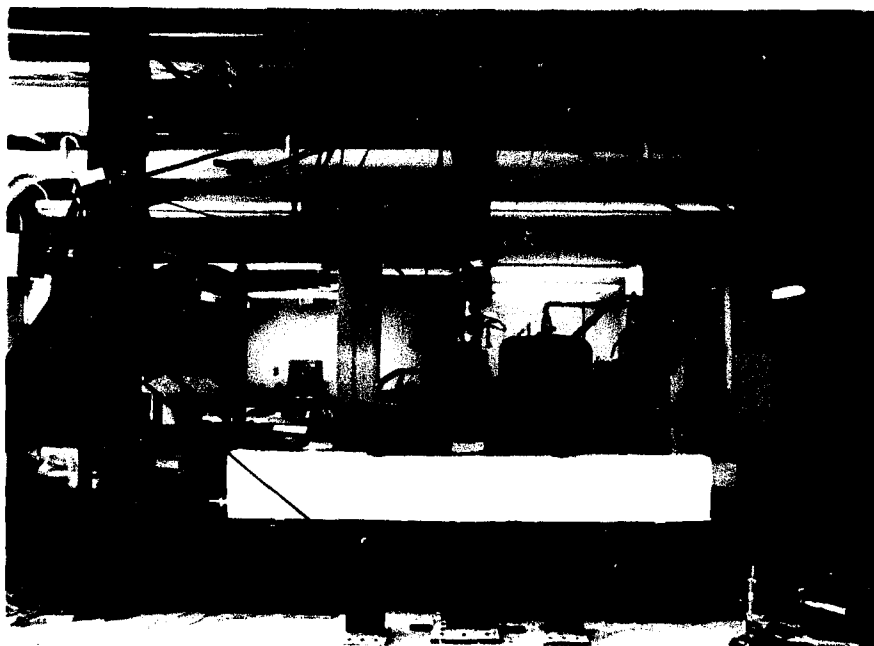


Fig. 3.6. Test Set-Up Inside the Frame

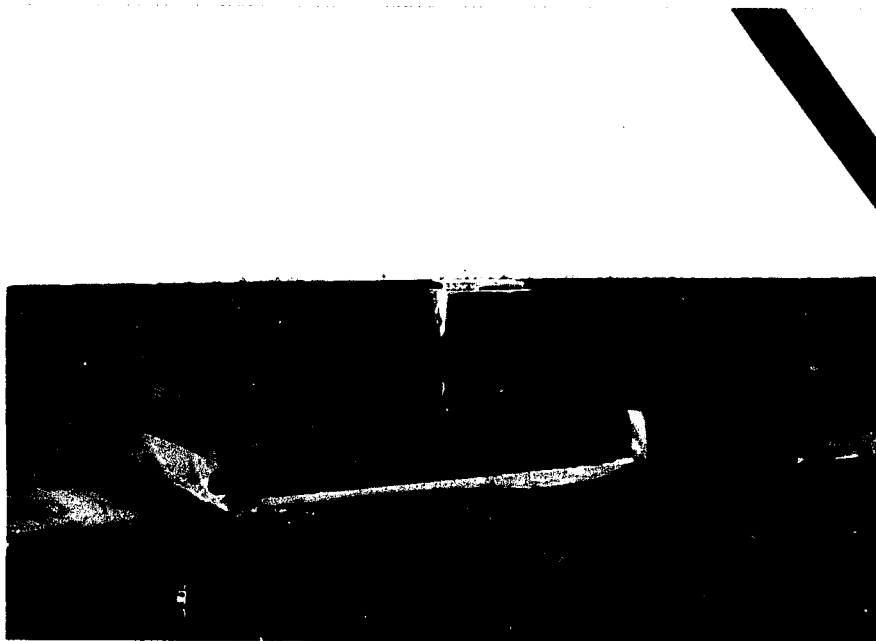


Fig. 3.7. A Typical Support for the Specimens

loads as shown in Fig. 3.8. For specimens 1 through 5, two LPSRSMs were placed at each location with 3/4 inch distance from the edge of the specimen and the average of the two was calculated and taken as the amount of deflection at that location. For the remaining specimens it was decided to use only one LPSRSM along the middle of the specimen at each location.

The strain gages were connected to the data acquisition system and the initial reading was recorded by an HP 9836 computer. Two load cells were then placed in the dead and live end of the beam. The dead end is defined as the anchored end of the strand while the live end refers to the end at which the jacking force is applied. Each load cell was tied and held in place by means of an anchor. Photographs of a typical anchor used as well as the dead and live end of specimen are shown in Figs. 3.9, 3.10a and 3.10b, respectively.

Each specimen was post-tensioned with a 50 ton capacity, 5 inches stroke, hollow core hydraulic jack which was driven by a hand pump. The amount of load applied to the tendon was measured by the dial gage of the hydraulic jack and more accurately by the strain gages. When the desired level of stress was reached, the pressure valve of the hydraulic jack was released and strain in the tendon was recorded and printed out by the computer. If there was

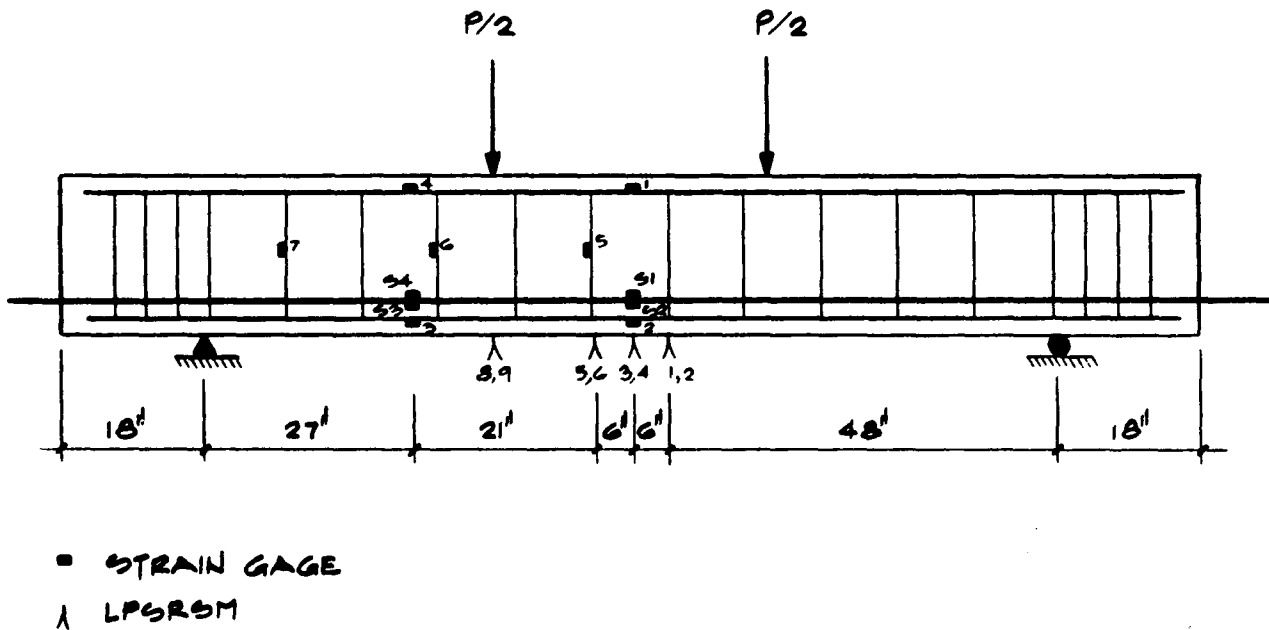


Fig. 3.8. Locations of LPSRSM's

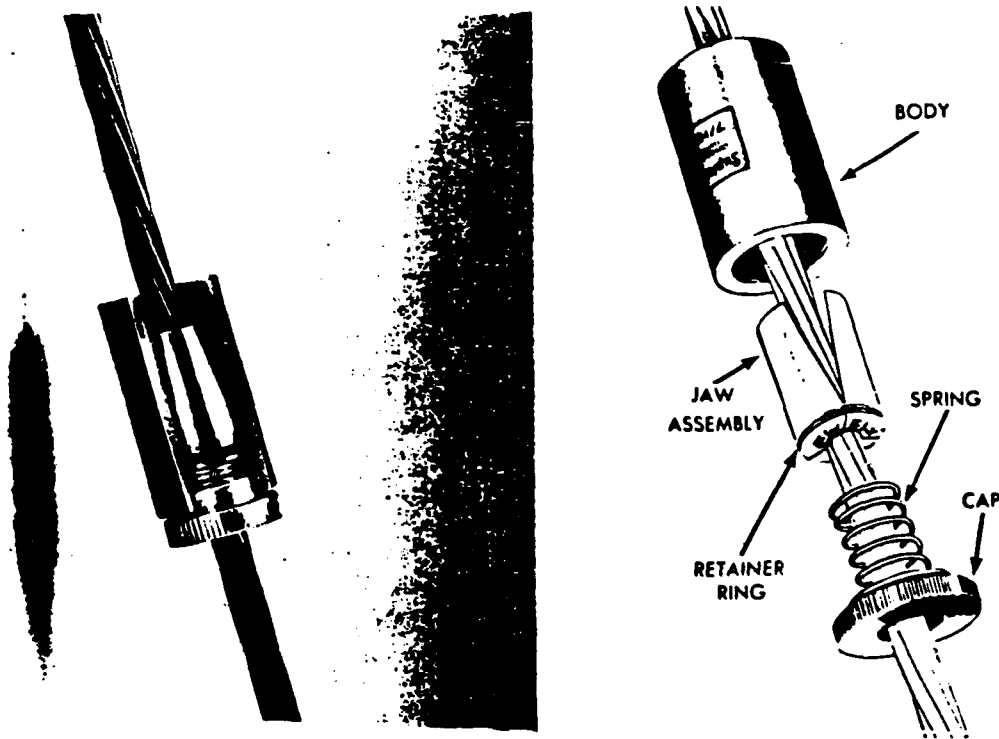


Fig. 3.9. Typical Chuck Anchor for a Single Tendon
(Courtesy Supreme Products Corporation)

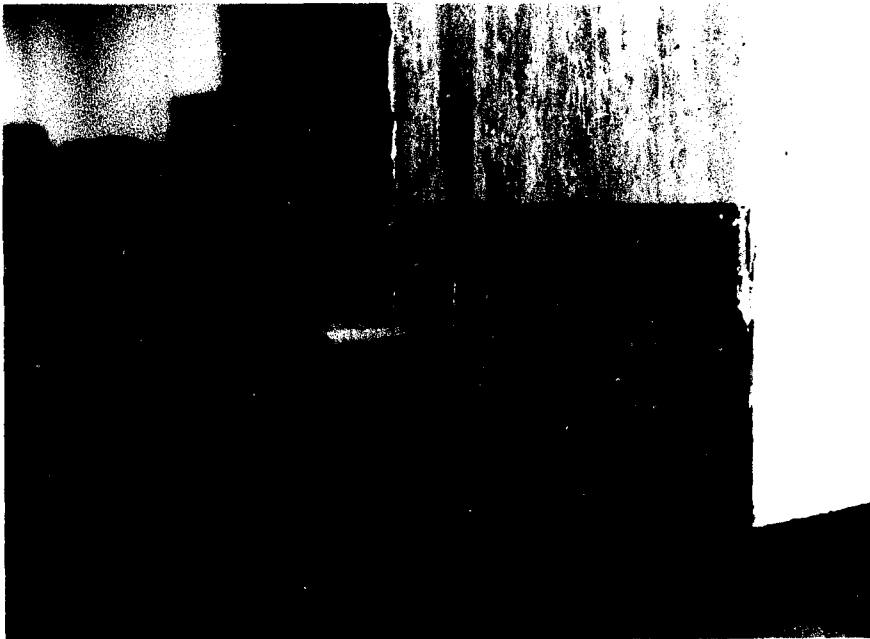


Fig. 3.10a. Assemblage of Dead End of the Specimens



Fig. 3.10b. Assemblage of Live End of the Specimen

a reduction in the stresses due to slippage of the anchor, the tendon was stressed again. This was done for a few times for each specimen until the desired level of stress was reached. The final value of stress was taken as the effective prestressing stress in the tendon for the specimen.

After the post-tensioning process was finished, the specimen was ready for the actual test. Before beginning the test, the specimen was loaded to a load of up to 3 kips and unloaded again. This was done for the purpose of stabilizing the specimen. The control unit for the actuator was set to the displacement control mode to prevent any accidental excessive deflection which could occur due to the change in the stiffness of the specimen.

The load was applied in 2 kips increments until the first flexural crack was observed, then 1 kip increment was applied until failure of the specimen occurred. At every load increment, the data from strain gages as well as the transducers and actuator were scanned by the data acquisition system, recorded on a floppy disk, and printed out by the HP printer. While this was being done, the cracks in the specimen were observed and marked and photographs were taken.

CHAPTER 4

BEHAVIOR OF SPECIMENS UNDER THE TEST

The behavior of all eight specimens tested for the purpose of this investigation are described in detail in this chapter. After a brief description of each specimen, the highlights of the test results for each specimen are pointed out. Plots of some of the strain gage readings and load versus deflection curve and photographs of specimen after the failure are also given for each specimen.

Actual dimensions and amount of reinforcement as well as the a/t ratio for all specimens are shown in Table 4.1. Locations of concentrated loads, strain gages and LPSRSM's for Specimen #1 are shown in Fig. 4.1. This specimen was loaded with a 2 kips load increment until a load of 19.9 kips was reached and the first flexural crack appeared. It was then loaded with 1 kip load increment until the end of the experiment. At a load of 42.6 kips, steel rebars at the bottom of the specimen started to yield, causing cracks to widen. A graph of load vs. strain for one of these rebars is shown in Fig. 4.2. At exactly the same load, the depth of the neutral axis was at the compression steel bars. The shift of the neutral axis from the bottom to the top of the compression steel can be

Table 4.1
Details of Specimens

Specimen Number	Size	A_{ps} sq. in.	A_s sq. in.	A'_s sq. in.	a in.	P_e (k)	f_{ps} (ksi)
1	12x18	0.1525	0.44	0.33	36	9.37	112.7
2	14x20	0.1525	0.62	0.51	36	15.13	159.6
3	14x20	0.1525	0.62	0.51	48	16.22	134.8
4	12x18	0.1525	0.44	0.33	28	10.36	72.13
5	14x20	0.1525	0.62	0.51	42	27.40	223.2
6	12x18	0.1525	0.44	0.51	36	15.00	160.4
7	12x18	0.1525	0.44	0.33	30	17.00	189.4
8	14x20	0.1525	0.62	0.51	36	21.41	171.5

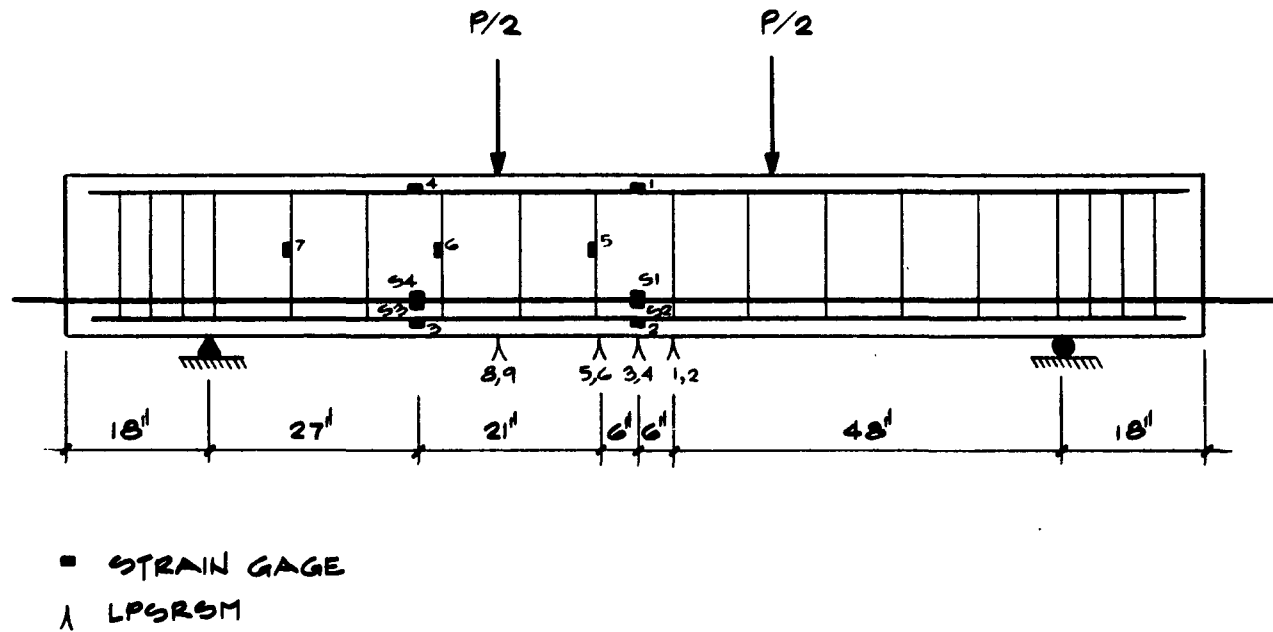


Fig. 4.1. Location of Strain Gages and LPSRSM's for Specimens 1, 2, 3, and 5

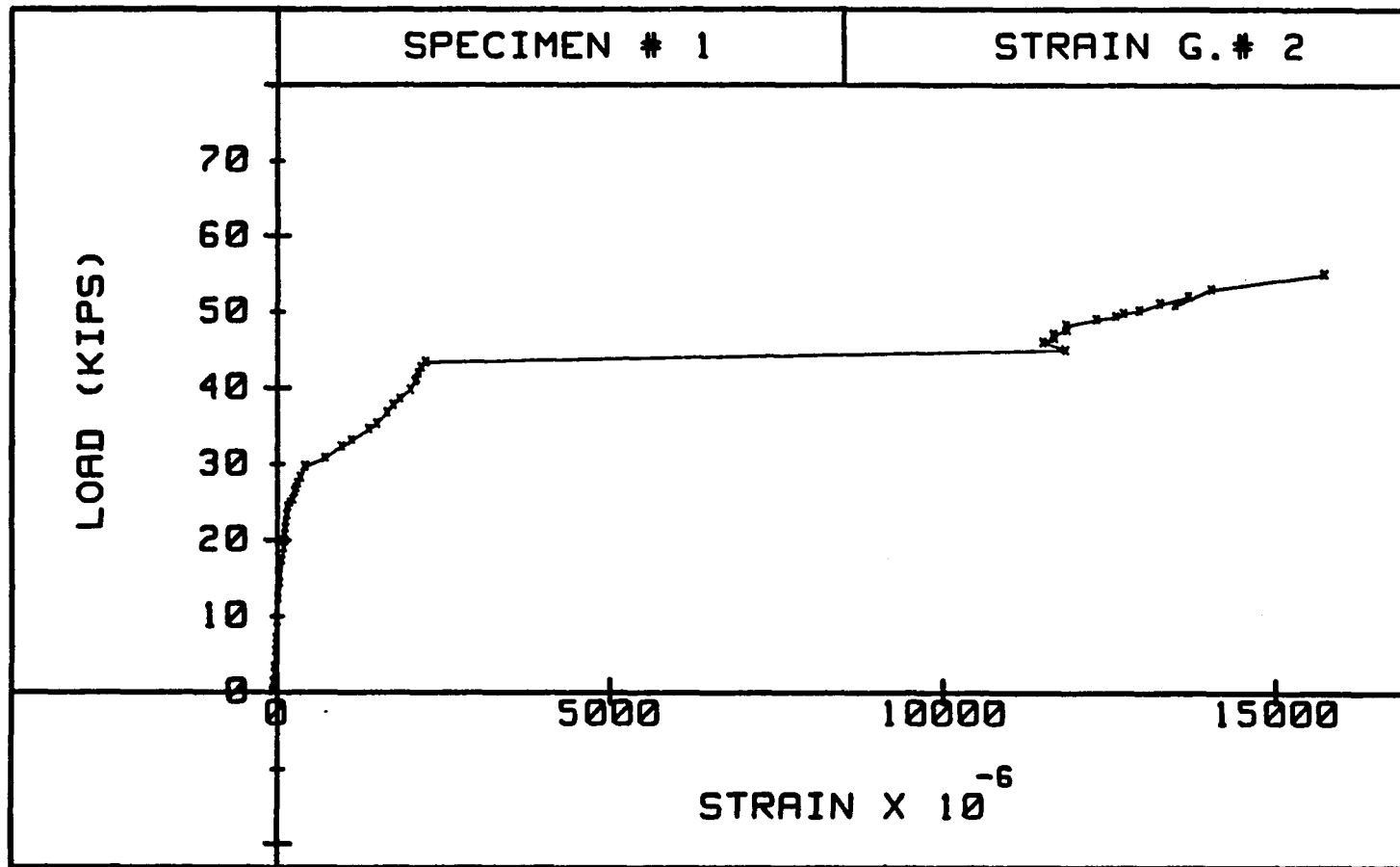


Fig. 4.2. Applied Load vs. Strain in the Longitudinal Reinforcement in the Bottom of Specimen 1

observed from Fig. 4.3. At a load of 47.6 kips, crack "A," which was under the right hand side concentrated load, was measured to be 4.5 mm wide. The specimen was loaded until a load of 55 kips was reached. At this point, due to some experimental problems, the test was stopped. The specimen did not fail completely. However, the depth of the neutral axis (propagation of crack) was very close to the top of the specimen (about 1 inch). This value of the load was taken as the ultimate load capacity of the specimen.

Only one of the four strain gages which were attached to the strand was working. The value of strain obtained from this strain gage was multiplied by the apparent E-value to obtain the ultimate stress in the strand which was found to be 112.7 ksi. This is 39 percent of the ultimate stress and 42 percent of the yielding stress of the strand. The maximum amount of deflection at midspan of this specimen was found to be 0.86 inches as shown in Fig. 4.4. A photograph of the specimen at ultimate load is shown in Fig. 4.5.

Actual details of Specimen #2 are listed in Table 4.1. The difference between this specimen and Specimen #1 was in the size and amount of effective prestressing force p_e . Locations of strain gages and LPSRSM's for this specimen are shown in Fig. 4.1. The first flexural crack for this specimen occurred at a load of 30.07 kips. At a

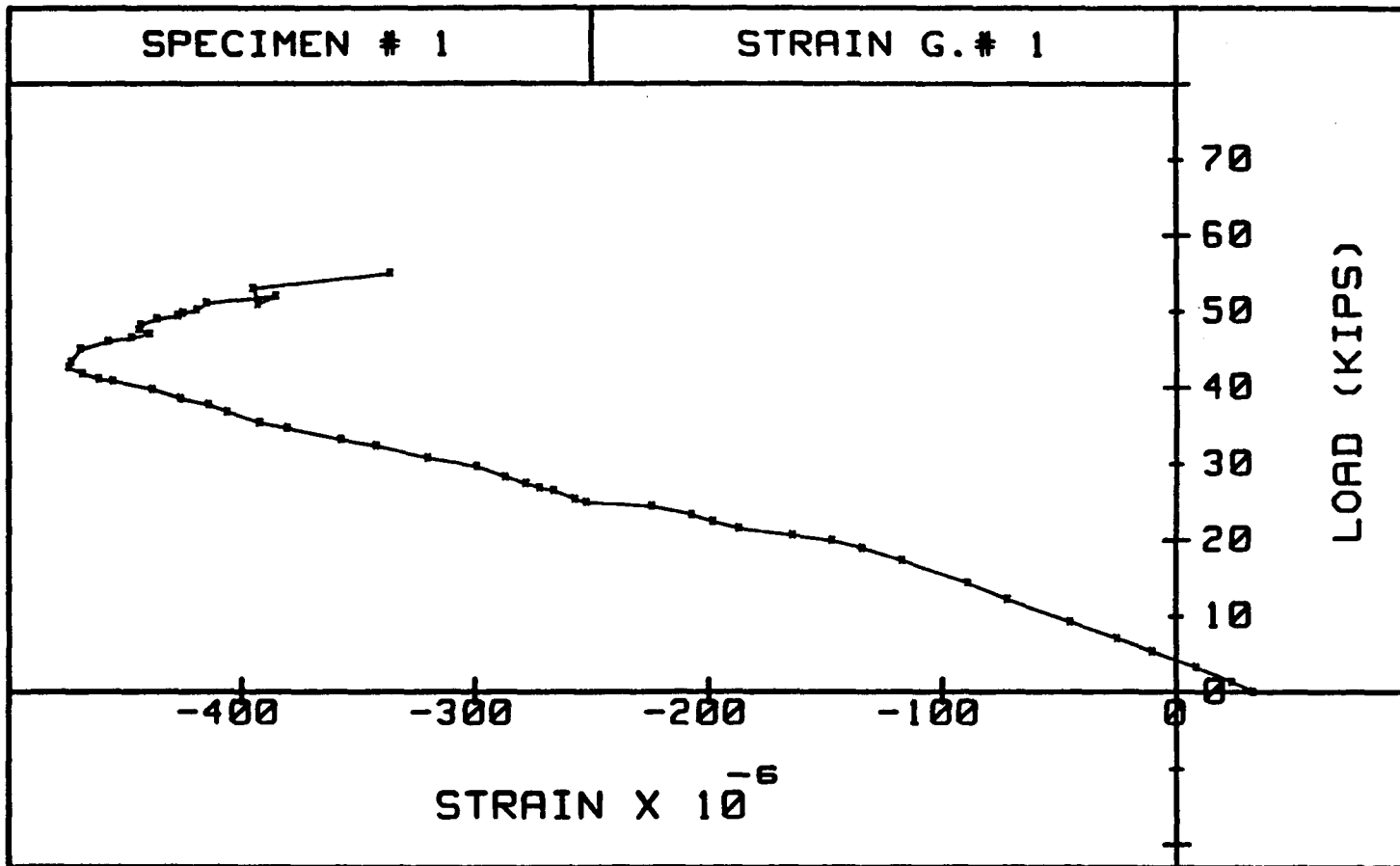


Fig. 4.3. Applied Load vs. Strain in the Compression Reinforcement for Specimen 1

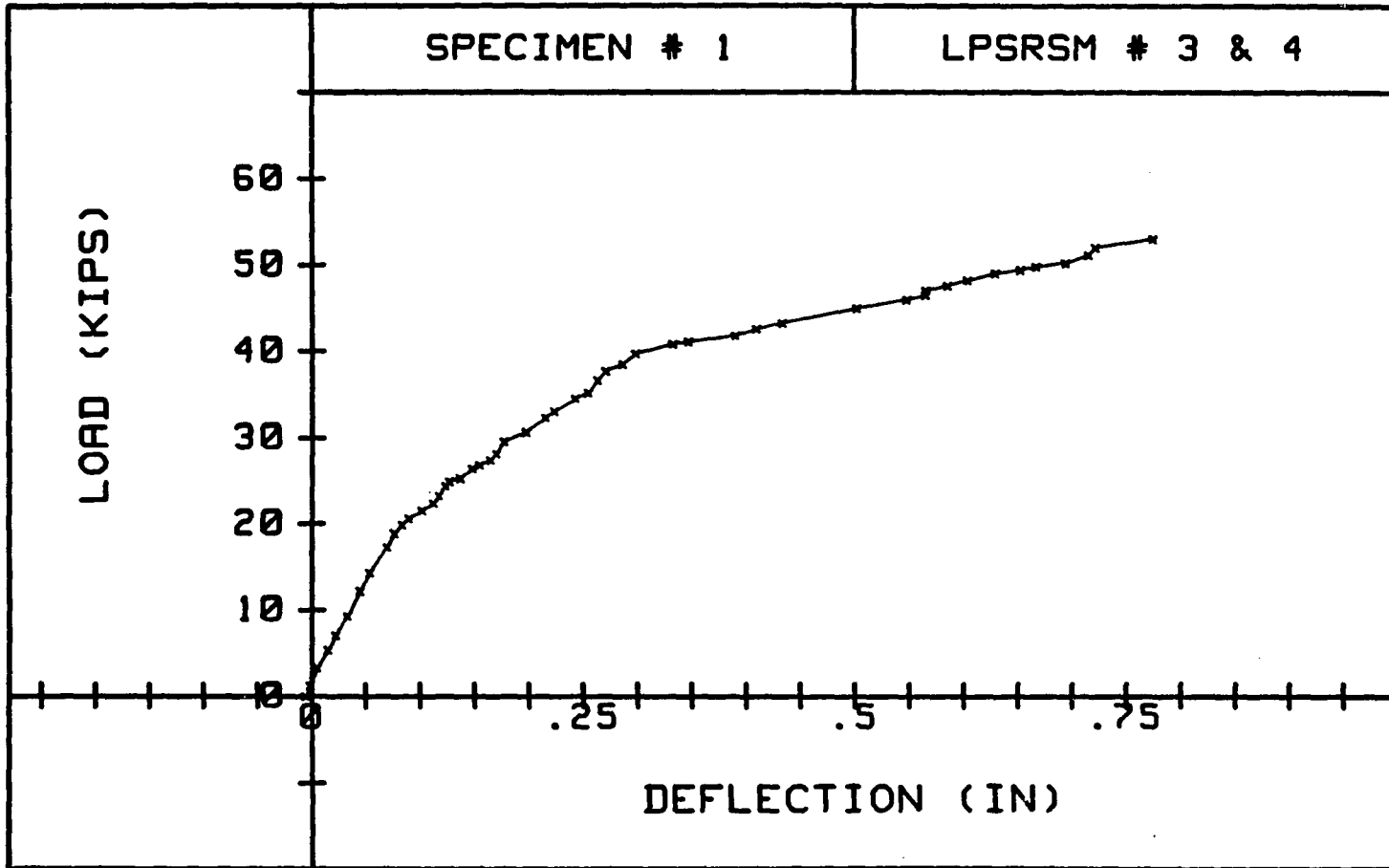


Fig. 4.4. Applied Load vs. Deflection for Specimen 1

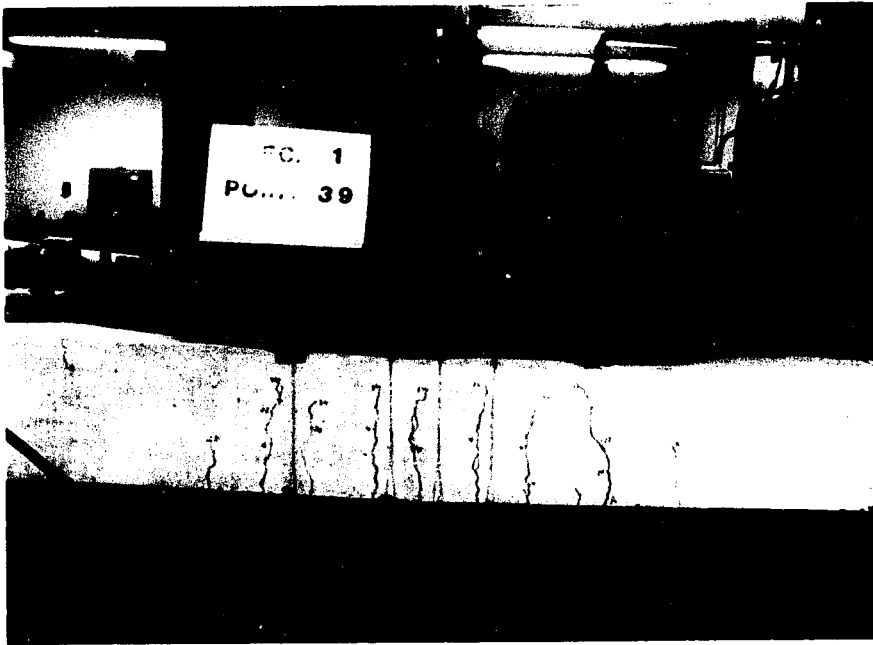


Fig. 4.5. Specimen 1 During the Test

load of 52.74 kips, cracks started to widen. This was the result of yielding longitudinal steel bars in the bottom of specimen. At a load of 54.06 kips, a flexural shear crack began to develop. At a load of 67.12 kips, the width of crack "A," which was located at the midspan of the beam, was measured to be 4 mm. The specimen was loaded until a load of 74.72 kips was reached and failed in flexure. The ultimate value of stress in the strand was obtained by averaging the amount of strain of three strain gages attached to the strand and multiplying it by the apparent E-value. The ultimate value of stress in strand, f_{ps} , for this specimen was found to be 159.6 kips which is 55 percent of ultimate stress, f_{pu} , and 60 percent of the yield stress of the strand. The maximum amount of deflection at the midspan for this specimen was found to be 0.575 in. as shown in Fig. 4.6. Photographs of this specimen at failure are shown in Fig. 4.7.

Specimen #3 had the same dimensions and reinforcement steel as Specimen #2. The major difference between the two specimens was the value of shear span, a , as shown in Table 4.1. Fig. 4.1 shows the locations of concentrated loads, strain gages and LPSRSM's for this specimen. The specimen was loaded with a 3-kip load increment until the first flexural crack occurred at a load of 23.31 kips. It was then loaded with a 2-kip load increment. At a load of

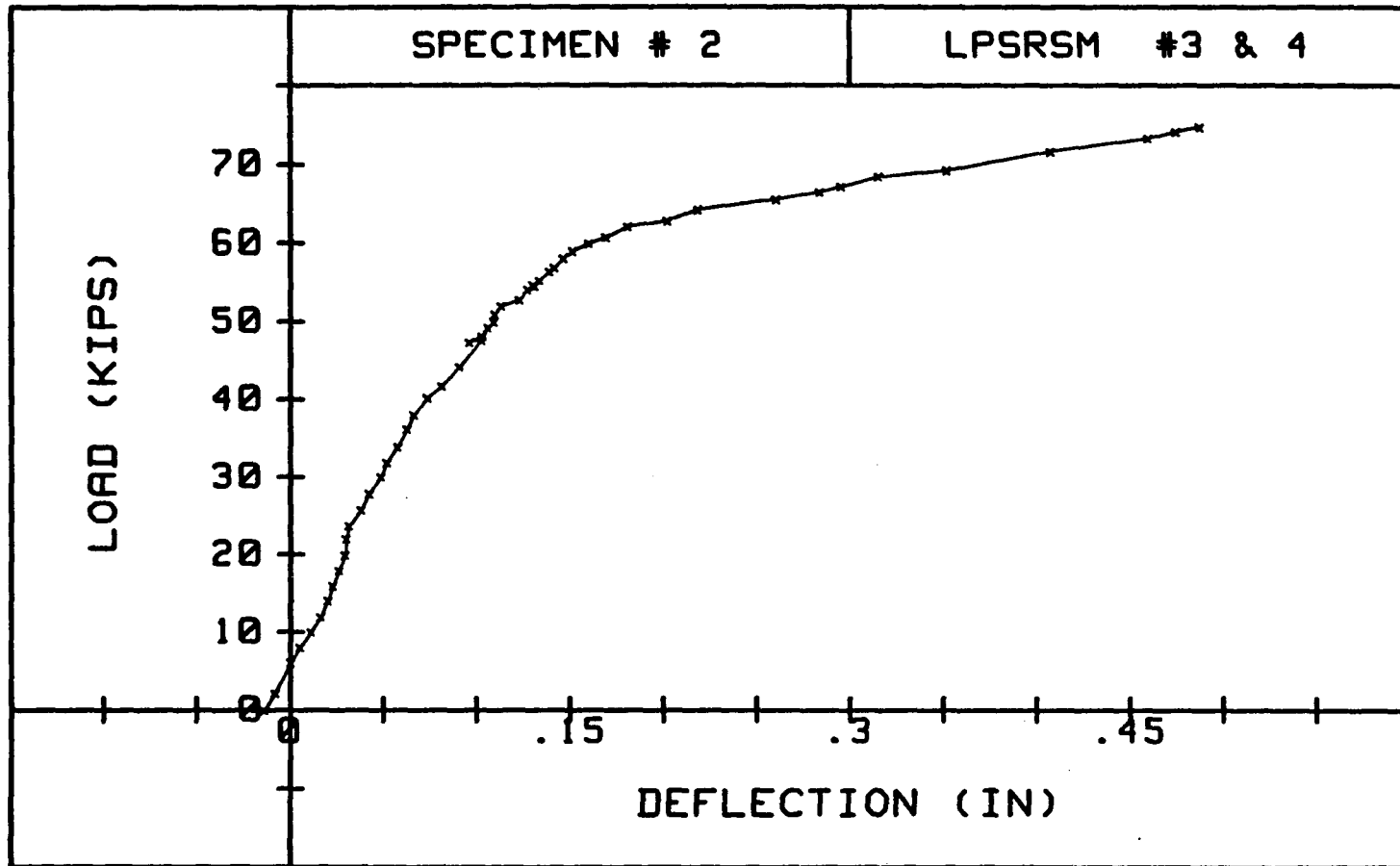


Fig. 4.6. Applied Load vs. Deflection for Specimen 2

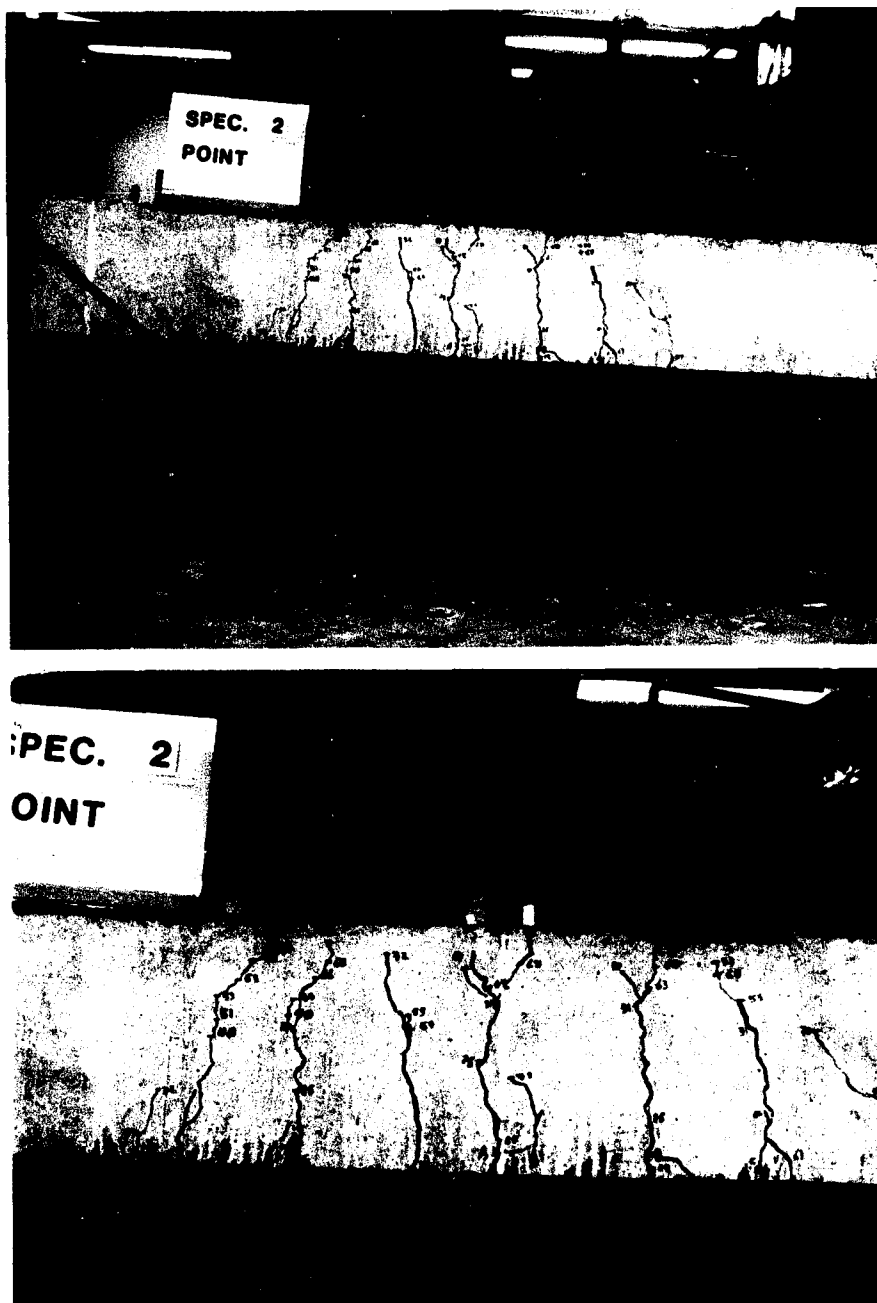


Fig. 4.7. Specimen 2 at the Conclusion of the Test

33.62 kips a flexural shear crack began to form. At a load of 46.12 kips the depth of the neutral axis reached to the compression steel as shown in Fig. 4.8 which gives the load vs. strain for one of the compression steel bars. Crack "A" which was located at the midspan of the beam was measured to be 2 mm wide at a load of 47.15 kips and 4 mm at a load of 49.65 kips. The specimen was loaded until a load of 51.8 kips was reached and failed in flexure. The value of stress in the strand at failure was found by averaging the values of strain obtained from the four strain gages attached to the strand and multiplying them by apparent E-value. This value was found to be 134.8 ksi. Maximum deflection in the midspan of the specimen was found to be 0.40 inches as shown in Fig. 4.9. A photograph of the specimen near the failure is shown in Fig. 4.10.

Specimen #4 had the same dimension and reinforcement steel as Specimen #1. This specimen had a shear span of 28 inches and was post-tensioned with an effective prestressing force of 10.36 kips. Locations of strain gages and LPSRSM's for this specimen are shown in Fig. 4.11. The specimen was loaded with 3 kips load increment until the first flexural crack appeared at a load of 27.21 kips. Due to some experimental problem the test was stopped at a load of 40.36 kips. The specimen was unloaded and reloaded again until a load of 55.45 kips was reached and the test

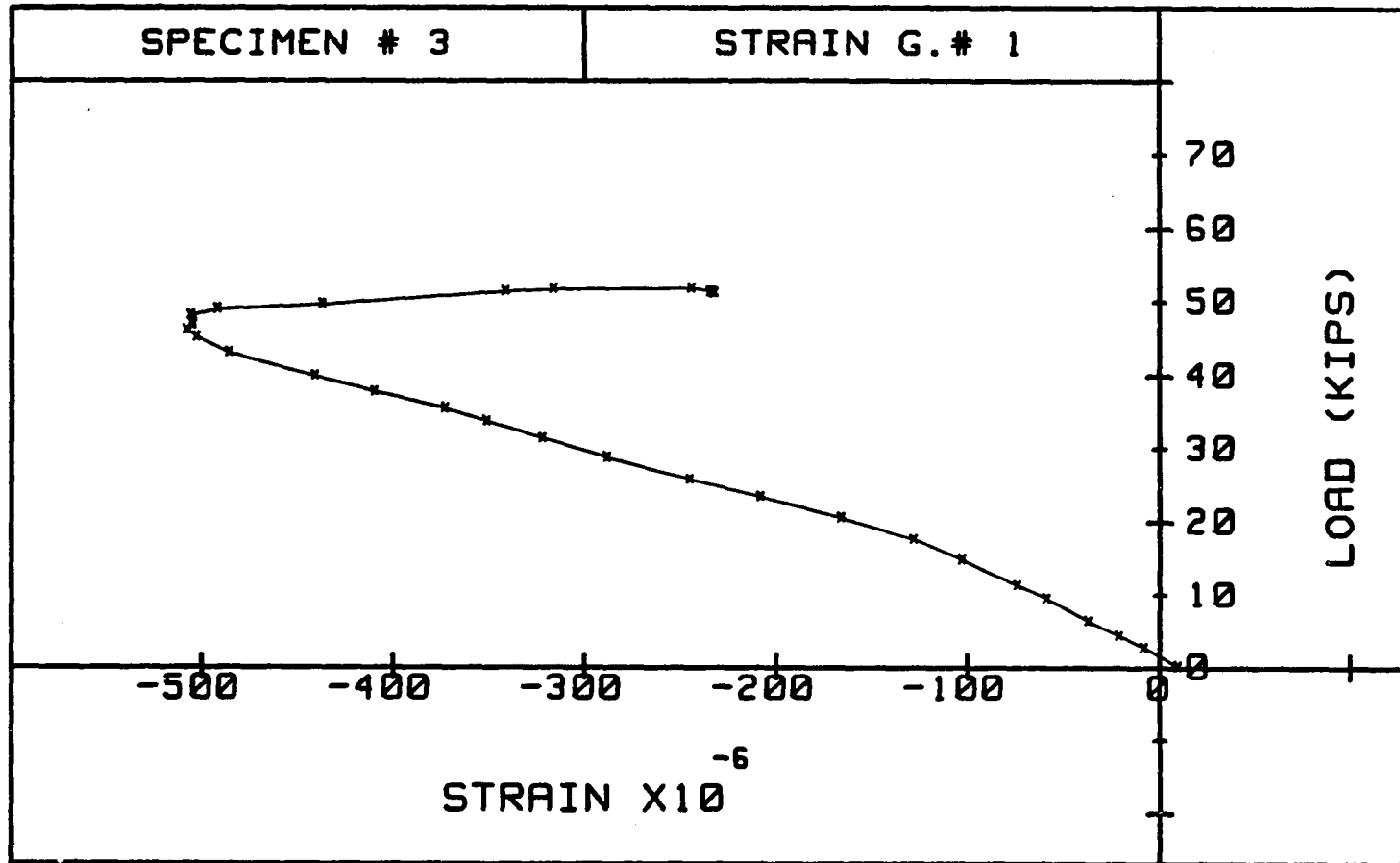


Fig. 4.8. Applied Load vs. Strain in the Compression Reinforcement for Specimen 3

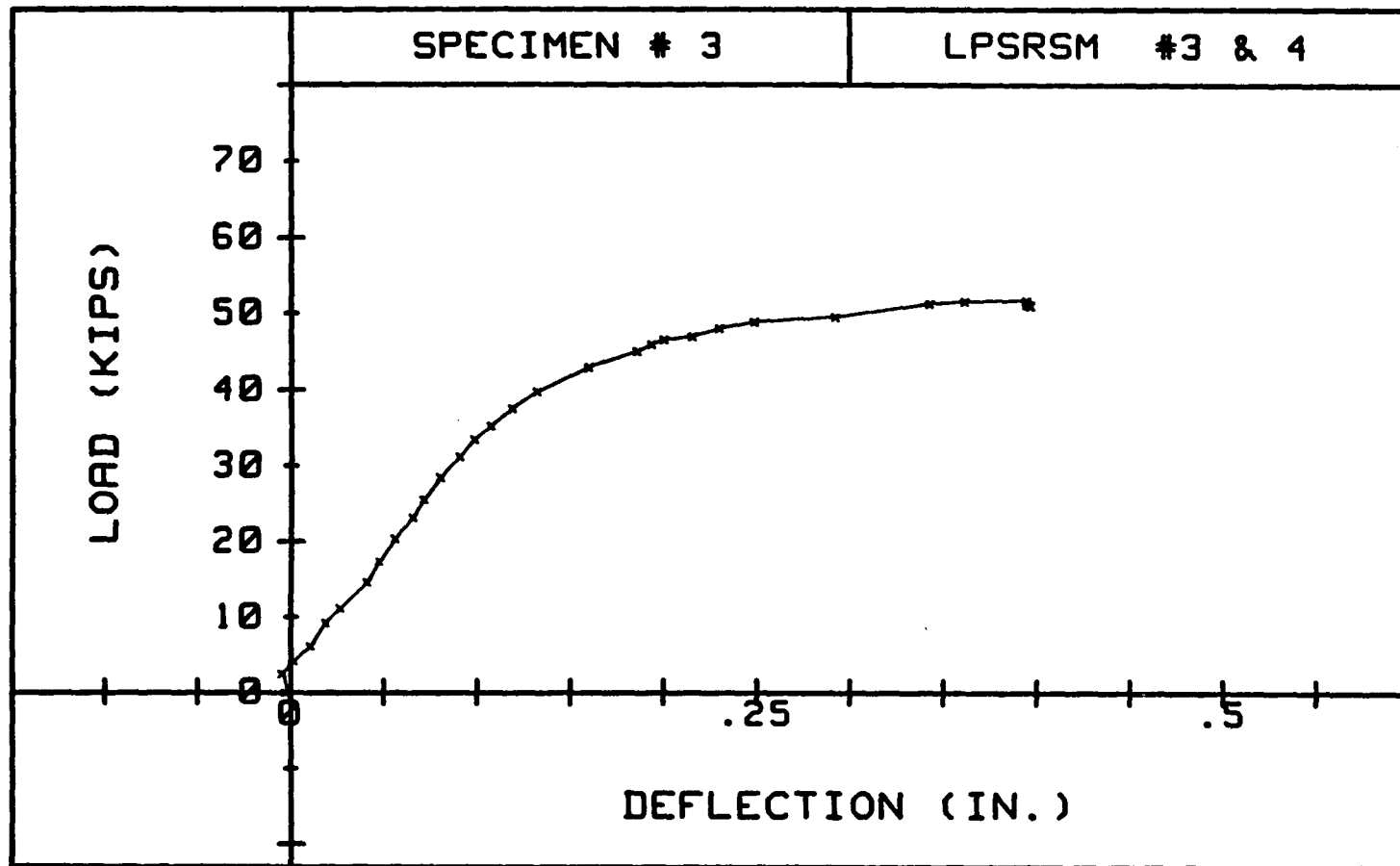


Fig. 4.9. Applied Load vs. Deflection for Specimen 3

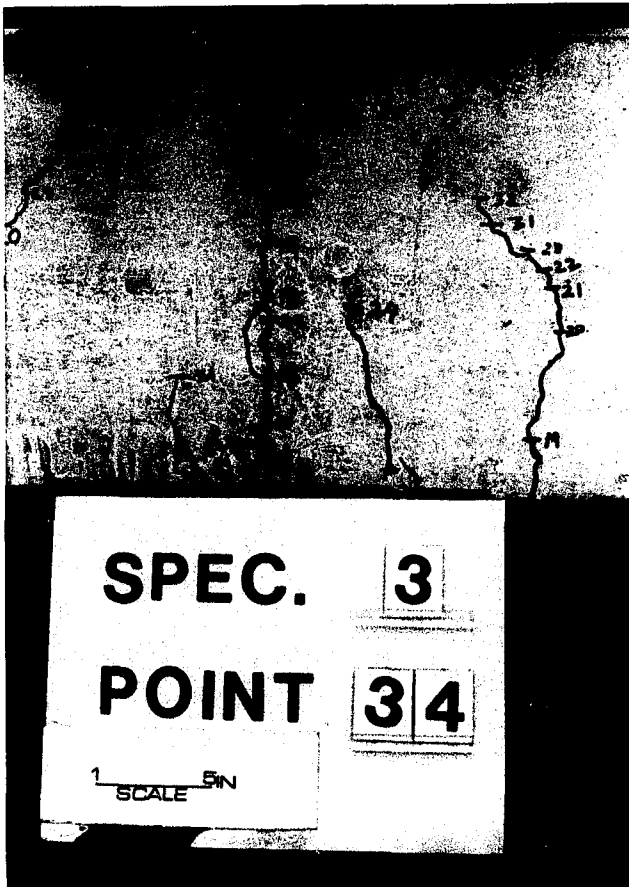


Fig. 4.10. Specimen 3 Near the Failure

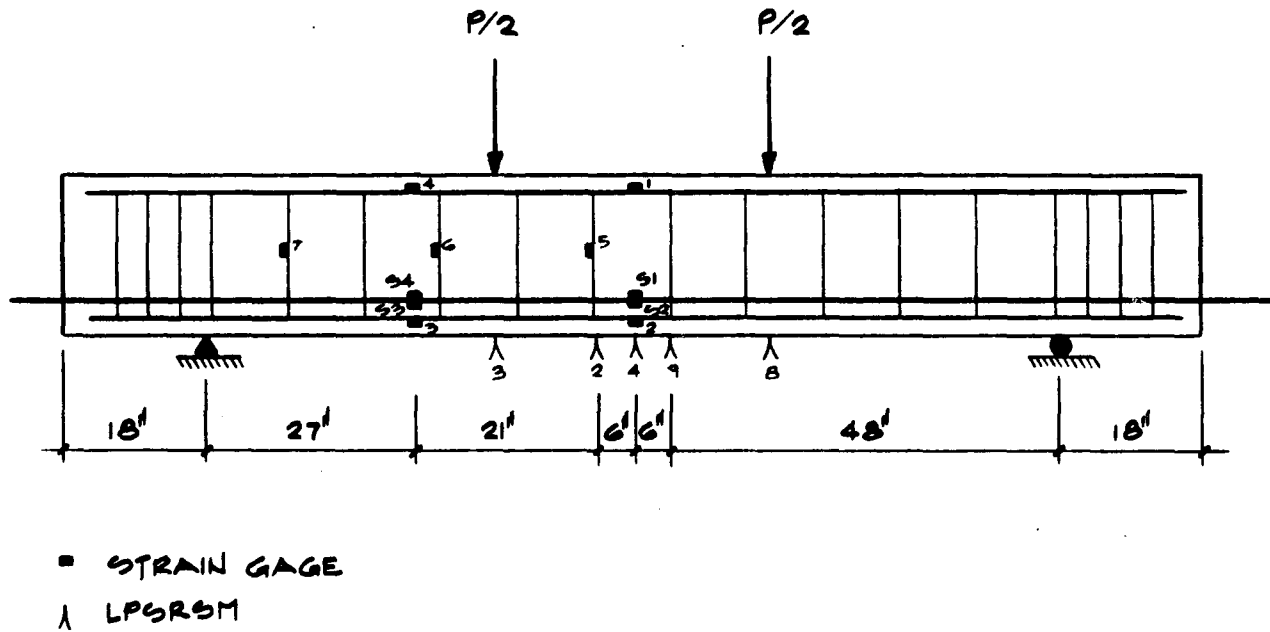


Fig. 4.11. Location of Strain Gages and LPSRSM's for Specimens 4, 6, 7, and 8

had to be stopped again. A photograph of specimen during the first loading and a plot of load vs. deflection at midspan of specimen for the second loading are shown in Figs. 4.12 and 4.13 respectively.

Actual dimensions, the amount of reinforcement, and a/d ratio for Specimen #5 are shown in Table 4.1. The locations of strain gages and LPSRSM's for this specimen are shown in Fig. 4.1. The first flexural crack occurred at a load of 35.95 kips. At a load of 54.73 kips, the longitudinal steel bars in the bottom of the specimen started to yield. At a load of 63.03 kips, cracks started to widen and flexural cracks under the concentrated loads started to move diagonally and form a flexural shear crack. The specimen was loaded until an ultimate load of 68.5 kips was reached and failed in flexure. The value of stress in the strand at ultimate load f_{ps} for this specimen was found to be 223.2 ksi. This is 77 percent of ultimate and 84 percent of yield stress of the strand. Maximum deflection at midspan of specimen was found to be 0.76 inch. A plot of load vs. deflection and a photograph of specimen at failure are shown in Figs. 4.14 and 4.15 respectively.

Actual dimensions and the amount of reinforcement, as well as a/d ratio for Specimen #6 are shown in Table 4.1. The location of concentrated loads, strain gages, and

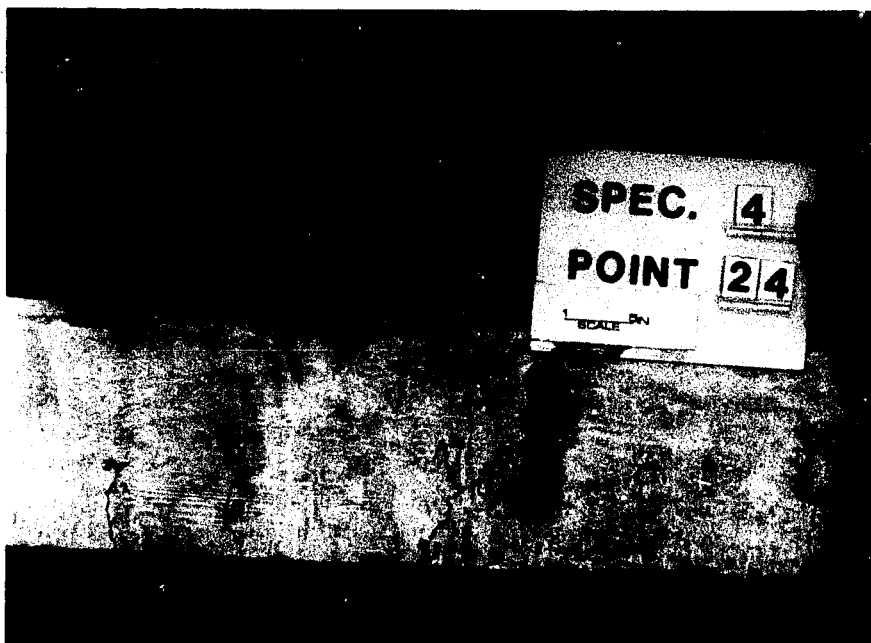


Fig. 4.12. Specimen 4 During the Test

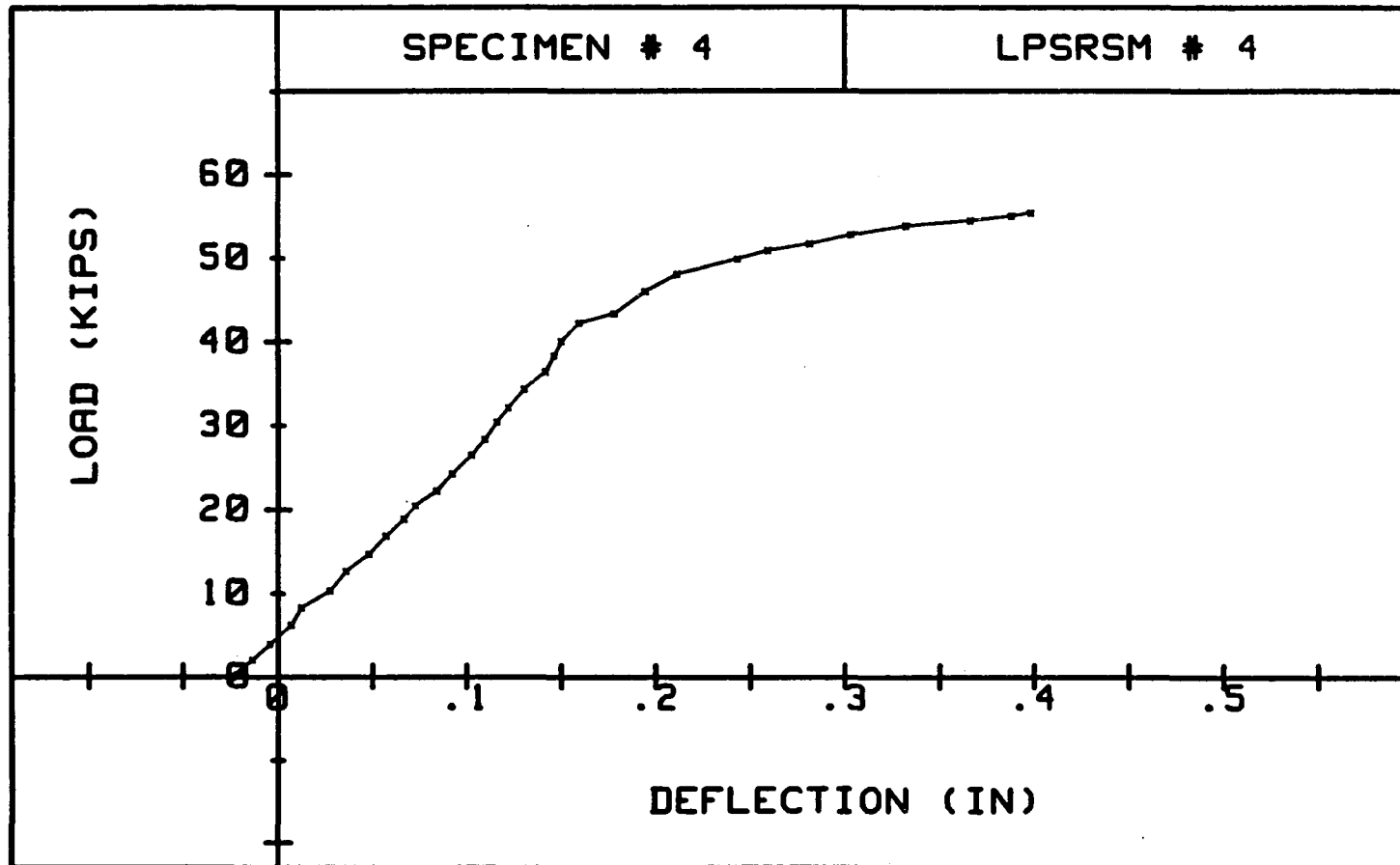


Fig. 4.13. Applied Load vs. Deflection for Specimen 4

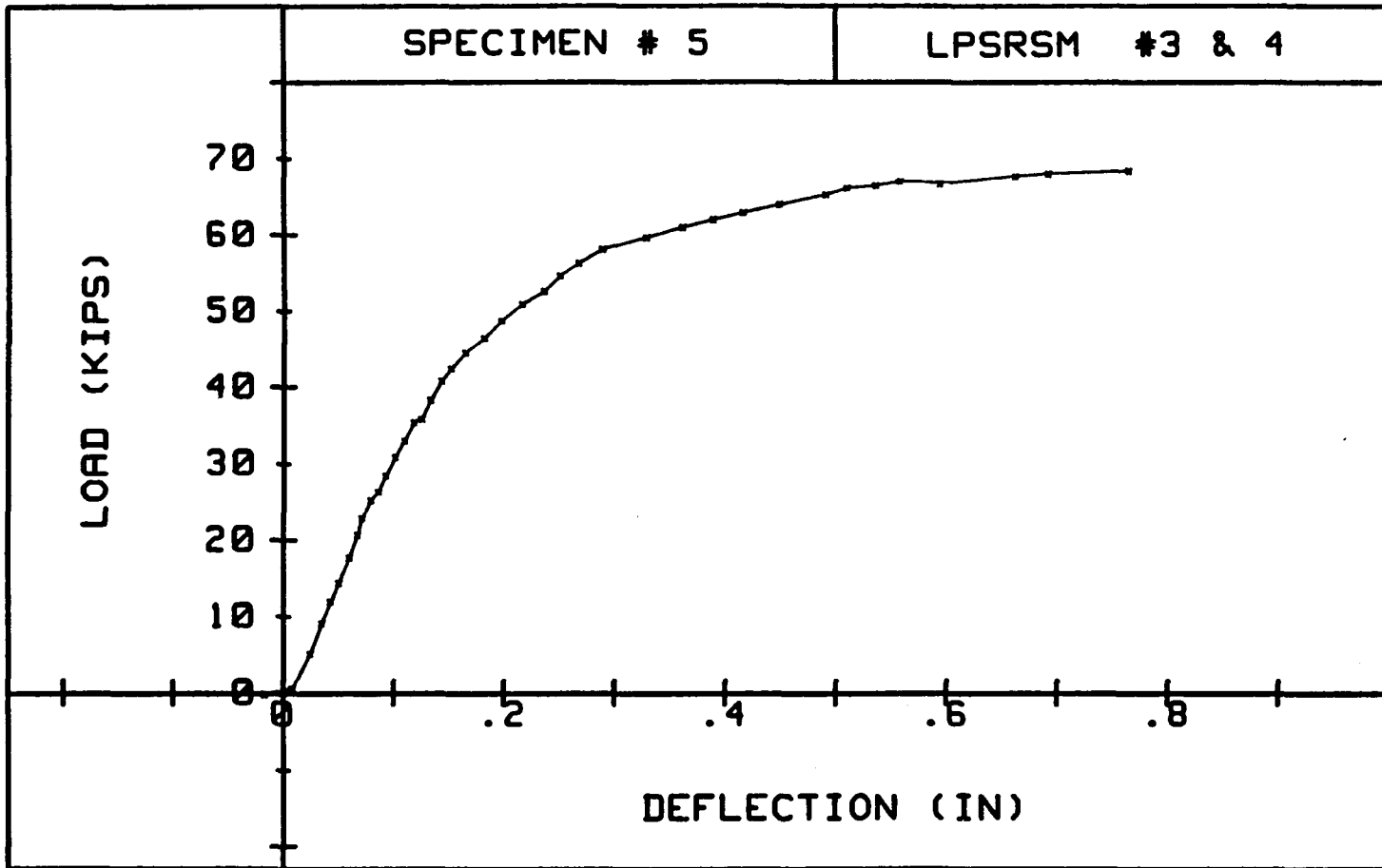


Fig. 4.14. Applied Load vs. Deflection for Specimen 5



Fig. 4.15. Specimen 5 at the Conclusion of the Test

LPSRSM's are shown in Fig. 4.10. This specimen was loaded with a 2 kips load increment until a load of 26.92 kips was reached and the first flexural crack appeared. At a load of 42.66 kips, a flexural-shear crack development was observed. At a load of 45.45 kips, the longitudinal steel bars in the bottom of the specimen started to yield, causing the cracks to widen. At a load of 61.55 kips, crack "B," which was located between the centerline of the beam and one of the concentrated loads was measured to be about 5 mm wide. This specimen was loaded up to a load of 63.63 kips and failed in flexure. The value of stress in the strand was found to be 160.41 ksi which was 56 percent of the ultimate and 60 percent of the yield stress of strand. Maximum deflection at the midspan of the specimen was found to be 1.24 inches as shown in Fig. 4.16. A photograph of the specimen at failure is shown in Fig. 4.17.

Actual details of Specimen #7 are shown in Table 4.1. Locations of the strain gages and LPSRSM's for this specimen are shown in Fig. 4.10. The first flexural crack for this specimen appeared at a load of 32.23 kips. At a load of 56.89 kips flexural cracks started to widen and small hair crack branches started to appear. The longitudinal steel bars in the tension zone were yielded at a load of 71.87 kips causing cracks to widen. A plot of stress

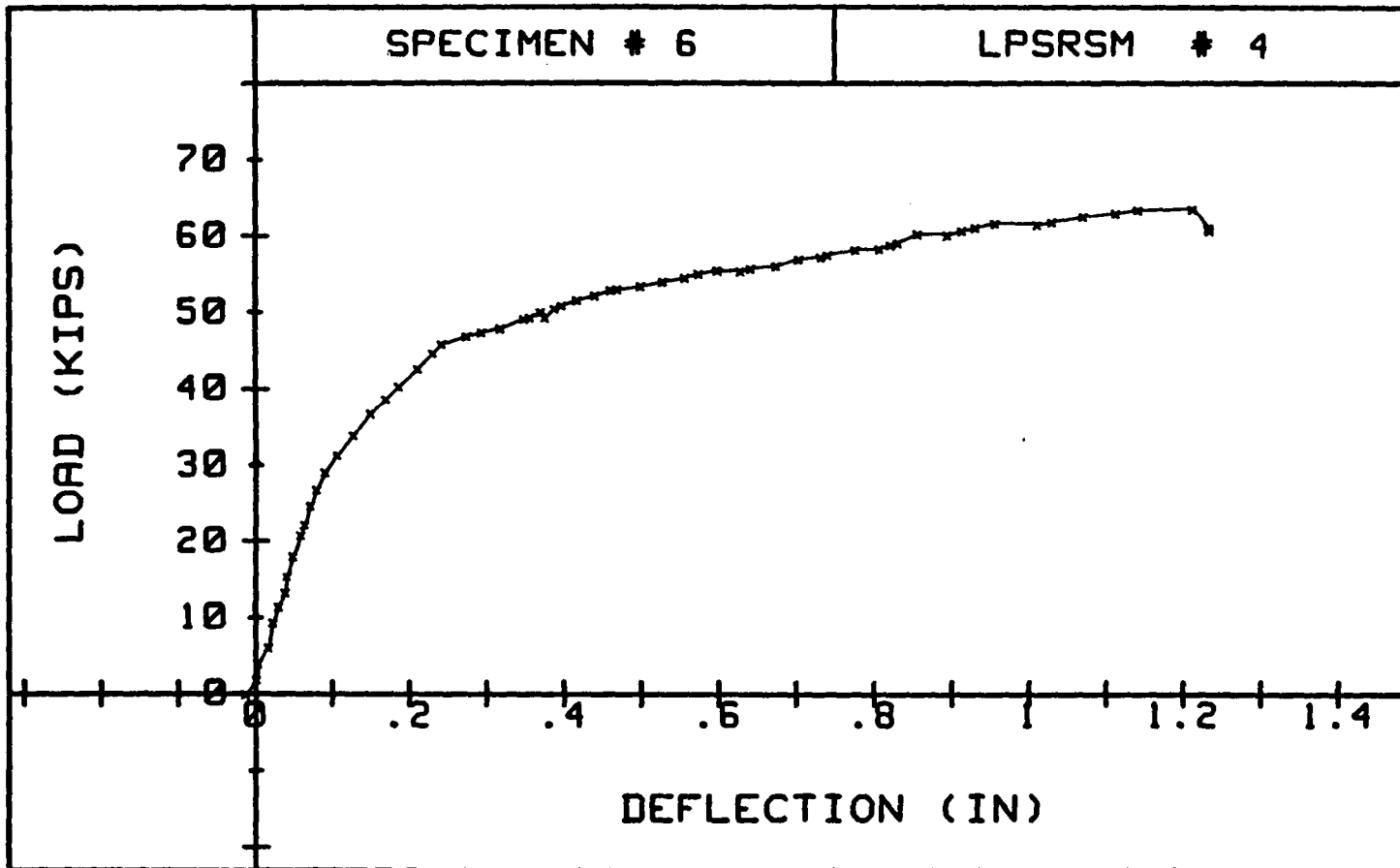


Fig. 4.16. Applied Load vs. Deflection for Specimen 6

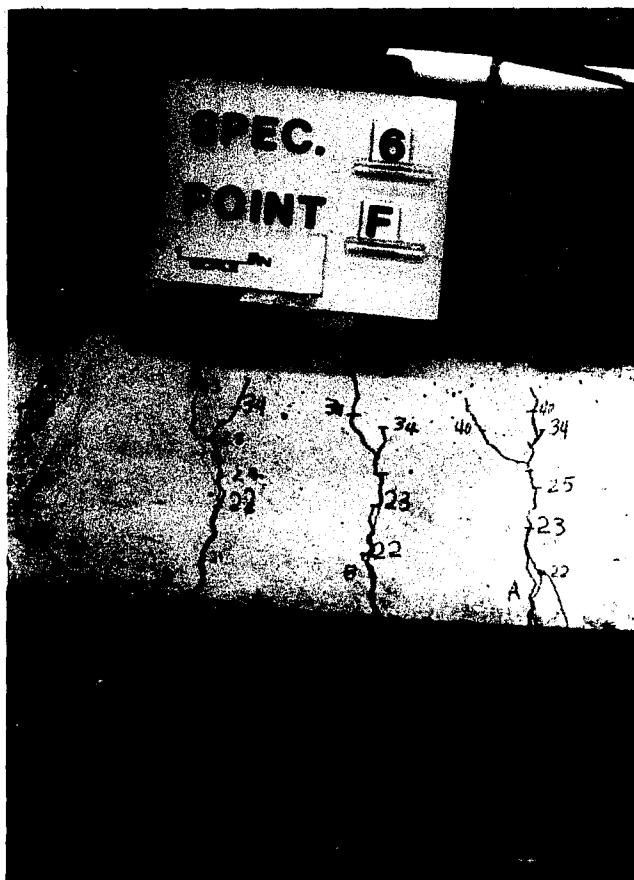


Fig. 4.17. Specimen 6 at the Conclusion of the Test

vs. strain for one of these bars is given in Fig. 4.18. At a load of 74.12 kips crack "B," which was located in the centerline of the beam, was measured to be 4.5 mm wide, and at a load of 79 kips, it was measured to be 6 mm wide.

The specimen was loaded up until a load of 80.05 kips was reached and failed in flexure. The value of stress in the strand at ultimate load was found to be 189.4 ksi, which was 66 percent of ultimate and 71.2 percent of the yield stress of the strand. Maximum deflection of the midspan was found to be 1.46 in. as shown in Fig. 4.19. Photographs of the specimen during the test and after failure are shown in Fig. 4.20 and 4.21 respectively.

Specimen #8 had the same dimension and amount of reinforcement as specimen #5. The shear span of this specimen was 36 inches and was prestressed with an effective prestressing force of 21.41 kips. Fig. 4.10 shows the location of concentrated loads, strain gages and LPSRSM's for this specimen. This specimen was loaded with a 2 kips load increment until a load of 35.4 kips was reached and first flexural crack appeared. At a load of 55.93 kips, the reinforcing steels in the bottom of the specimen started to yield causing widening of cracks. A plot of stress vs. strain for one of these steel bars is shown in Fig. 4.22. At a load of 66.2 a web shear crack

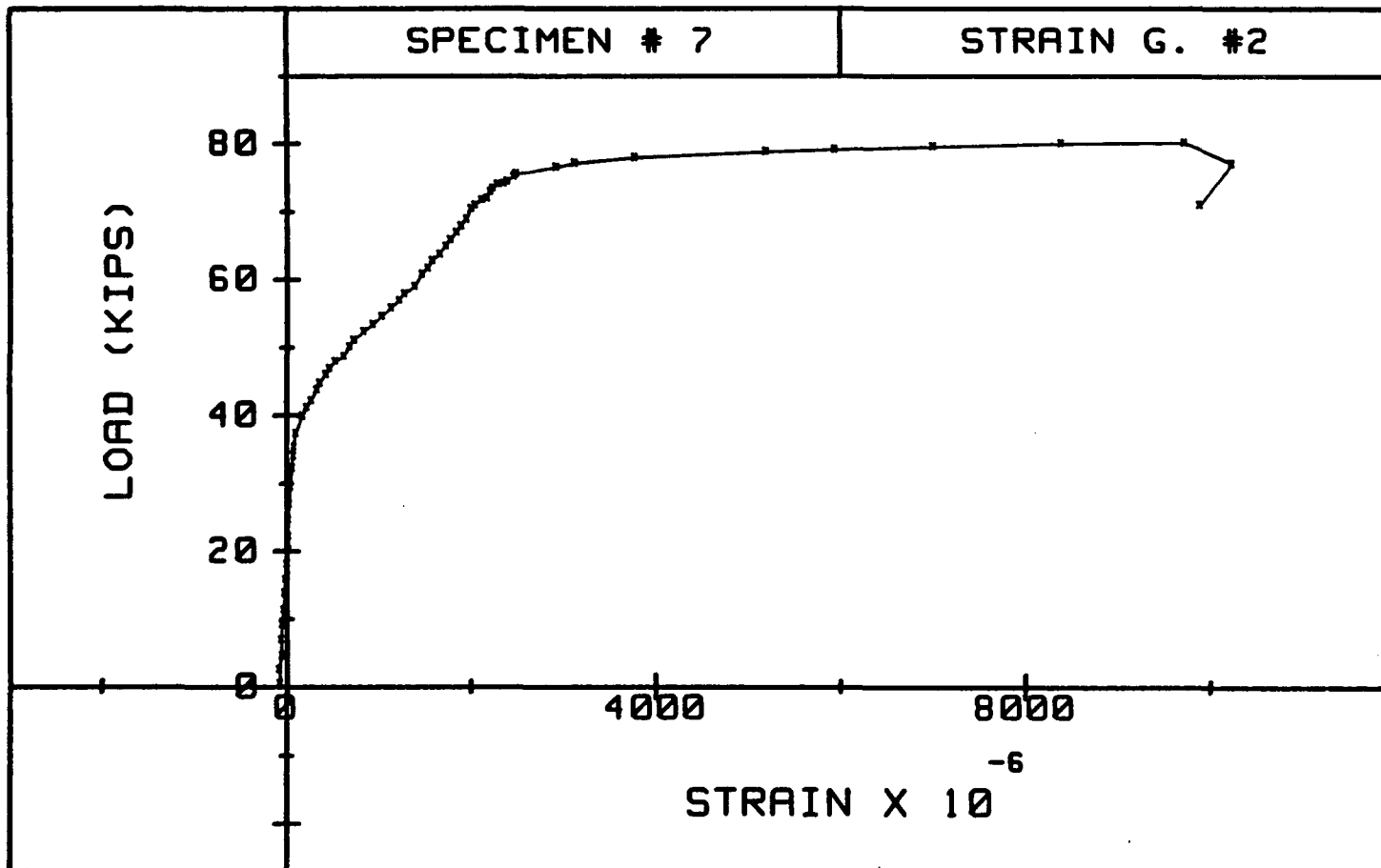


Fig. 4.18. Applied Load vs. Strain in the Longitudinal Reinforcement in the Bottom of Specimen 7

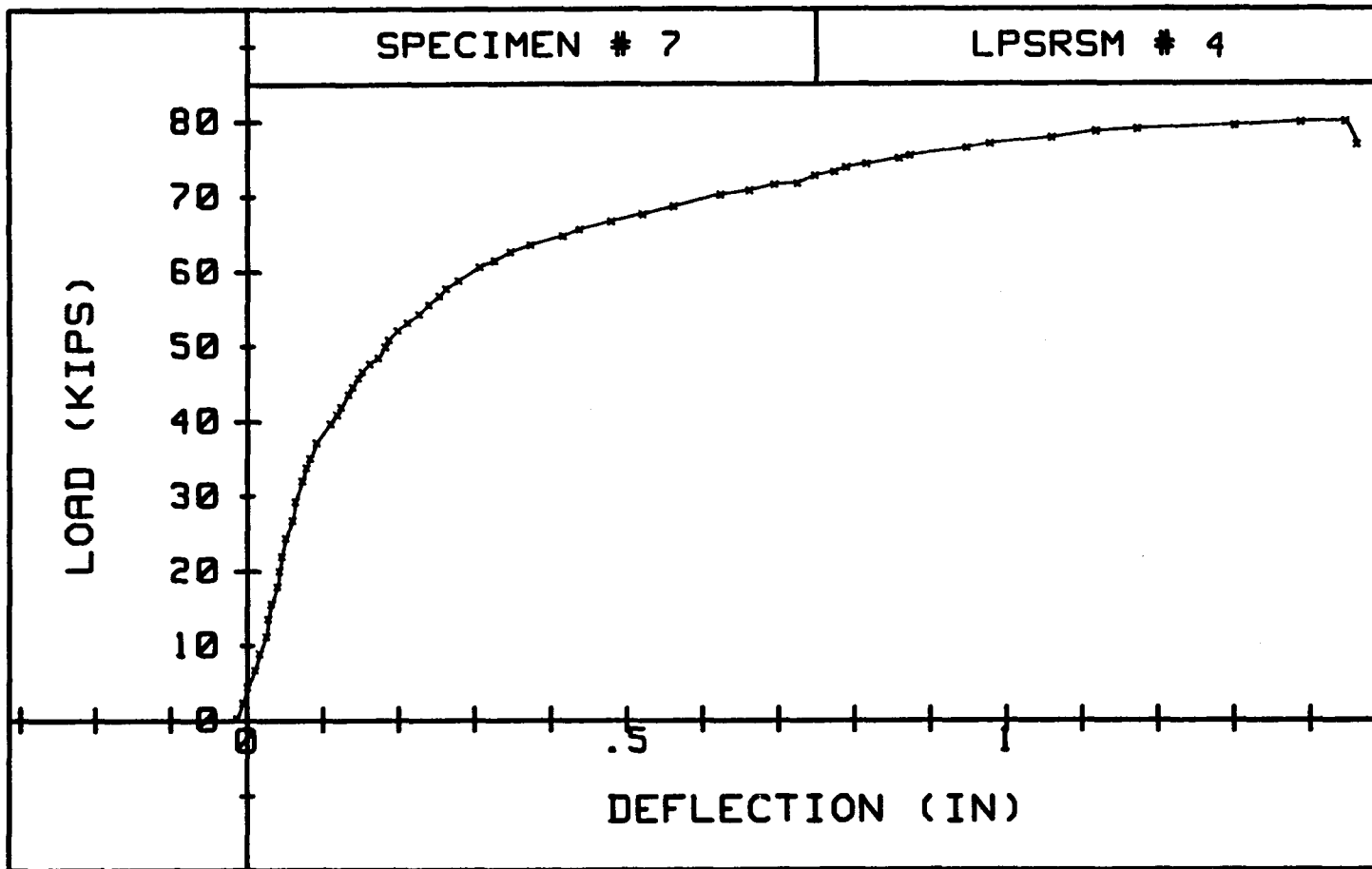


Fig. 4.19. Applied Load vs. Deflection for Specimen 7



Fig. 4.20. Specimen 7 Near the Failure

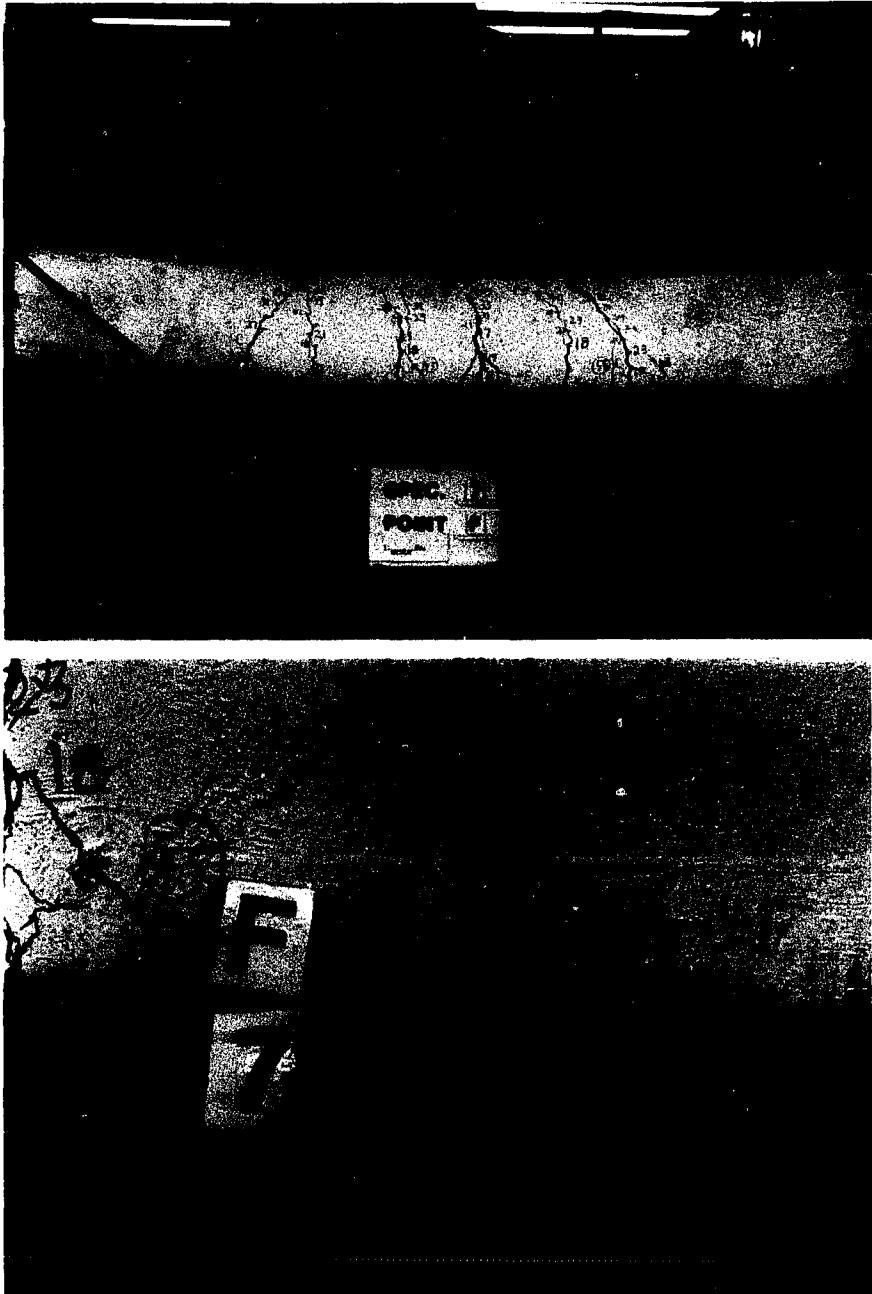


Fig. 4.21. Specimen 7 at the Conclusion of the Test

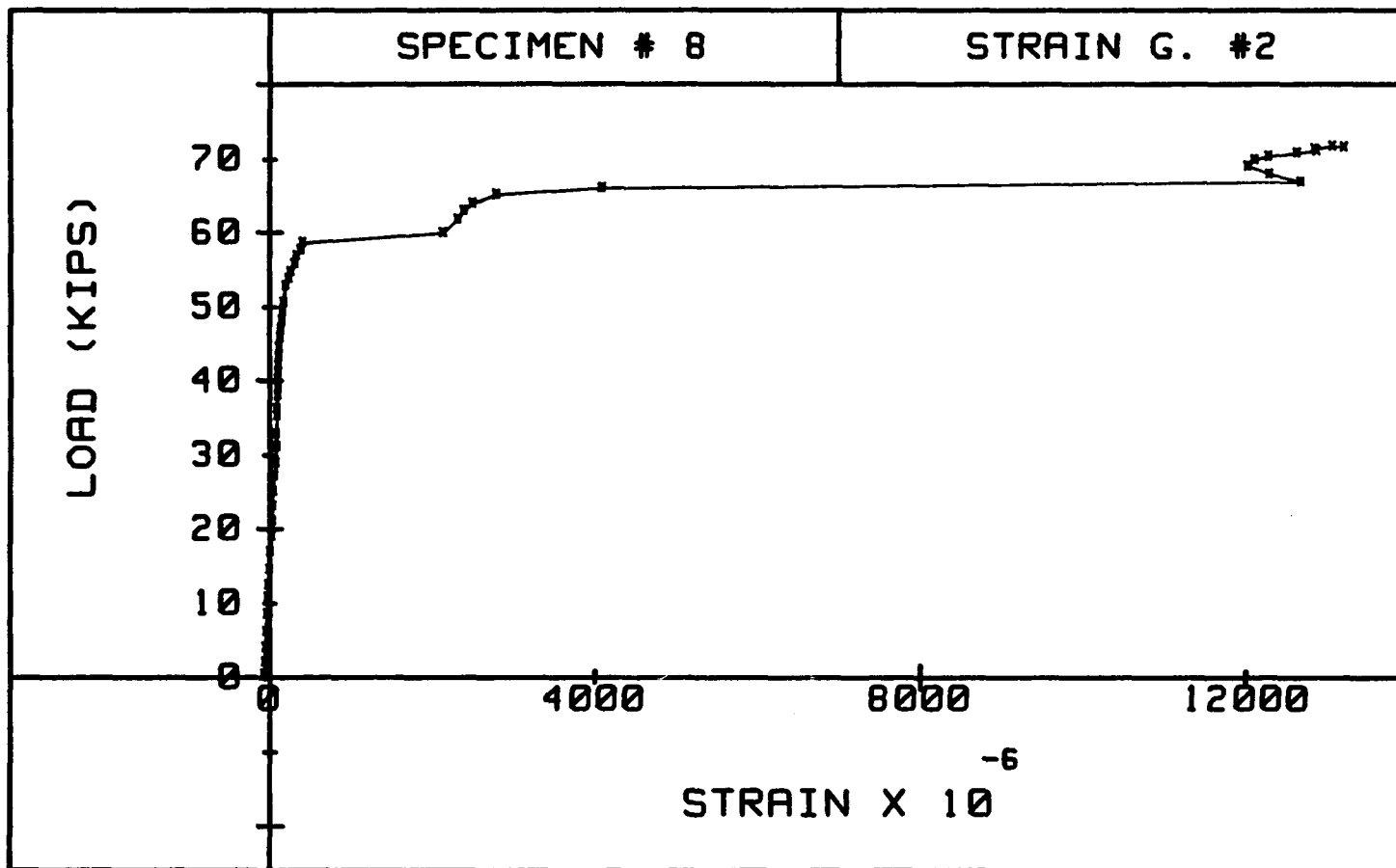


Fig. 4.22. Applied Load vs. Strain in the Longitudinal Reinforcement in the Bottom of Specimen 8

started to form. The specimen was loaded up until a load of 72 kips was reached and actuator went out of alignment. After fixing the actuator, specimen was reloaded again until a load of 76.24 kips was reached and it failed with a combined flexure-shear failure mode. Maximum value of f_{ps} for this specimen was found to be 171.5 ksi which was 60 percent of ultimate and 64 percent of yield stress of the strand. Maximum deflection at the midspan of specimen was found to be 0.57 inches, as shown in Fig. 4.23. Photographs of this specimen at failure are shown in Fig. 4.24.

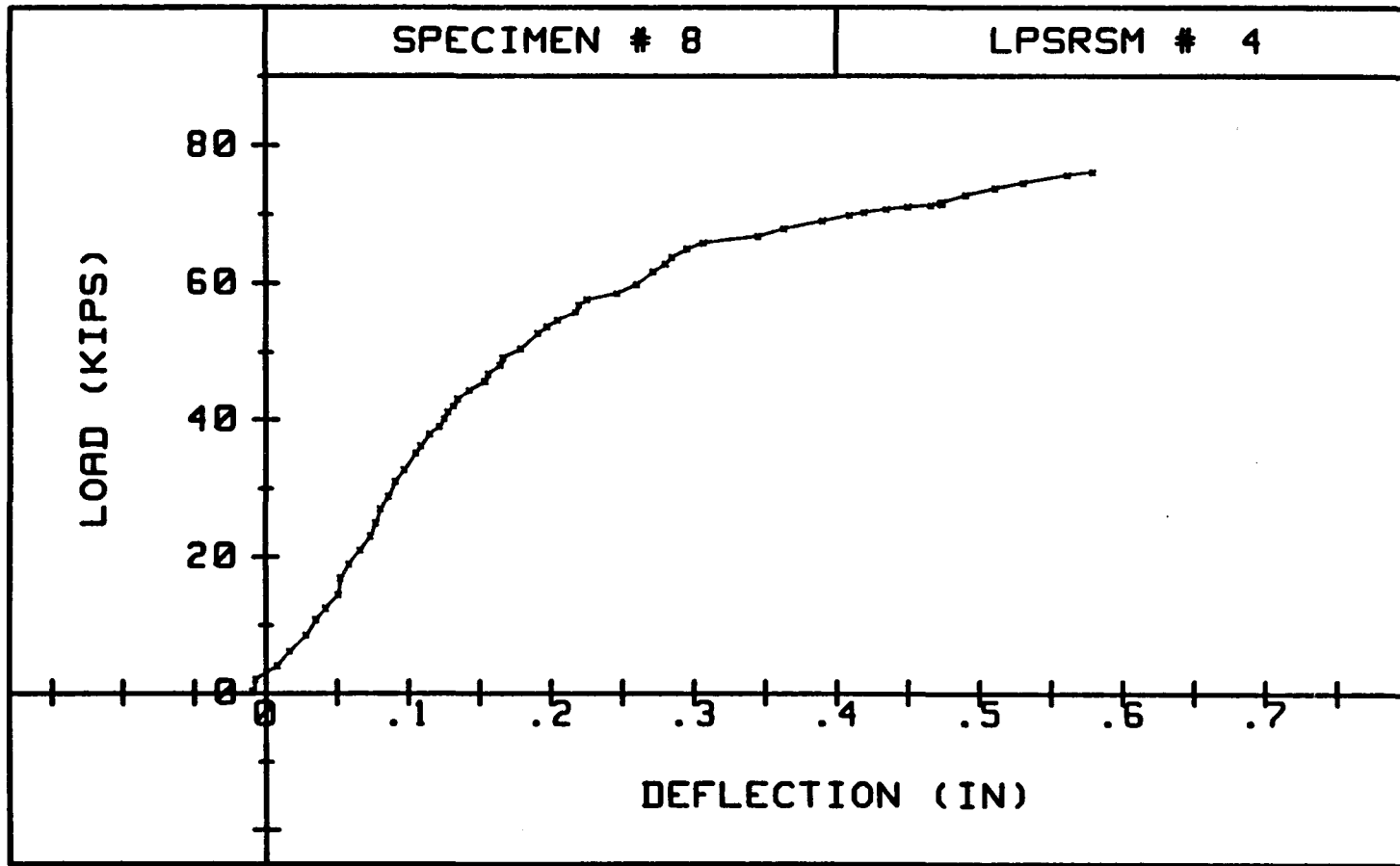


Fig. 4.23. Applied Load vs. Deflection for Specimen 8

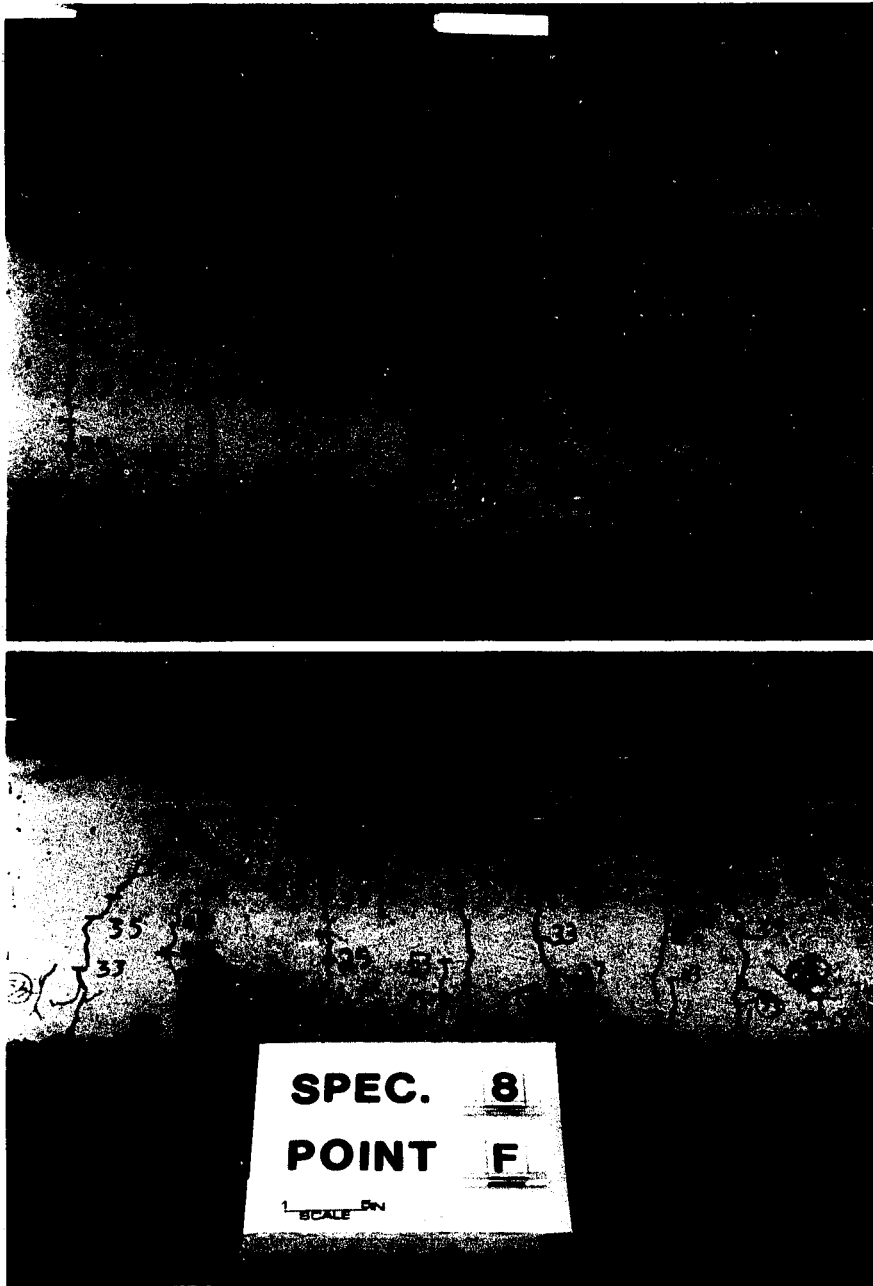


Fig. 4.24. Specimen 8 at the Conclusion of the Test

CHAPTER 5

DISCUSSION OF RESULTS

5.1. Effects of Primary Variables

Table 5.1 lists the primary variables as well as some of the test results. As can be seen in this table, the increase in the size of the specimen and/or effective prestressing force, P_e , resulted in an increase in cracking (M_{cr}) and in ultimate moment (M_u). However, the ratio of ultimate moment (M_u) to the cracking moment (M_{cr}) was found to be larger for the smaller cross sections and smaller for larger cross sections. This indicates that the increase in the size of the specimen increases the cracking moment (M_{cr}) more rapidly than it increases the ultimate moment (M_u).

From Table 5.1, it can also be observed that Specimen #3, with the largest value of shear span, a , gives the lowest value of additional stress in the strands due to externally applied loads, Δf_s , while Specimen #7, with the smallest value of " a " gives the highest value of Δf_s . To have a better observation of this variation, the values of Δf_s vs. the ratio of b/l , where b is the length of constant moment region and l is the clear span of the beam, is given in Fig. 5.1. It should be mentioned that specimens #4 and

Table 5.1
Primary Variables and Some of the Test Results

Specimen Number	Size (in.)	a (in.)	P _e (k)	f' _c (ksi)	f _{ps} (ksi)	f _{pe} (ksi)	Δf _s (ksi)	M _{cr} (k-in)	M _{ult} (k-in)	Mode of Failure
1	12x18	26	9.37	4.47	112.7	61.4	51.3	410	990	Flex.
2	14x20	26	15.13	4.47	159.6	99.2	60.4	570	1345	Flex.
3	14x20	48	16.22	4.47	134.8	106.4	28.4	738	1243	Flex.
4*	12x18	28	10.36	4.47	72.13	67.9	4.23	390	777	None
5	14x20	42	27.40	4.47	223.2	179.7	43.5	828	1439	Flex.
6	12x18	36	15.00	4.27	160.4	98.31	62.09	484	1145	Flex.
7	12x18	30	17.00	4.27	189.4	111.31	78.09	498	1201	Flex.
8	14x20	36	21.41	4.27	171.5	140.4	31.1	684	1397	Flex. Shear

*Specimen did not fail.

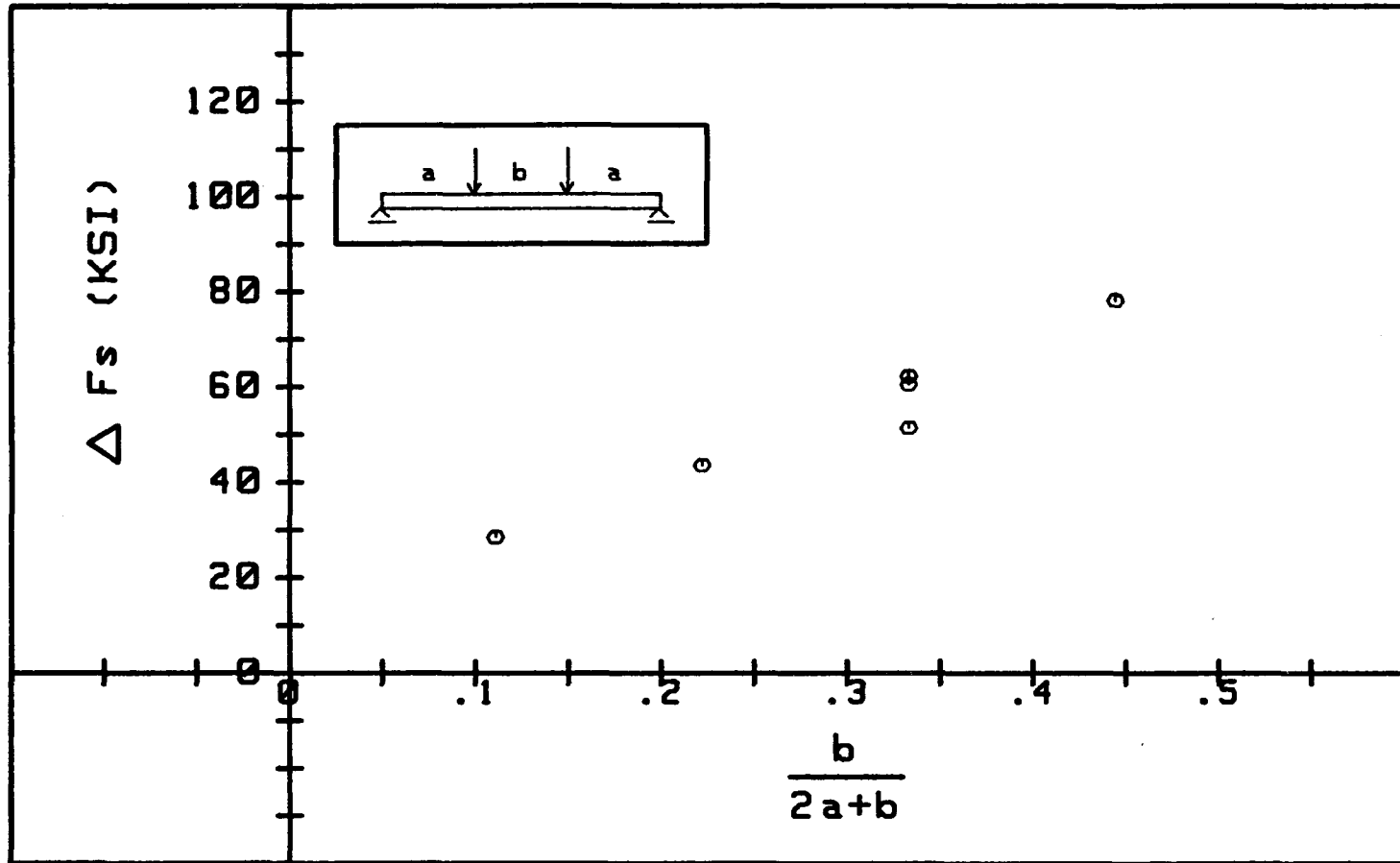
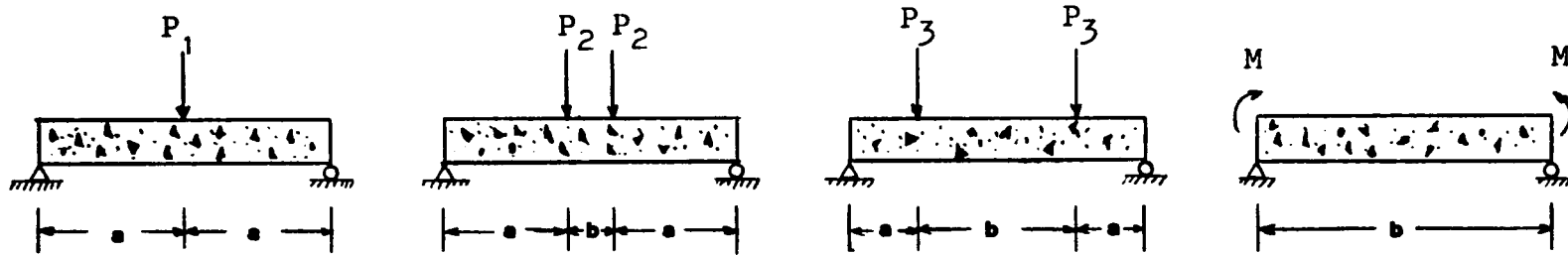


Fig. 5.1. Effect of Shear Span on Δf_s

8 are not included in Fig. 5.1. Due to experimental problems, Specimen #4 did not fail and Specimen #8 failed with a combined mode of flexure-shear failure, and therefore did not reach its ultimate flexural capacity. From Fig. 5.1, it can be concluded that Δf_s and b/l are directly proportional to each other.

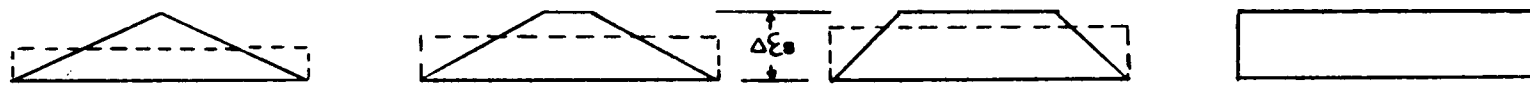
The reason for this relationship can be explained by referring to Fig. 5.2. Since the ultimate moment capacity of a cross section is independent of the shear span, a , the magnitude of ultimate moment (M_u) in Fig. 5.2 will be the same for all conditions of loading. Additional strain in the strands due to externally applied loads, $\Delta \epsilon_s$, for a bonded tendon will be similar to the moment diagram as shown in Fig. 5.2c. However, if the tendon is unbonded, $\Delta \epsilon_s$ will be uniformly distributed over the entire length of the span. Having a longer length of constant moment region, b , results in a larger value of average strain, $\Delta \epsilon_a$, as shown in Fig. 5.2c. This effect of b/l on the magnitude of Δf_s has not been mentioned by any of the researchers and is not included in any of the existing expressions for calculation of Δf_s . In the following section, the results of this experiment will be compared to those values obtained from some of the existing expressions, namely those proposed by Tam and Pannell⁽¹⁵⁾, ACI 318-83 code⁽¹⁹⁾ and British Code of Practice, CP110⁽²³⁾.



(a) Loaded Specimens.



(b) Moment Diagrams.



(c) Strain Distribution.

--- UNBONDED
 — BONDED

Fig. 5.2. Distribution of $\Delta\epsilon_s$ in Unbonded Tendons for Different Loading Conditions

5.2. Comparison of Test Results With Existing Theories

Equation 18-4 of the ACI code gives the following expression for calculation of ultimate stress in prestressed tendons at nominal strength, f_{ps} , for flexural members with unbonded tendons and the l/d ratio of less than or equal to 35.

$$f_{ps} = f_{se} + \Delta f_s \leq f_{py} \quad (5.1)$$

where

$$\Delta f_s = 10,000 + \frac{f'_c}{100\rho_p} \leq 60,000 \text{ psi}$$

f_{se} = effective stress in prestressed reinforcement, after allowance for all prestress losses, psi

f'_c = specified compressive strength of concrete, psi

ρ_p = ratio of prestressed reinforcement $\frac{A_{ps}}{b_w d_p}$

The values obtained from this equation are shown in Table 5.2 and are compared to the test results in Fig. 5.3. From this figure it can be seen that the values obtained from Eq. 5.1 are inconsistent with the test results. For smaller values of b , the values obtained from Eq. 5.1 are much higher than those obtained from the test results. As the value of b increases, the difference between the two values becomes smaller. This could be based on the

Table 5.2
 Values of Δf_s in ksi

Specimen Number	a (in.)	ACI* (ksi)	Tam (ksi)	B.C. (ksi)	Test (ksi)
1	36	57.92	82	27.63	51.3
2	36	74.12	94	44.64	60.4
3	48	77.35	97.15	47.88	28.4
4**	28	--	--	--	--
5	42	72.73	94.3	80.86	43.5
6	36	57.03	83.2	44.24	62.09
7	30	57.03	86.49	50.1	78.09
8***	36	74.4	95.45	63.18	31.1

*These are the values obtained from Eq. 18.4. However, these values are limited to a maximum value of 60 ksi.

**Beam did not fail (test was not completed).

***Failed with flexural-shear mode.

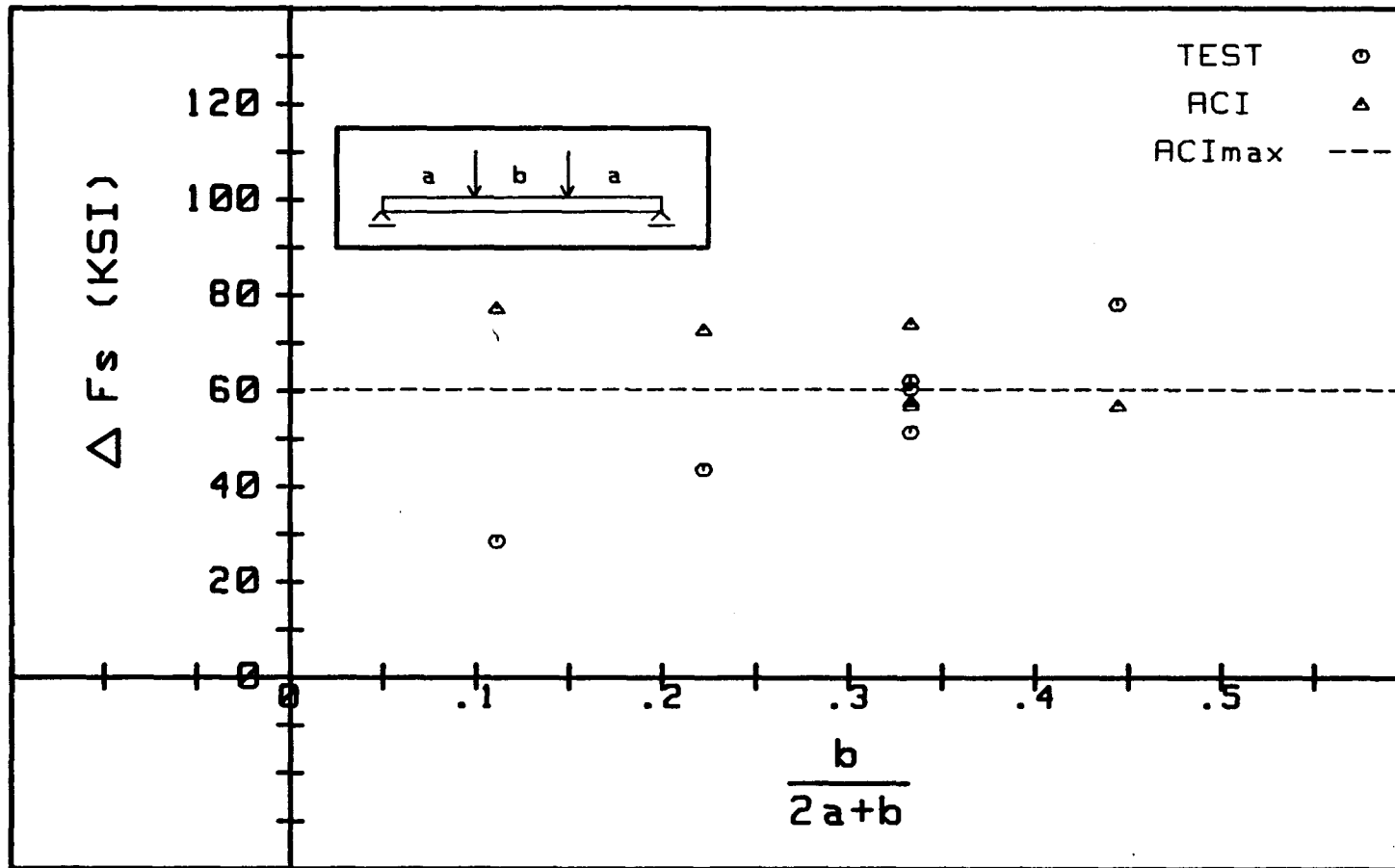


Fig. 5.3. Comparison of Eq. 18-4 of ACI-318-83 Code to the Test Results

following reasons. First, the effects of b/t ratio are not included in the ACI code equation. As discussed earlier, the length of the constant moment region does influence the magnitude of the additional strains. Secondly, the specimens tested in this experiment were lightly reinforced. However, the above equation was obtained from the testing of specimens with a higher percentage of reinforcement. Since the value of ρ in Eq. 5.1 is in the denominator of the equation, a decrease in the value of ρ results in an increase of the value of Δf_s . The results of the equation could become compatible with the test results by introducing a modification factor (λ), which includes the effect of the b/t ratio. Within the limitation of this experiment, this modification factor was found to be as follows:

$$\lambda = 11000 \frac{b}{f'_c t} \quad (5.2)$$

and should be applied to Eq. (5.1) in the following fashion:

$$\Delta f_{sm} = 10,000 + \frac{f'_c}{100 \rho_p} \cdot \lambda$$

or

$$\Delta f_{sm} = 10,000 + 110 \frac{b}{\rho_p l} \quad (5.3)$$

where Δf_{sm} = modified Δf_s .

The values obtained from Eq. 5.3 were plotted in Fig. 5.4 and were found to be very close to the actual values (less than 5% difference) for values of Δf_s less than 60 ksi. As the value of Δf_s goes beyond 60 ksi, the values of this equation become more conservative (about 20% lower than the measured values).

The following equation was proposed by Tam and Pannell⁽¹⁵⁾ for calculation of Δf_s in unbonded tendons:

$$\Delta f_s = \Psi \epsilon_u \left(1 - \frac{c}{d}\right) E_s \frac{d}{L} \quad (5.4)$$

where

Ψ = (plastic hinge length)/c

ϵ_u = ultimate strain of the concrete (0.003)

c = depth of neutral axis at failure

d = effective depth of the beam (from the compression fiber to the centroid of prestressing steel)

E_s = modulus of elasticity of steel

L = length of prestressing tendon from anchorage to anchorage.

Calculation of the factor Ψ can be achieved by using the following equation, which was also suggested by Tam and Pannell⁽¹⁵⁾.

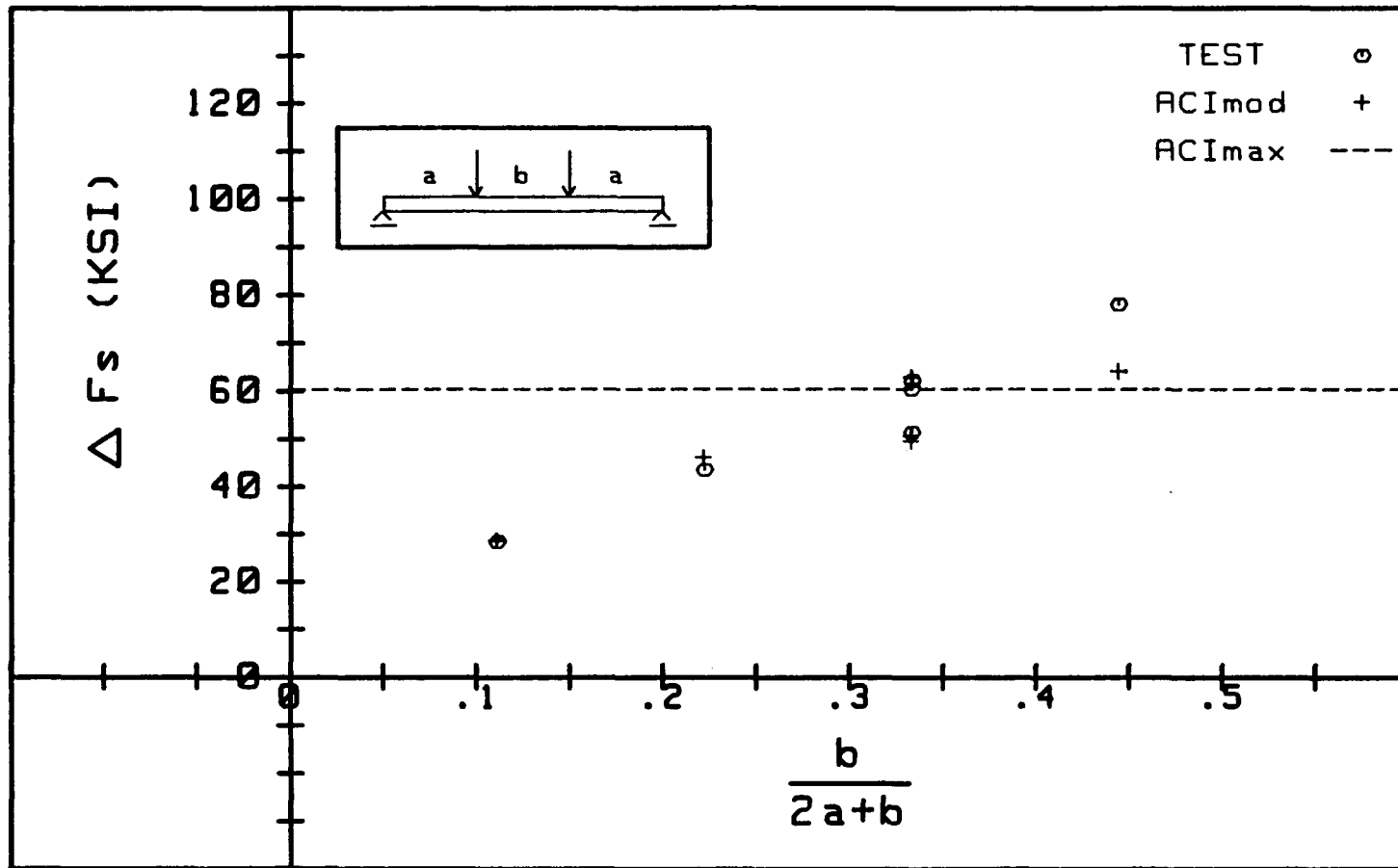


Fig. 5.4. Comparison of Modified Eq. 18-4 of ACI-381-83 Code to the Test Results

$$\nu = \frac{f_{ps} - f_{pe}}{\epsilon_u [1 - (\omega_p f_{ps} + \omega f_y) / 0.85 \beta_1 f'_c] \frac{d}{L} E_s} \quad (5.5)$$

where

f_{ps} = stress in prestressed reinforcement at nominal strength, psi

f_{pe} = effective stress in prestressed reinforcement, psi.

$$\omega_p = \rho_p f_{ps} / f'_c$$

$$\rho_p = \frac{A_{ps}}{b_w d_p}$$

A_{ps} = area of prestressed reinforcement in tension zone (sq. in.)

b_w = width of compression face of member

d_p = distance from extreme compression fiber to centroid of compression reinforcement.

$$\omega = \rho f_y / f'_c$$

$$\rho = A_s / b d_p$$

A_s = area of nonprestressed tension reinforcement, sq. in.

Based on the results of their experiment, Tam and Pannell obtained a single value of 10.5 for ν . This value of ν was used in Eq. 5.4 and Δf_s was calculated for each individual specimen. The results are shown in Table 5.2 and are compared with the test results in Fig. 5.5. As can be seen in the figure, the results of Eq. 5.4 are

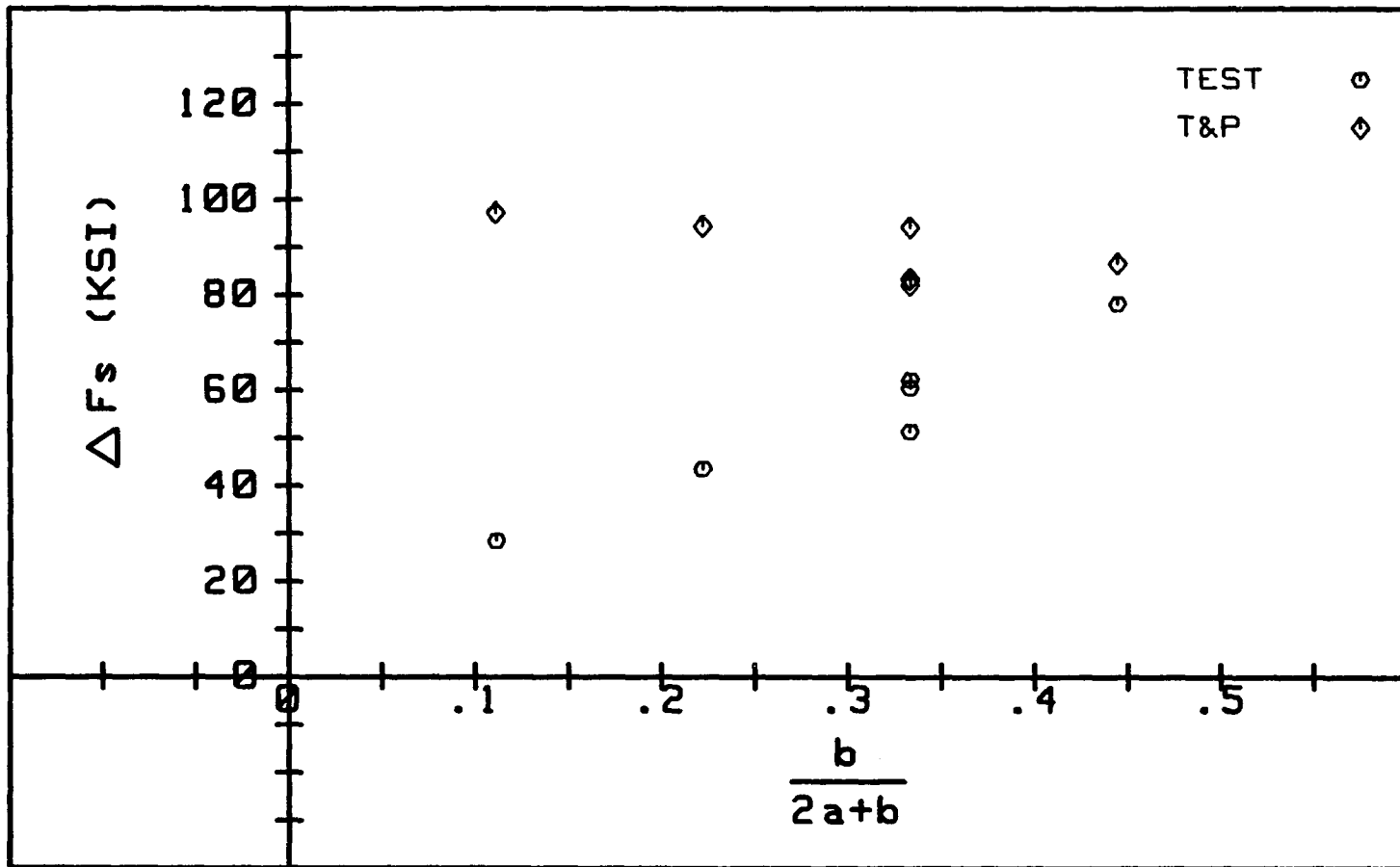


Fig. 5.5. Comparison of Pannell-Tam Equation to the Test Results

unconservative and independent of b/l ratio. This difference is due to the following. First, the specimens tested by Tam and Pannell were heavily reinforced beams with reinforcement indices ($\bar{\omega}$) ranging from 0.125 to 0.269, but the specimens in this experiment were lightly reinforced with reinforcement indices ranging from 0.052 to 0.071. Secondly, they tested all of their specimens with a single point load which resulted in exclusion of b/l effects from their expression for Δf_s .

Eq. 5.5 was used and values of Ψ for each specimen were calculated. The results are plotted vs. the ratio of b/l in Fig. 5.6. From this figure, it was concluded that the value of Ψ is not constant but is varying with the b/l ratio.

By using the least squares method the relationship between the Ψ and b/l was found to be:

$$\Psi = 18.75 \frac{b}{l} + 0.825 \quad (5.6)$$

If Eq. 5.6 is substituted in Eq. 5.4, the modified Tam-Pannell's equation within the limitation of this experiment will be given as:

$$\Delta f_s = \frac{1}{l \cdot L} (E_s \epsilon_n)(d-c)(18.75b + 0.825l) \quad (5.7)$$

where

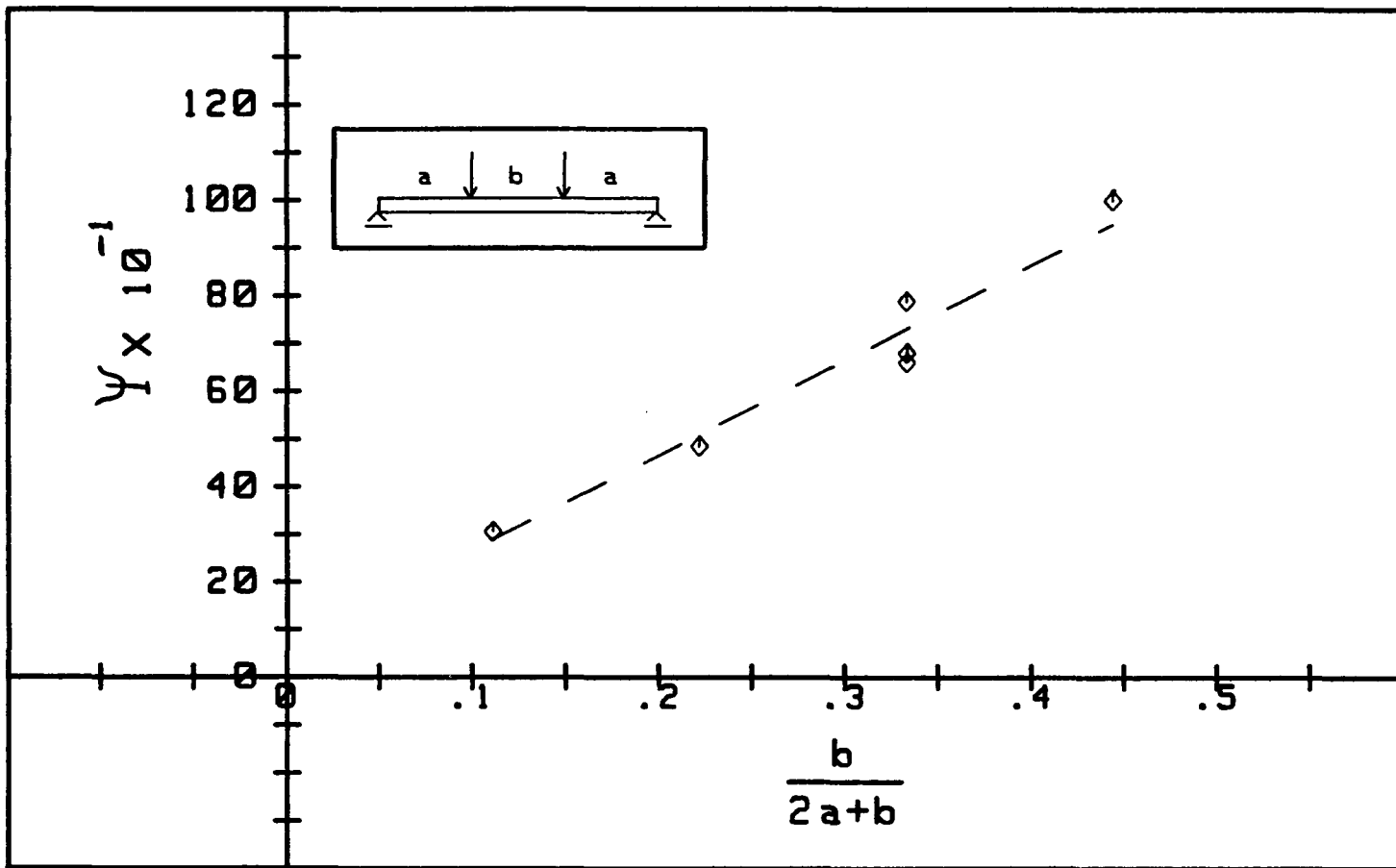


Fig. 5.6. Effect of Shear Span on the Coefficient Ψ

l = clear span of the beam

L = length of prestressing tendon from anchorage to anchorage.

The values obtained from this modified equation are compared to the test results in Fig. 5.7. As can be seen from the figure, the values obtained from the equation are very close to the test results (less than 5% difference) for values of Δf_s less than 60 ksi. As the value of Δf_s goes beyond 60 ksi, the values of this equation become more conservative, with a maximum difference of 12.5%.

British Code of Practice CP110⁽²³⁾ gives the ratio of f_{ps}/f_{pe} as a function of $\frac{f_{pe} A_{ps}}{f'_c b_w}$ and l/d ratio as shown in Table 5.3.

Since f_{ps} is equal to $f_{pe} + \Delta f_s$, the ratio f_{ps}/f_{pe} can be written as $\frac{f_{pe} + \Delta f_s}{f_{pe}}$ or simply $1 + \frac{\Delta f_s}{f_{pe}}$. In other words, Δf_s can be obtained by using the following equation $\Delta f_s = (x-1)f_{pe}$, where x is the ratio of f_{ps}/f_{pe} obtained from Table 5.3. This equation was used and Δf_s for each specimen was calculated. The values of Δf_s obtained from this equation and the experiment are plotted against the b/l ratio and the effective prestressing force (P_e) in Fig. 5.8 and Fig. 5.9 respectively. As it is shown in Fig. 5.8, the values obtained from Table 5.3 are inconsistent with

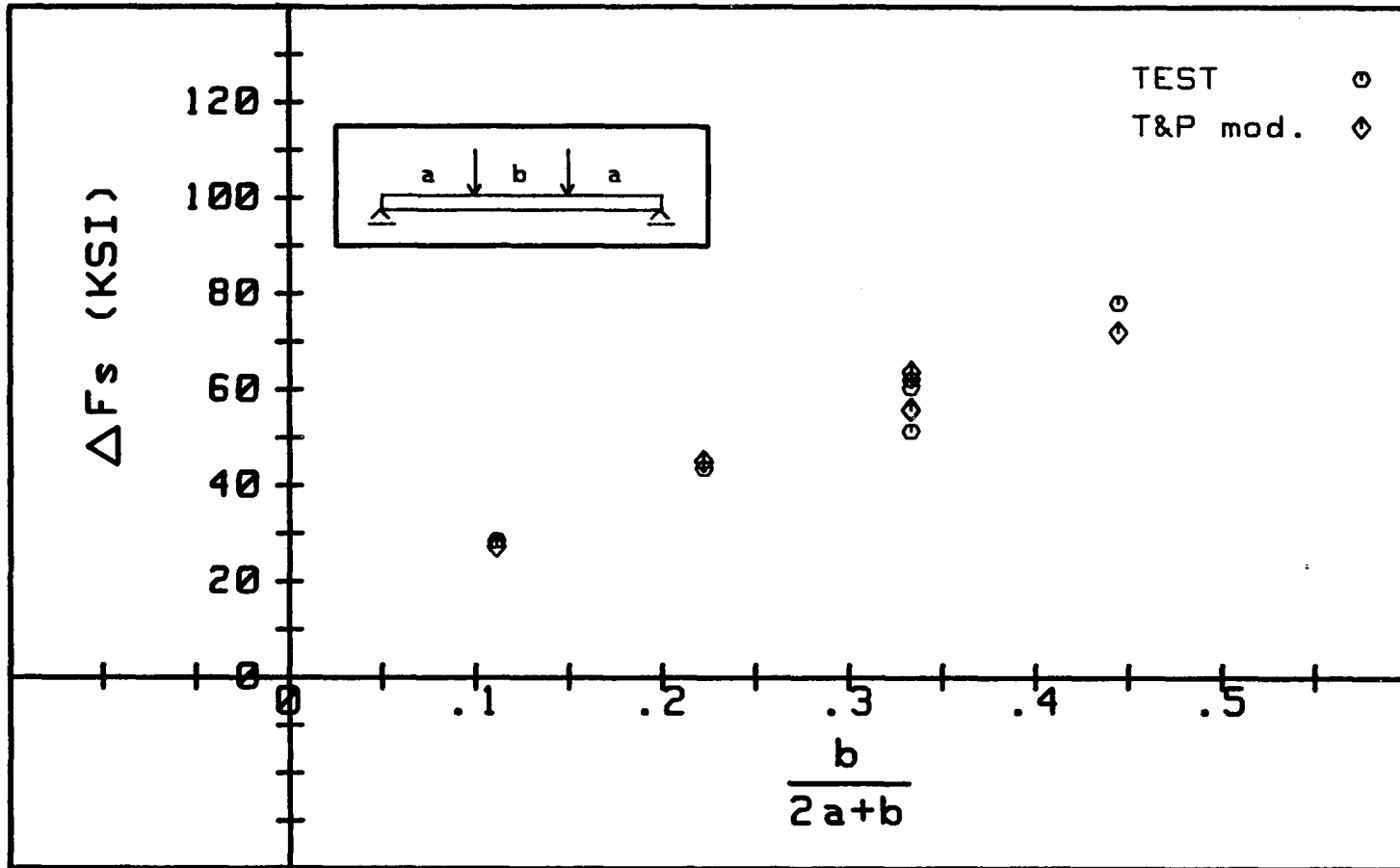


Fig. 5.7. Comparison of Modified Pannell-Tam Equation to the Test Results

Table 5.3

Stress in Tendons as a Proportion of Effective
 Prestress f_{ps}/f_{pe} for values of

$$\frac{l}{d} \left[\frac{\text{effective span}}{\text{effective depth}} \right]$$

$\frac{f_{pe} A_{ps}}{f'_c b_w d}$	30	20	10
0.025	1.23	1.34	1.45
0.05	1.21	1.32	1.45
0.10	1.18	1.26	1.45
0.15	1.14	1.20	1.36
0.20	1.11	1.16	1.27

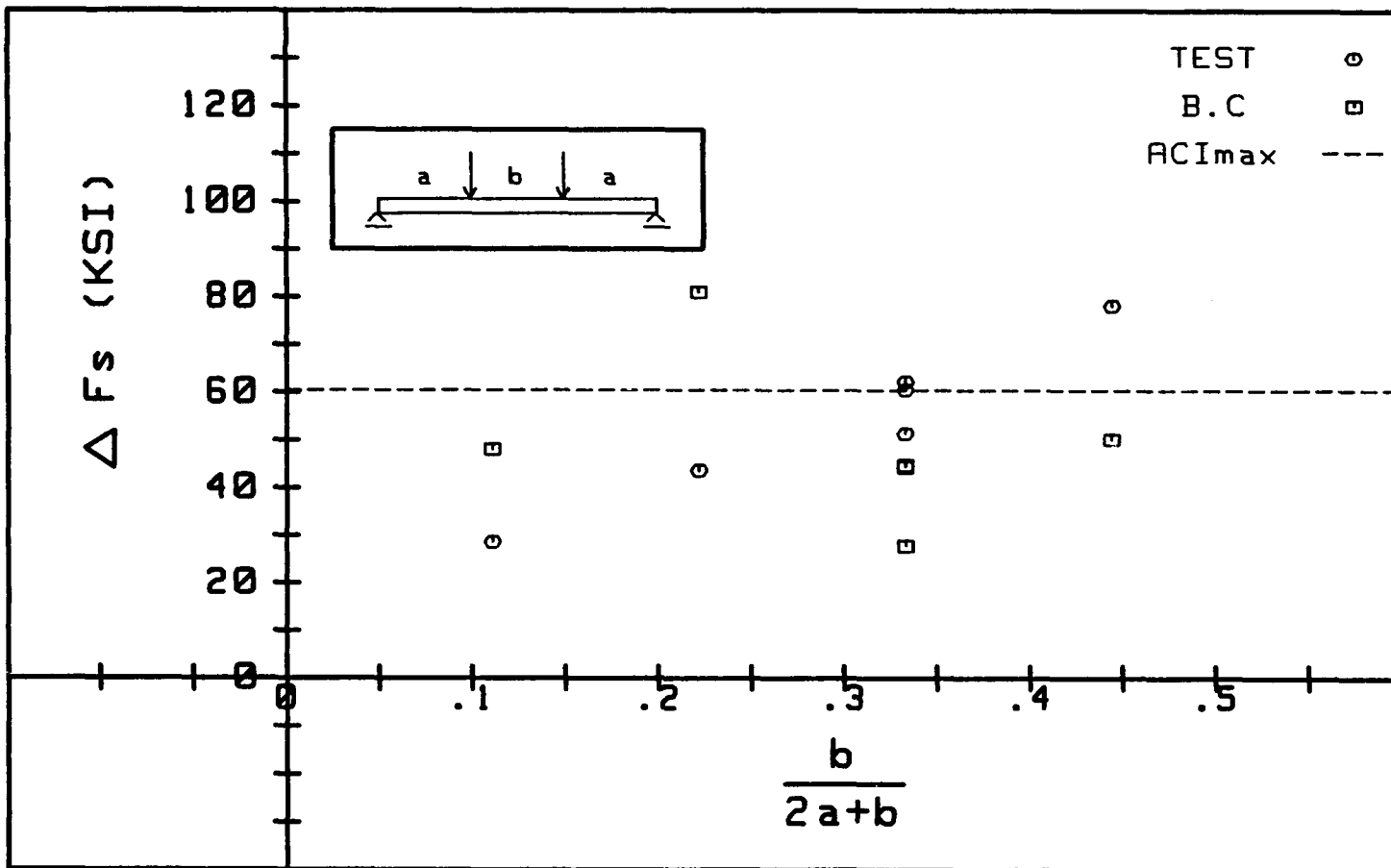


Fig. 5.8. Comparison of the British Code Values to the Test Results

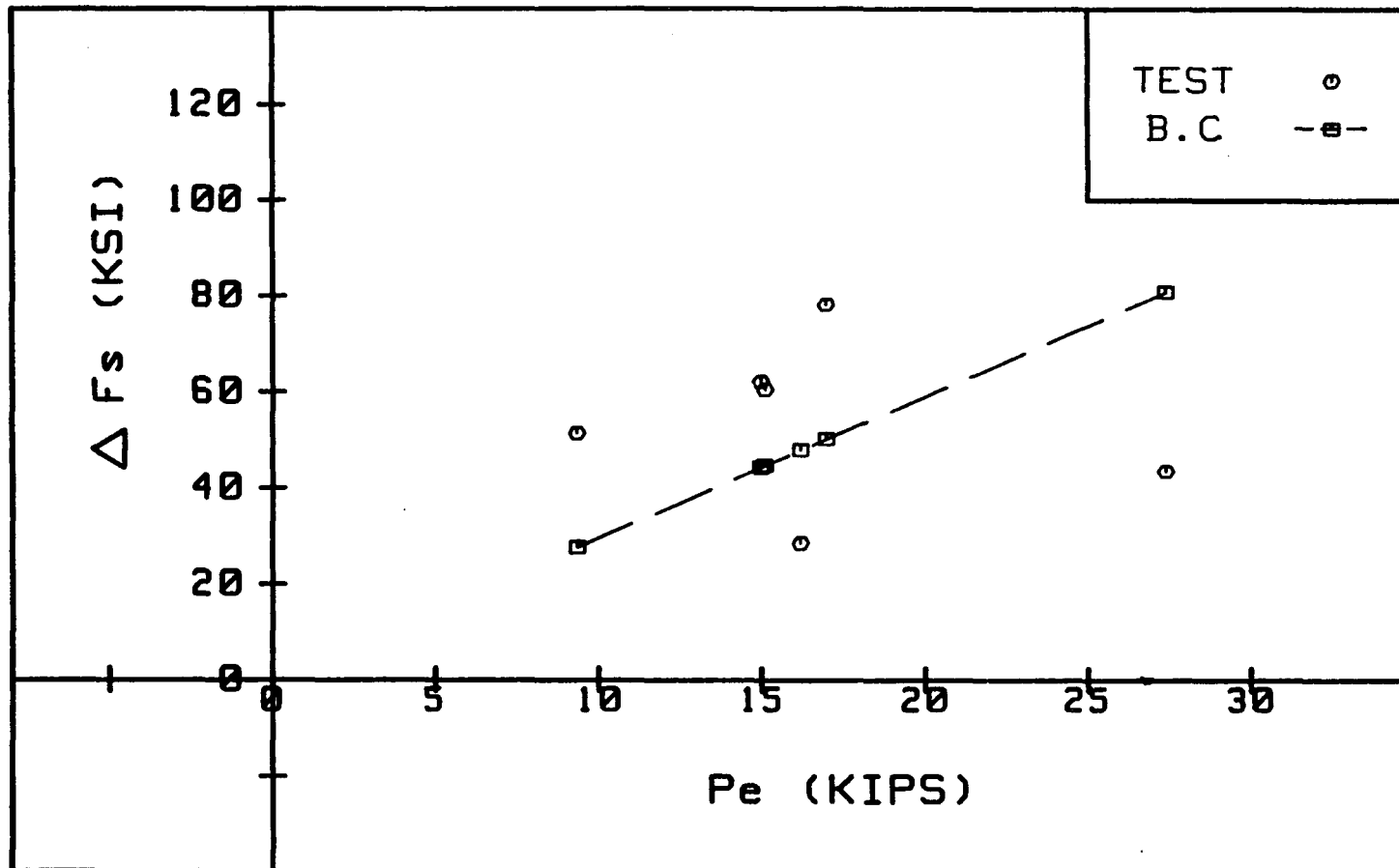


Fig. 5.9. Comparison of the British Code Values to the Test Results

the test results and independent of b/l ratio. However, these values are directly proportional to the effective prestressing force (P_e) as shown in Fig. 5.9. This is because the table gives the value of Δf_s as a percentage of effective prestress (f_{pe}), i.e., for a set of beams with $l/d \leq 10$ and $\frac{f_{pe} A_{ps}}{f'_c b_w} \leq 0.1$, the value of Δf_s is 45 percent of f_{pe} . But the results of this experiment indicate that the value of Δf_s is independent of the effective prestressing force, P_e , as shown in Fig. 5.9.

It is therefore concluded that additional test data is needed to modify Table 5.3, taking into account the following parameters:

- 1) The values given in Table 5.3 should become independent of the effective prestressing stress (f_{pe}).
- 2) The effect of b/l should be included in the entries of Table 5.3.
- 3) The ratio of l/d should be extended to higher values than 30.

5.3. Reinforcing Index, $\bar{\omega}$

ACI 318-83⁽¹⁹⁾ gives the minimum amount of reinforcement in a reinforced concrete member in terms of the steel ratio, ρ . This was obtained by setting the cracking moment of a plain concrete section equal to the nominal moment of a reinforced concrete section of the same size

and solving for the steel ratio, ρ . The result was then multiplied by a factor of safety of 2.

For prestressed concrete members, the minimum amount of reinforcement is not given in terms of steel ratios or reinforcing index, $\bar{\omega}$. It is rather given indirectly in terms of ultimate resisting moment (M_u) and cracking moment (M_{cr}). The same approach used for the development of ρ_{min} in reinforced concrete members can be used to find an expression for the minimum amount of reinforcement in prestressed and partially prestressed concrete members in terms of reinforcing index, $\bar{\omega}$. This was first done by Naaman⁽²¹⁾ for a typical prestressed concrete beam, and an equation was obtained. However, Naaman did not include any compression steel in that expression. The following equation was derived in Appendix A of this report and it gives the value of $\bar{\omega}$, which would result in a cross section with nominal moment capacity of equal value to that of cracking moment.

$$\bar{\omega}_{eq} = 0.85 (1 - \sqrt{1 + \mu}) \quad (5.8)$$

where

$$\nu = \frac{2}{0.85 f'_c b_w d^2} \left(A_s F_y [v(d-d'_s) + 2] - P_e \left(d - \frac{h}{3} \right) - 1.25 b_w h^2 \sqrt{f'_c} \right)$$

$$v = \frac{A'_s}{A_s} \cdot \frac{f'_s}{F_y}$$

When the test specimens were designed, an effort was made to make the actual $\bar{\omega}$ of all specimens 10 to 30 percent higher than the $\bar{\omega}$ obtained from the above equation. However, due to the difference between the design and the actual value of the material properties, the actual value of $\bar{\omega}$ turned out to be as high as twice the value obtained from Eq. 5.8, as shown in Table 5.4 and Fig. 5.10. From this figure it can be concluded that the following equation gives the value of $\bar{\omega}$ for the tested specimens.

$$\bar{\omega}_T = 1.7(1 - \sqrt{1+\nu}) \quad (5.9)$$

where ν is given by Eq. 5.8.

Eq. 5.9 is compatible to Eq. 10-3 of the ACI Code which gives the minimum amount of reinforcement ratio in reinforced concrete members (ρ_{\min}). The highest value of $\bar{\omega}$ obtained from Eq. 5.9 is 0.066. This is 34 percent lower than the value of 0.1 suggested by Lin⁽²⁴⁾ for the minimum

Table 5.4
Reinforcing Index

Specimen Number	$\bar{\omega}$ Actual	$\bar{\omega}$ Equation	$\frac{\bar{\omega}_{act.}}{\bar{\omega}_{eq.}}$
1	0.0571	0.030	1.9
2	0.0539	0.025	2.156
3	0.0539	0.0317	1.70
4*	--	--	--
5	0.0640	0.0317	2.02
6	0.0658	0.0323	2.04
7	0.071	0.0329	2.158
8**	--	--	--

*Specimen did not fail.

**Specimen failed with flexural-shear mode.

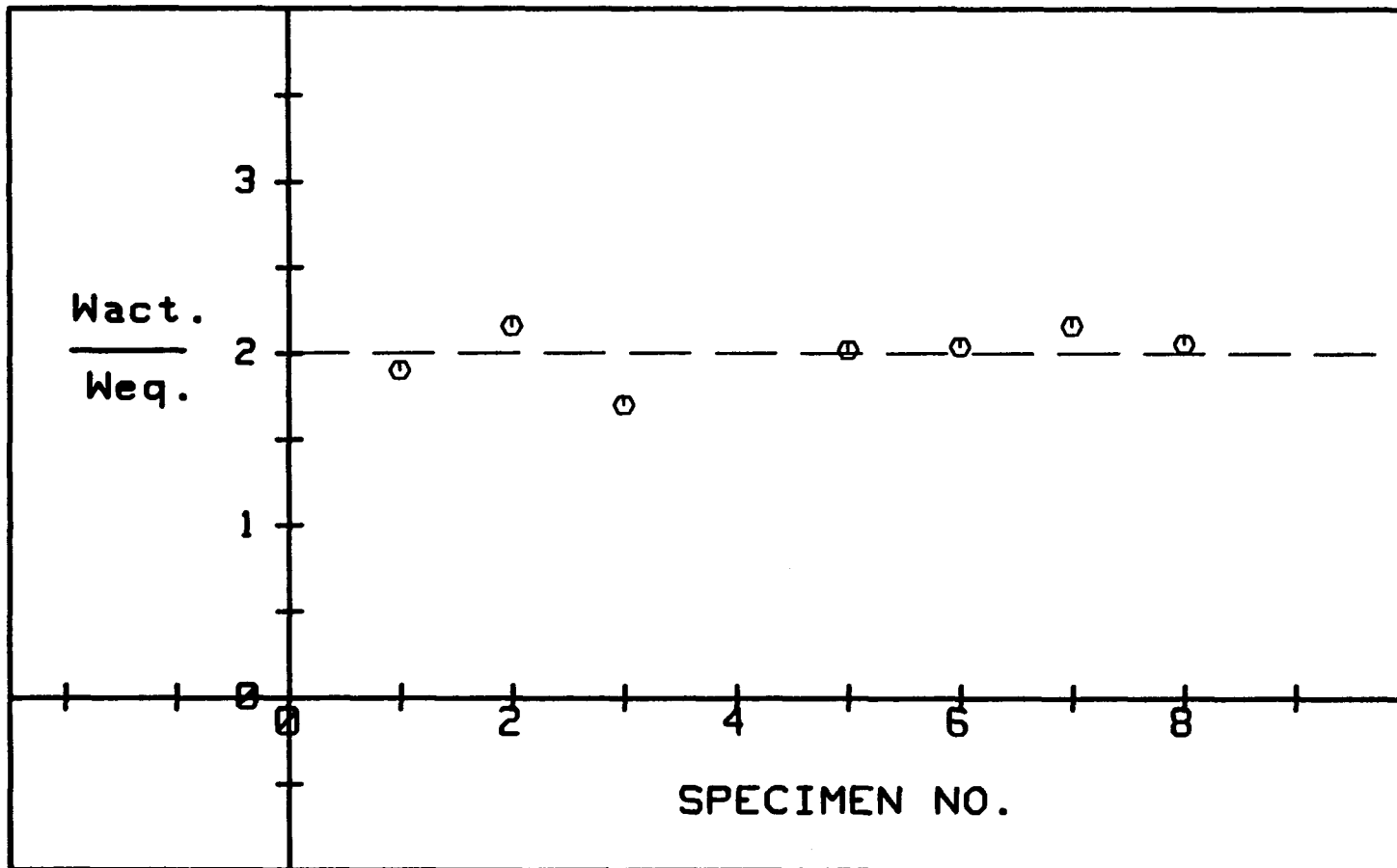


Fig. 5.10. Ratio of Actual \bar{w} to the \bar{w} Obtained from Eq. 5.8 vs. Specimens

amount of reinforcement in prestressed concrete beams. Eq. 5.9 can be used to find the minimum amount of reinforcement in a prestressed concrete flexural member.

Fig. 5.11 shows the ratio of $M_u/b_w d$ vs. $\bar{\omega}$. From this figure it can be concluded that $M_u/b_w d$ is proportional to $\bar{\omega}$. This relationship was found to be linear with a slope of 90. This results in the following equation.

$$\frac{M_u}{b_w d \bar{\omega}} = 90$$

or

$$M_u = 90 \bar{\omega} b_w d \quad (5.10)$$

However, it should be mentioned that the above relationship was obtained for this experiment. More experimental data are needed to justify such relationship.

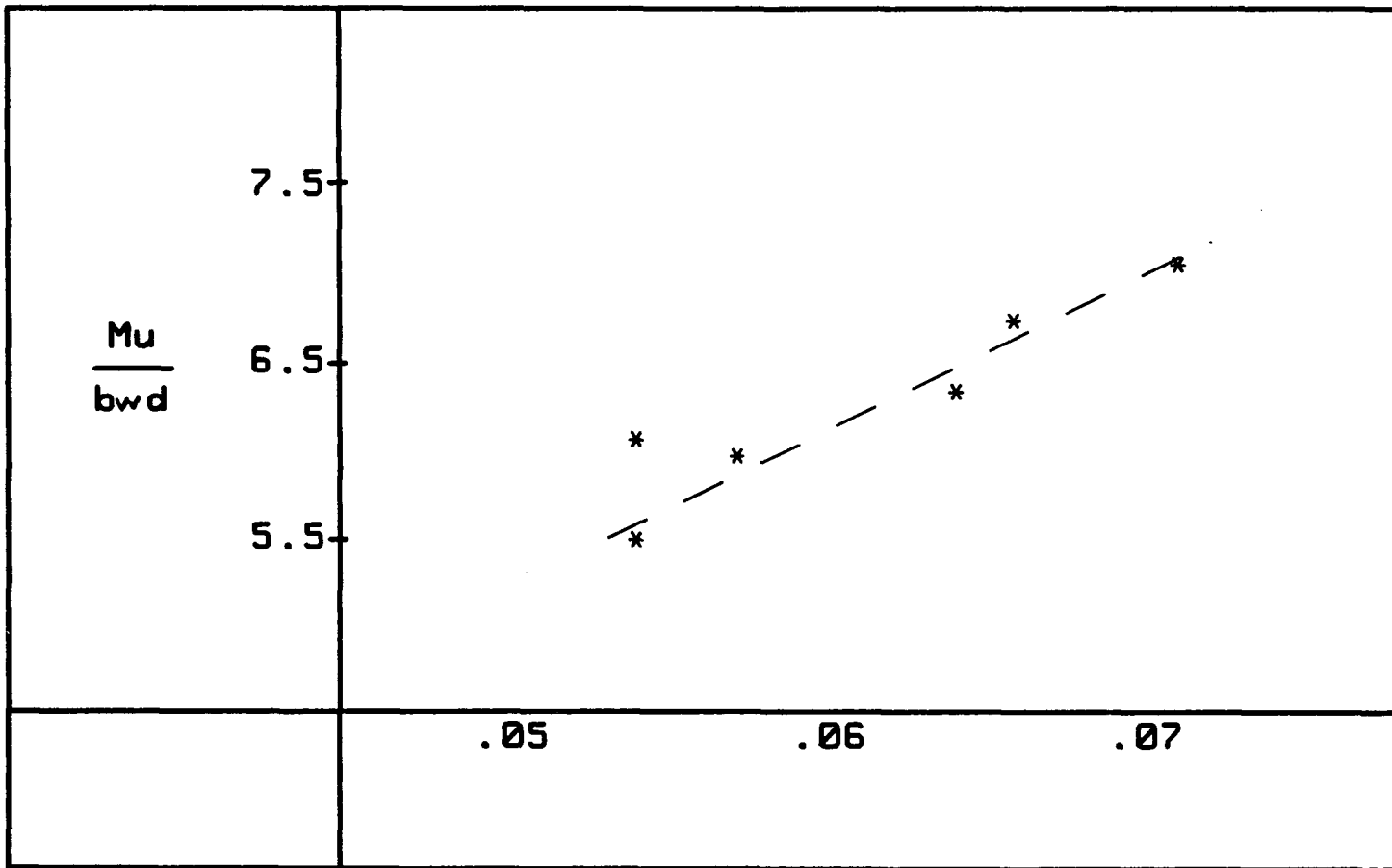


Fig. 5.11. Ratio $M_u/b_w d$ vs. Reinforcing Index ρ

CHAPTER 6

SUMMARY AND CONCLUSIONS

6.1. Summary

Due to the lack of bond between the prestressing steel and the concrete in unbonded post-tensioned members, compatibility of strain between concrete and steel cannot be assumed. In the past three decades, several experiments have been performed and expressions have been proposed for calculating the stress in the unbonded strands at ultimate flexural failure. All of these expressions were obtained from experiments with constant shear span (a). This has resulted in exclusion of (a) from those expressions.

The primary objective of this experiment was to show that Δf_s is influenced by the b/l ratio in addition to the material properties and the l/d ratio, which are included in the existing expressions.

Eight post-tensioned rectangular beams with unbonded tendons and a minimum amount of reinforcement were built and tested for this study. The primary variables of the experiment consisted of the shear span, the size of the specimen and the effective prestressing force.

All beams were tested under a displacement control mode with an MTS hydraulic actuator.

Six out of eight specimens failed in flexure. Because of some experimental problem, Specimen #4 did not fail and Specimen #8 failed with a combined flexural-shear failure mode.

Even though the specimens were lightly reinforced and contained a considerably low amount of reinforcement with reinforcing indices ranging from 0.052 to 0.071, the overall flexural behavior of the specimens was found to be fairly satisfactory. Cracking moments of specimens ranged from 410 (k-in) to 828 (k-in) and ultimate moment capacities ranged from 990 (k-in) to 1439 (k-in). The behavior of the specimens is discussed in detail in Chapters 4 and 5.

6.2. Conclusions

The following conclusions are drawn from the results of this experiment.

- 1) Δf_s , the increase in prestressing steel above the effective prestressing stress (f_{pe}), was found to be influenced by the ratio of b/λ in addition to the material properties and λ/d , which are included in the existing equations.
- 2) Equation 18-4 of the ACI code was found to be unconservative for minimally reinforced beams. Within the limitations of this experiment, a modification factor, (λ), which includes the effect of b/λ , was found and

applied to the original equation. The values obtained from the modified equation were found to be in very good agreement with the test results.

- 3) The value of Ψ in Tam and Pannell's equation (Eq. 5.4) was found to be changing with the b/l ratio rather than being a constant value as was proposed by Tam and Pannell. It was also concluded that the magnitude of Ψ was dependent on the amount of steel reinforcement in the specimens. Based on the results of this experiment, a linear equation for Ψ was obtained and defined in Chapter 5. By applying this new value of Ψ to Equation 5.4 and using the modified equation of Tam and Pannell (Eq. 5.7), the value of Δf_s for this experiment could be predicted accurately.
- 4) Δf_s was found to be independent of the effective prestressing force (p_e).
- 5) Equation (5.9) can be used to find the minimum amount of reinforcement in a prestressed concrete beam in terms of reinforcement index $\bar{\omega}$.
- 6) $\frac{M_u}{b_w d \bar{\omega}}$ was found to be proportional to reinforcing index, $\bar{\omega}$. The ratio $\frac{M_u}{b_w d}$ was found to be equal to 90.

6.3. Recommendations for Further Research

The results of this experiment have answered many questions with regards to the additional stress due to externally applied loads in unbonded post-tensioned concrete beams with minimum amount of flexural reinforcement. Some modification factors have been recommended. However, additional experiments are needed before generalization of these modification factors and before their inclusion in the existing codes can be justified.

All the specimens that were tested were lightly reinforced beams, with a maximum value of reinforcing index, $\bar{\omega}$, of only 0.071. Additional specimens with $\bar{\omega}$ ranging from 0.1 to 0.3 with the same ratio of b/t should be tested. Modification factors for these specimens should be obtained and compared to those obtained from the current study.

APPENDIX A

DERIVATION OF $\bar{\omega}$

Using equation of equilibrium and summing the forces in the section equal to zero, the following equation can be obtained.

$$0.85 f'_c b_w \beta_1 C = A_{ps} f_{ps} + A_s f_y - A'_s f'_s \quad (A.1)$$

Dividing both sides of Equation (A.1) by $b_w d f'_c$ it becomes:

$$\frac{0.85 \beta_1 C}{d} = \frac{A_{ps} f_{ps} + A_s f_y - A'_s f'_s}{b_w d f'_c} \quad (A.2)$$

$$\bar{\omega} = \omega_p + \omega - \omega' \quad (A.3)$$

where

$$\omega_p = \frac{A_{ps} f_{ps}}{f'_c b_w d}, \quad \omega = \frac{A_s f_y}{f'_c b_w d}, \quad \omega' = \frac{A'_s f'_s}{f'_c b_w d}$$

Let $\omega' = v \cdot \omega$

$$\text{and } v = \frac{A'_s}{A_s} \cdot \frac{f'_s}{f_y}$$

From the results of this experiment value of $\frac{f'_s}{f_y}$ found to

be equal to $\frac{1}{3}$. This ratio can be obtained for any cross section by strain compatibility equations.

$$\bar{\omega} = \frac{A_{ps} f_{ps}}{f'_c b_w d} + \frac{A_s f_y}{f'_c b_w d} (1-\nu)$$

or

$$A_{ps} f_{ps} = \bar{\omega} f'_c b_w d - A_s f_y (1-\nu) \quad (A.4)$$

Substituting Eq. A.3 into Eq. A.2:

$$\frac{0.85 \beta_1 C}{d} = \bar{\omega} \quad \text{or} \quad \beta_1 C = \frac{\bar{\omega} d}{0.85 \beta_1} \quad (A.5)$$

Writing equation for nominal moment capacity of cross section as follows:

$$\begin{aligned} M_n = & A_{ps} f_{ps} \left[d - \frac{\beta_1 C}{2} \right] + A_s f_s \left[d - \frac{\beta_1 C}{2} \right] \\ & - A'_s f'_s \left[d' - \frac{\beta_1 C}{2} \right] \end{aligned} \quad (A.6)$$

and cracking moment for a rectangular cross section as:

$$M_{cr} = P_e \left[\frac{h}{6} + e_0 \right] + 1.25 b_w h^2 \sqrt{f'_c} \quad (A.7)$$

Substituting Eqs. A.4 and A.5 in Eq. A.6 and setting that equal to Eq. A.7. Solving the quadratic equation for $\bar{\omega}$

$$\bar{\omega}_{eq} = 0.85(1 + \sqrt{1+\mu}) \quad (A.8)$$

where

$$\mu = \frac{2}{0.85 f'_c b_w d^2} \left(A_s f_s [v(d-d'_s) + d_s - d] - \left[P_e \left(d - \frac{h}{3}\right) + 1.25 b_w h^2 \sqrt{f'_c} \right] \right)$$

APPENDIX B

LIST OF NOTATION

a	shear span, distance between concentrated load and face of support, in.
A	area of that part of the cross section between flexural tension face and the center of gravity of cross section, sq.in.
A_c	cross area of section, sq.in.
A_{ps}	area of prestressed reinforcement in tension zone, sq.in.
A_s	area of nonprestressed steel in tension zone, sq.in.
A'_s	area of compression reinforcement, sq.in.
b	length of constant moment region, in.
b_w	width of compression face of member, in.
c	distance from extreme compression fiber to neutral axis, in.
d	distance from extreme compression fiber to centroid of prestressed reinforcement, in.
d_s	distance from extreme compression fiber to centroid of nonprestressed reinforcement, in.
d'_s	distance from extreme compression fiber to centroid of compression steel, in.
e_0	distance from centroid of prestressing steel to the center of gravity of cross section, in.
E_s	modulus of elasticity of reinforcement, psi.
f'_c	specified compressive strength of concrete, psi.
f_{ps}	stress in prestressed reinforcement at nominal strength, psi.

f_{pu}	specified tensile strength of prestressing tendon, psi.
f_{py}	specified yield strength of prestressing tendon, psi.
f'_s	stress in compression reinforcement, psi.
f_{pe}	effective stress in prestressed reinforcement, psi.
f_y	specified yield strength of nonprestressed reinforcement, psi.
h	overall height of member, in.
I	moment of inertia of section, in ⁴ .
l	span length of member, in.
L	length of prestressing tendon from anchorage to anchorage, in.
M_{cr}	cracking moment of concrete, k-in.
M_n	nominal moment strength, k-in.
M_{ult}	ultimate moment of section, k-in.
P_e	effective prestressing force, lb.
r	radius of gyration of cross section, in.
V	shear force, lbs.
β_1	a factor given by ACI code.
$\Delta\epsilon_s$	additional strain in prestressing steel due to externally applied loads
Δf_s	additional stress in prestressing steel due to externally applied loads.
ρ	ratio of nonprestressed tension reinforcement = $A_s/b_w d$
ρ'	ratio of compression reinforcement = $A'_s/b_w d$
ρ_p	ratio of prestressed reinforcement = $A_{ps}/b_w d$

ϕ strength reduction factor

ψ (plastic hinge length)/c

$$\omega = \rho \frac{f_y}{f'_c}$$

$$\omega = \rho' \frac{f'_s}{f_i}$$

$$\omega_p = \rho_p \frac{f_{ps}}{f'_c}$$

$$\bar{\omega} = \omega_p + \omega - \omega'$$

REFERENCES

- 1) Winter, G., Nilson, A.H., "Design of Concrete Structures," McGraw-Hill Book Company, 1979, p. 2.
- 2) Bennett, E. W., "Partial Prestressing--A Historical Overview." PCI Journal Vol. 29, No. 5, September-October 1984, pp. 104-117.
- 3) Libby, J.R., "Modern Prestressed Concrete," Van Nostrand Reinhold Company, San Diego, 1971.
- 4) Nilson, A.H., "Design of Prestressed Concrete," John Wiley and Sons, New York, 1978.
- 5) Baker, A.L.L., "A Plastic Theory of Design for Ordinary Reinforced and Prestressed Concrete Including Moment Redistribution in Continuous Members." Magazine of Concrete Research, Vol. 1, No. 2. June 1949, pp. 57-66.
- 6) Janney, J.R., Hognestand, E., and MacHenry., "Ultimate Flexural Strength of Prestressed and Conventionally Reinforced Concrete Beams." Journal of ACI, Vol. 56, pp. 601-620.
- 7) American Concrete Institute, "Building Code Requirements for Reinforced Concrete (ACI 318-63)," Detroit, Michigan, 1963.
- 8) Warwaruk, J., Sozen, M.A., and Siess, C.P., "Strength and Behavior in Flexure of Prestressed Concrete," Bulletin No. 464, Engineering Experiment Station, University of Illinois, 1982.
- 9) Mattock, A.H., Yamazaki, J., and Kattula, T., "Comparative Study of Prestressed Concrete Beams, With and Without Bond," ACI Journal, Vol. 68, No. 2, February 1971, pp. 116-125.
- 10) Mattock, A.H., "A Study of the Ultimate Moment of Resistance of Prestressed and Reinforced Concrete Beams, with Particular Reference to Bond Conditions," Ph.D. Dissertation, University of London, 1955.

- 11) Baker, A.L.L., "Tests on Concrete Beams Reinforced with 12 Gauge Wires of an Ultimate Strength of 120 Tons per sq.in.," Magazine of Concrete Research (London), V. 3, No. 9, March 1952, pp. 121-127.
- 12) Gifford, F.W., "Tests on End Anchored, Unbonded Prestressed Beams Having Parabolic Steel Eccentricity, Subject to Uniformly Distributed Loading," Magazine of Concrete Research (London), V. 5, No. 13, Aug. 1953, pp. 27-36.
- 13) ACI Committee 318, "Building Code Requirements for Reinforced Concrete (ACI 318-71)," American Concrete Institute, Detroit, Michigan, 1971.
- 14) Pannell, F.N., "The Ultimate Moment of Resistance of Unbonded Prestressed Concrete Beams," Magazine of Concrete Research, Vol. 21, No. 66, March 1969, pp. 43-53.
- 15) Tam, A., and Pannell, F.N., "The Ultimate Moment of Resistance of Unbonded Partially Prestressed Reinforced Concrete Beams," Magazine of Concrete Research, Vol. 28, No. 97, December 1976, pp. 203-208.
- 16) Mojtahedi, S., and Gamble, W.L., "Ultimate Steel Stress in Unbonded Prestressed Concrete," Journal of Struct. Div. ASCE, Vol. 104, No. S17, July 1978, pp. 1158-1165.
- 17) Cook, N., Rark, R., and Young, P., "Flexural Strength of Prestressed Concrete Members with Unbonded Tendons," PCI Journal, Vol. 26, No. 6, November-December 1981, pp. 53-77.
- 18) Park, R., and Gamble, W.L., "Reinforced Concrete Slabs," John Wiley and Sons, Canada, 1980, p. 559.
- 19) ACI Committee-318, "Building Code Requirements for Reinforced Concrete (ACI-83)," American Concrete Institute, Detroit, Michigan, 1983.
- 20) ACI-ASCI Committee 423, "Tentative Recommendations for Concrete Members Prestressed with Unbonded Tendons," ACI Journal, Vol. 66, No. 2, Feb. 1969, pp. 81-86.

- 21) Naaman, A.E., "A Proposal to Extend Some Code Provisions on Reinforcement to Partial Prestressing," PCI Journal, Vol. 26, No. 2, March-April 1981, pp. 74-91.
- 22) Naaman, A.E., "Prestressing Concrete Analysis and Design," McGraw-Hill Book Company, Chicago, IL, 1982, pp. 149-181.
- 23) British Code of Practice for the Structural Use of Concrete, Part I. Design, Materials and Workshop, CP110, November 1972, p. 70.
- 24) Lin, T.Y., "Design of Prestressed Concrete Structures," John Wiley and Sons, San Francisco, 1981, p. 149.